AD-A035 500   TENNESSEE UNIV KNOXVILLE   F/G 20/8
LIST OF PUBLICATIONS FOR REPORTING PERIOD 1 JULY 1976 - 30 NOVE--ETC(U)
NOV 76   I A SELLIN   N00014-75-C-0474

UNCLASSIFIED   7603   NL

1 OF 1
ADA035500

END
DATE
FILMED
3-77

See A026577
title from next page

ADA035500

REPORT DOCUMENTATION PAGE		READ INSTRUCTIONS BEFORE COMPLETING FORM
1. REPORT NUMBER [redacted] 7603	2. GOVT ACCESSION NO.	3. RECIPIENT'S CATALOG NUMBER
4. TITLE (and Subtitle) LIST of Publications for ~~Technical Report 7603, November, 1976~~ Reporting Period 1 July 1976 - 30 November 1976.		5. TYPE OF REPORT & PERIOD COVERED Technical Report, 1 July 1976 - 30 November 1976
		6. PERFORMING ORG. REPORT NUMBER
7. AUTHOR(s) [redacted] I. A. Sellin		8. CONTRACT OR GRANT NUMBER(s) N00014-75-C-0474
9. PERFORMING ORGANIZATION NAME AND ADDRESS University of Tennessee Knoxville, Tennessee 37916		10. PROGRAM ELEMENT, PROJECT, TASK AREA & WORK UNIT NUMBERS 121103
11. CONTROLLING OFFICE NAME AND ADDRESS Office of Naval Research Arlington, Va 22217		12. REPORT DATE November, 1976
		13. NUMBER OF PAGES 94p.
14. MONITORING AGENCY NAME & ADDRESS (if different from Controlling Office) Office of Naval Research Resident Representative P. O. Box 1247 Huntsville, Alabama		15. SECURITY CLASS. (of this report) Unclassified
		15a. DECLASSIFICATION/DOWNGRADING SCHEDULE

16. DISTRIBUTION STATEMENT (of this Report)

Defense Documentation Center (12 copies)
T. A. Bryant, ONR Resident Representative (1 copy)
NRL, Technical Library (3 copies)
Dr. W. J. Condell, Physics Program, ONR (3 copies)
Dr. W. F. Krupke, LRL (1 copy)

DISTRIBUTION STATEMENT A
Approved for public release;
Distribution Unlimited

17. DISTRIBUTION STATEMENT (of the abstract entered in Block 20, if different from Report)

COPY AVAILABLE TO DDC DOES NOT PERMIT FULLY LEGIBLE PRODUCTION

DDC
RECEIVED
JAN 31 1977
C

18. SUPPLEMENTARY NOTES

19. KEY WORDS (Continue on reverse side if necessary and identify by block number)

Copy available to DDC does not permit fully legible reproduction

20. ABSTRACT (Continue on reverse side if necessary and identify by block number)

This document is a serial technical report concerning work performed to date on the project entitled "Structure of High Ionized Heavy Ions and Associated Collision Phenomena in the MeV/Nucleon Range." Specifically, a list of reprints of books and articles plus preprints and other abstracts of work to be published is included. An updated list of preprints and reprints will be forthcoming when available. This report supplements serially our June, 1976 Technical Report.

346650

List of Publications for reporting period 1 July 1976 - 30 November 1976

Articles:

1. "Strong Isotope Dependence of K-Vacancy Production in Slow Ne^{+}-Ne Collisions," Phys. Rev. Lett. 37, 984 (1976).

2. "Overcoming the Doppler Limitation in Beam-Foil Experiments by Target Ion Spectroscopy," to be published in Proceedings of the IEEE, for the Fourth Conference on Application of Small Accelerators.

3. "Charge Dependence of K X-Ray Production in Nearly Symmetric Collisions of Highly Ionized S and Cl Ions in Gases," accepted by Phys. Rev. A.

4. "Projectile Charge-State Dependende in K-Shell Ionization of Neon, Silicon, and Argon Gases by Lithium Projectiles," submitted to Physics Letters.

5. "Lifetime Measurements in Si IX-Si XII using Beam-Foil Excitation," submitted to Phys. Rev. A.

6. "The Splitting and Oscillator Strengths for the $2s^2S$ - $2p^2P°$ Doublet in Lithiumlike Sulfur," submitted to Astrophysical J.

7. "Differences in the Production of Non-Characteristic Radiation in Gaseous and and Solid Targets," Phys. Rev. Lett. 36, 1574 (1976).

8. "Radiative Lifetimes and Transition Probabilities for Electric Dipole $\Delta n=0$ Transitions in Highly Stripped Sulfur Ions," Phys. Rev. A14, 1036 (1976).

9. "An Experimental Survey of Electron Transfer in keV Collisions in Multiply Charged Ions with Atomic Hydrogen," in Proceedings of the Fifth International Conference on Atomic Physics, R. Marrus, M. H. Prior, and H. A. Shugart, eds. University of California, Berkeley, California (1976), p. 126.

10. "Lifetimes and Transition Rates for Allowed In-Shell Transitions in Highly Stripped Sulfur," in Proceedings of the Fifth International Conference on Atomic Physics, R. Marrus, M. H. Prior, and H. A. Shugart, eds., University of California, Berkeley, California (1976), p. 166.

11. "Applications of Beam-Foil Spectroscopy to Atomic Collisions in Solids," Nucl. Inst. and Meth. 132, 397 (1976).

12. "Differences in the Production of Non-Characteristic Radiation in Solid and Gas Targets," in Beam-Foil Spectroscopy: Heavy Ion Atomic Physics, I. A. Sellin and D. J. Pegg, eds., Plenum Press, New York (1976), Vol. 2, p. 497.

13. "Angular Distribution Studies on Non-Characteristic X-Radiation," in Beam-Foil Spectroscopy: Heavy Ion Atomic Physics, I. A. Sellin and D. J. Pegg, eds., Plenum Press, New York (1976) Vol. 2, p. 497.

14. "Autoionizing States in Highly Ionized O, F, and Si," in Beam-Foil Spectroscopy: Heavy Ion Atomic Physics, I. A. Sellin and D. J. Pegg, eds., Plenum Press, New York (1976), Vol. 1, p. 451.

15. "Lebensdauern und Oszillatorenstärken von n=2 Zuständen in Be-ähnlichem S," to be published in Verhandl. Deutsche Physikalische Gesellschaft.

16. "Der $2s^2S-2p^2P°$ Doublettübergang in Li-ähnlichen Schwefel," to be published in Verhandl. Deutsche Physikalische Gesellschaft.

17. Invited Paper," High Ionization-Excitation States of Ne^{q+} Ions and their Mass-Dependent Symmetric Collision Interactions," to be published in Bull. Am. Phys. Soc.

18. "Measurement of the H^++H Charge Exchange Cross Section, 0.8-2.5 MeV," to be published in Butl. Am. Phys. Soc.

19. "A Beam-Foil Study of the $2s^2S-2p^2P°$ Doublet in Li-like sulfur," to be published in Bull. Am. Phys. Soc.

20. "Radiative Lifetimes and Oscillator Strengths for the n=2 States of Be-like Sulfur," to be published in Bull. Am. Phys. Soc.

21. "Mass Dependence of Ne K X-Ray Yields from Ne^+-Ne Collisions at keV Energies," to be published in Bull. Am. Phys. Soc.

W. Gruebler and V. Konig (Birkhauser-Verlag, Basel and Stuttgart, 1976), p. 940.
[5]Sr. M. A. Doyle et al., to be published.
[6]L. Brown and U. Rohrer, Nucl. Phys. A221, 325 (1974).
[7]Th. Stammbach and R. L. Walter, Nucl. Phys. A180, 225 (1972).
[8]R. C. Byrd et al., to be published.
[9]J. R. Smith and S. T. Thornton, Nucl. Phys. A186, 161 (1972).
[10]C. A. Kelsey, B. Hoop, and P. Van der Maat, Nucl. Phys. 51, 395 (1964).
[11]R. L. Walter, W. Benenson, P. S. Dubbledam, and T. H. May, Nucl. Phys. 30, 292 (1962).
[12]D. S. Cramer and L. Cranberg, Nucl. Phys. A171, 59 (1971).
[13]W. Tornow, S. E. Skubic, R. C. Byrd, P. W. Lisowski, and R. L. Walter, Phys. Rev. C 13, 2080 (1976).
[14]W. Tornow, H. Spiegelhauer, and G. Mack, Nucl. Instrum. Methods 125, 373 (1975).
[15]H. Davis and R. B. Galloway, Nucl. Instrum. Methods 108, 561 (1973).
[16]C. Werntz and W. E. Meyerhof, Nucl. Phys. A121, 38 (1968).

Strong Isotope Dependence of K-Vacancy Production in Slow Ne$^+$-Ne Collisions*

R. S. Peterson, S. B. Elston, and I. A. Sellin
University of Tennessee, Knoxville, Tennessee 37916, and Oak Ridge National Laboratory, Oak Ridge, Tennessee 37830

and

R. Laubert, F. K. Chen, and C. A. Peterson
New York University, New York, New York 10003
(Received 17 June 1976)

Large isotope effects in the K x-ray yields from collisions of ^{A}Ne$^+$-^{B}Ne (A,B = 20, 22) have been observed. For slow collisions (relative velocities ~$\frac{1}{3}$ a.u.) the K x-ray yields do not scale well with either relative velocity or center-of-mass energy, whereas at higher collision velocities, the yields appear to scale well with relative velocity.

The dominant mode of production of K-shell vacancies in slow, symmetric ion-atom collisions was originally predicted[1] to be due to the transfer of an initial $2p$ vacancy into the K shell by the rotational coupling of the $2p\sigma$-$2p\pi$ molecular orbitals of the collisionally formed quasimolecule. Quantitative predictions of vacancy production rates in Ne$^+$-Ne collisions were made[2] by scaling collision trajectories in D$^+$-D collisions and scaling the molecular energy levels of the H$_2^+$ molecule. For Ne$^+$-Ne collisions the K-vacancy production rate for a given impact parameter was taken as the product of the probability that the initial $2p$ vacancy occupied the $2p\pi$ molecular orbital and the probability of rotational coupling of the $2p\sigma$ and $2p\pi$ orbitals. Isotope effects in the trajectory scaling were considered negligible if the ratio of the nuclear charge to the reduced mass of the collision partners was near unity (i.e., $Z/M_r \approx 1$) and the screened nuclear charge was a constant fraction of the bare nuclear charge.[2]

Within the approximations used in Ref. 2, it was expected[2] that K-vacancy production in symmetric collisions between different isotopes of the same element would be approximately the same in collisions of the same relative velocity. The present experiment provides the first precise test of this prediction using K x-ray production as a measure of the K-vacancy production. For ^{A}Ne$^+$-^{B}Ne collision velocities of about $\frac{1}{2}$ a.u. or greater, we have verified the accuracy of this prediction. For velocities ~$\frac{1}{3}$ a.u., we find a 40% isotope effect in the K-vacancy production rate for equal relative velocities!

A central purpose of this Letter is to describe sensitive means for making quantitative tests[3] of mass-dependent corrections to scaling calculations like those of Briggs and Macek[3] and to illustrate the success of such tests for Ne$^+$-Ne collisions. It is surprising that such sensitive tests can be obtained from such relatively simple total cross-section measurements.

For $Z_A = Z_B$, and given internuclear separation, isotopic effects on energy levels of the Ne-Ne collision system and on corresponding electronic screening of the nuclei may be neglected. For equal relative velocities, isotopic effects on fluorescent yields are also expected to be small. The dominant isotope effects are due to differences in internuclear trajectory, slight variations in which strongly influence the probability of rotational coupling near the threshold (Figs. 2 and 3 of Ref. 2). Such variations in beam trajectory depend strongly on the reduced mass in the threshold region. In this region, the cross section for K x-ray production varies steeply with velocity due to the rapid variation in K-shell interpenetration.

In the present experiment, Ne$^+$ beams of atomic masses 20 and 22 from the 400-kV Cockroft-Walton accelerator of the New York University Physics Department were directed through a differentially pumped gas cell and collected in a biased Faraday cup, whose output was used for normalization. A collimated lithium-drifted silicon detector counted the Ne K x rays emitted at right angles to the beam direction. The target gas pressure of ^{20}Ne or ^{22}Ne, typically less than 3 mTorr, was monitored by a capacitance manometer. This manometer controlled a variable gas leak in order to maintain a constant target density. From such data, absolute K x-ray production cross sections were established and found to agree within overlapping error bars with earlier data.[4-6]

A ratio method of examining the isotope effects was devised to eliminate errors stemming from absolute cross-section measurement errors. To avoid errors from the measurement of absolute target densities for a given isotope, the target gas density was held constant while K x-ray yields were measured with ^{20}Ne$^+$ and ^{22}Ne$^+$ beams of magnetically selected velocities established to better than 1%. At least three measurements for each beam isotope were made at each velocity. Scatter in these yields arose from target density fluctuations, beam current measurement errors, x-ray counting statistics, and errors in the absolute beam energy. Measuring the ratios of the x-ray yields from different isotopic beams on an undisturbed target (for constant target density) eliminated errors from imperfect measurements of the absolute target density. Errors in the ratios were calculated from the scatter of the individual yield measurements. The rms yield errors obtained were typically 3% (counting statistics were better than 2%). To compare x-ray yields between different isotopic targets, differences in absolute target densities for ^{20}Ne and ^{22}Ne target gases were measured by observing the Ne K x-ray yields for 250-keV protons on Ne. It was assumed that the K-vacancy cross sections and fluorescent yields were identical for these two collision systems. The measured cross-section ratio was 1.008 ± 0.032, which was used to correct x-ray yield ratios between collision systems with different isotopic targets. The isotopic purity of the ^{22}Ne gas was measured to be greater than 99%, while the ^{20}Ne gas target was a natural isotopic mixture (~91% ^{20}Ne, ~9% ^{22}Ne). The error bars for measurements on ^{20}Ne targets do not reflect these isotopic impurities.

The results of K x-ray yield ratios as a function of relative velocity are shown in Fig. 1. The error bars reflect one standard deviation of the errors mentioned above. At velocities near threshold ($v_{rel}^2 \approx 8$ keV/amu) there are large deviations from simple relative velocity scaling. These deviations are larger for the collision systems with larger reduced masses and center-of-mass collision energies. In the approximation $Z/M_r \approx 1$, such an effect is not expected. For a given impact parameter, the energy available in the center-of-mass system determines the distance of closest approach. The possibility that the yield isotope effects could be accounted for by center-of-mass energy scaling was tested; the results are shown in Fig. 2. The symmetric-mass collisions do not scale with center-of-mass energy, while the asymmetric-mass collisions, shown as open squares in the inset, do scale with center-

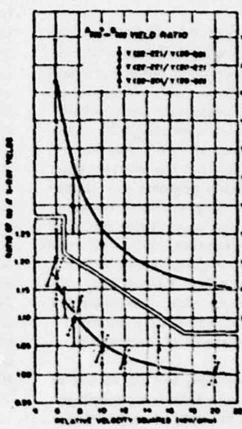

FIG. 1. Ratios of Ne K x-ray yields from ^{A}Ne$^+$-^{B}Ne collision systems for A,B = 20, 22 as a function of relative velocity. The Y(22-22)/Y(20-20) ratios are referenced to the right-hand axis, whereas all other ratios are referenced to the left-hand axis. Error bars represent one standard deviation of errors discussed in the text.

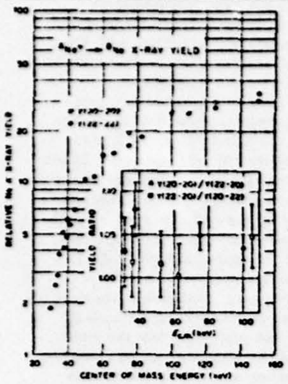

FIG. 2. Plot of Ne K x-ray yields from symmetric-mass collisions, $^{20}Ne^{+}$-^{20}Ne and $^{22}Ne^{+}$-^{22}Ne, as a function of center-of-mass energy. The inset is a plot of ratios of Ne K x-ray yields as a function of center-of-mass energy.

of-mass energy within experimental errors. The asymmetric-mass collision systems have identical relative velocities when their center-of-mass energies are identical. Therefore, the asymmetric-mass collisions also scale with the relative velocity. Screening of the nuclei should be nearly identical for $^{22}Ne^{+}$-^{20}Ne and $^{20}Ne^{+}$-^{22}Ne for equal relative velocities so that the internuclear potentials for these collision systems are identical. Because classical binary-collision trajectories are identical if different collision systems have identical relative velocities, center-of-mass energies, and potential energies, it can be concluded from the data in the Fig. 2 inset that, within error bars, the K x-ray yields, and hence the K-vacancy cross sections, are nearly identical for $^{A}Ne^{+}$-^{B}Ne collision systems if the trajectories are identical.

For large relative velocities, the trajectory in the localized region of large rotational coupling is dominated by relative velocity as opposed to nuclear Coulomb repulsion terms. Hence, relative velocity scaling should become a good approximation at sufficiently high relative velocities. Physically this implies that a rectilinear approximation to the true classical trajectory in the region of strong rotational coupling is approximately valid. Since the rotational coupling of $2p\sigma$-$2p\pi$ molecular orbitals maximizes for collisions with impact parameters of the order of the K-shell radius,[7] as the relative velocity of a collision is increased, the relative velocity scaling of the K-vacancy production cross section becomes a good approximation. This conclusion is borne out by the data of Fig. 1, where relative velocity scaling becomes valid above $v_{rel} = 0.5$ a.u. ($E_{lab}/M = v_{rel}^2/2 = 6$ keV/amu).

Near threshold velocities of $\sim \frac{1}{4}$ a.u., the relative velocity scaling fails badly, which implies that a rectilinear approximation to the trajectory in the localized region of strong rotational coupling is not adequate. For these velocities, the nuclear Coulomb repulsion prevents penetration into regions of large rotational coupling.[3,7,8] For a given impact parameter and relative velocity, the distance of closest approach is smallest for the collision system with the largest center-of-mass energy (and hence with the largest reduced mass). Therefore, the trajectories of collision systems with larger center-of-mass energies will have a larger probability to penetrate into this region of large rotational coupling. These collision systems will have the larger probability to couple the $2p\sigma$-$2p\pi$ molecular orbitals, which implies a larger K-vacancy cross section. For threshold velocities, the collision system with the largest center-of-mass energy has the largest x-ray yield, as is evident in Fig. 1. The results shown in Fig. 2 for the symmetric-mass collisions and in the Fig. 2 inset for the $^{20}Ne^{+}$-^{20}Ne to $^{22}Ne^{+}$-^{20}Ne ratio indicate that center-of-mass energy scaling is also invalid, even though the difference in distances of closest approach for systems of identical impact parameter and relative velocity is ~10%. Yet, the x-ray yields vary as much as 40%. A quantitative explanation of these large deviations from relative velocity scaling for threshold velocities must depend not only on distances of closest approach but also on the internuclear velocities at those distances. If the distance of closest approach did become the dominant factor in K-vacancy production near the threshold, the center-of-mass energy might be expected to become the valid scaling parameter. It is seen in Fig. 1 that for relative velocities greater than about 0.5 a.u. the relative velocity scaling is good, but that near threshold velocities, neither the relative velocity nor the center-of-mass energy scalings are adequate. Thus, calculations of the rotational coupling of the $2p\sigma$ and $2p\pi$ molecular orbitals of the quasimolecule formed in the collision which take explicit account

of the detailed Coulomb trajectories are required. Hence, the validity of scaling the D^{+}-D collision[8] depends strongly upon $Z/M_r = 1.00$ for velocities near the threshold. Collision systems where $Z/M_r = 0.91$ (i.e., $^{22}Ne^{+}$-^{22}Ne) can lead to variations of K vacancy yields as high as 40%. At higher relative velocities, however, the relative velocity scaling does appear to be valid for collision systems with $Z/M_r = 1$ as predicted.[8]

Since we completed these experiments, Taulbjerg and Macek[3] have kindly provided explicit calculation of the isotope effects we observed for the collision system used in our experiment, based on a mass-dependent refinement of their original papers[2] to be published in the very near future.[9,10] The solid curves in Fig. 1 display the results of their mass-dependent treatment, excellently accounting for the large isotope effects seen in our experiments. The new mass-dependent treatment of vacancy production in assymmetric collisions by Taulbjerg, Briggs, and Vaaben[9] has thereby been shown to be excellent. The demonstrated size of such isotope effects even in total crosssection measurements provides a promising experimental tool for use in studying other collision systems.

We acknowledge stimulating discussions with J. H. Macek, W. Brandt, and J. S. Briggs concerning these experiments.

*Work supported in part by the U. S. Office of Naval Research, the National Science Foundation, and the U. S. Energy Research and Development Administration.

[1]W. Lichten, Phys. Rev. 164, 131 (1967).
[2]J. S. Briggs and J. Macek, J. Phys. B 5, 579 (1972).
[3]K. Taulbjerg and J. H. Macek, private communication.
[4]F. W. Saris and D. Onderdelinden, Physica (Utrecht) 49, 441 (1970).
[5]K. H. Schartner, H. Schafer, and R. Hippler, Phys. Lett. 46A, 31 (1973).
[6]N. Stolterfoht, D. Schneider, D. Burch, B. Aagaard, E. Bøving, and B. Fastrup, Phys. Rev. A 12, 1313 (1975).
[7]J. S. Briggs, in Proceedings of the International Conference on Inner-Shell Ionization Phenomena and Future Applications, Atlanta, Georgia, 1972, edited by R. W. Fink, S. T. Manson, J. M. Palms, and P. V. Rao, CONF-720 404 (U. S. Atomic Energy Commission, Oak Ridge, Tenn., 1973), Vol. 2, p. 1209.
[8]B. Fastrup, G. Hermann, and O. C. Kessel, Phys. Rev. Lett. 27, 771 (1971).
[9]K. Taulbjerg, J. S. Briggs, and J. Vaaben, to be published.
[10]K. Taulbjerg, in Proceedings of the Second International Conference on Inner-Shell Ionization Phenomena, Freiburg, Germany, 29 March–2 April 1976 (to be published).

Angular Distributions of Electrons from Resonant Two-Photon Ionization of Sodium

J. A. Duncanson, Jr., M. P. Strand, A. Lindgård, and R. S. Berry
Department of Chemistry, The University of Chicago, Chicago, Illinois 60637
(Received 13 July 1976)

Sodium atoms are excited to either the $3^2P_{1/2}$ or $3^2P_{3/2}$ state using a linearly polarized dye-laser beam and are subsequently ionized using a linearly polarized nitrogen-laser beam. Angular distributions of the ejected electron have been both measured and calculated for several relative orientations of the photon polarization vectors. The difference between the s- and d-continuum partial-wave phase shifts $\delta_s - \delta_d$ and the ratio of the radial dipole matrix elements (d_s/d_d) are obtained.

We report the first measurement of anisotropic angular distributions of electrons from resonant two-photon ionization of atoms. An isotropic ensemble of sodium atoms in their $3^2S_{1/2}$ ground state is excited to either the $3^2P_{1/2}$ or the $3^2P_{3/2}$ level by a linearly polarized beam from a tunable dye laser, producing an aligned intermediate state. After a 5-nsec delay, they are ionized by a linearly polarized nitrogen laser beam of wavelength 337.1 nm. For the two-step ionization process, the intensity of electrons ejected in direction $\hat{\Omega}$ is given by

$$\frac{d\sigma}{d\Omega} = \text{const} \sum_{\substack{\Lambda_1\Lambda_2 \\ LM}} Y_{LM}(\hat{\Omega})(\rho_{\Lambda_1}{}^{(1)}\rho_{\Lambda_2}{}^{(2)})_{LM} C(\Lambda_1, \Lambda_2, L), \tag{1}$$

OVERCOMING THE DOPPLER LIMITATION IN BEAM-FOIL SPECTROSCOPY BY TARGET ION SPECTROSCOPY: HIGH IONIZATION-EXCITATION STATES OF SLOW Ne^{q+} IONS AND THEIR MASS-DEPENDENT, SYMMETRIC COLLISION INTERACTIONS*

(2)

Ivan A. Sellin
University of Tennessee
Knoxville, Tennessee 37916

and

Oak Ridge National Laboratory
Oak Ridge, Tennessee 37830

Summary

Two modern techniques, one for overcoming the Doppler limitation in beam-foil experiments and the second permitting pursuit of the study of collisional interactions and lifetimes of keV energy, multiply charged ions are described. In particular, high ionization-excitation states of Ne^{q+} ions and their mass-dependent symmetric molecular collision interactions are discussed.

Introduction

A primary limitation on the spectroscopic accuracy of beam-foil measurements has always been the Doppler spread associated with the high beam velocities needed to generate the high ionization-excitation states of interest. This limitation is especially severe for beam-foil Auger experiments in which the ratio of electron emission velocity to beam velocity rather than c is the important parameter. Resolution of this problem would permit not only great improvement of the spectroscopic accuracy of conventional beam-foil measurements in the xuv and x-ray regions but also precision measurements of fundamental quantities pertaining to highly ionized ions by standard resonance techniques now impracticable because of the Doppler spread problem.

For some time it has been known that impact of highly ionized, foil-transmitted heavy ions generates high ionization-excitation states of lighter target atoms.[1] For example, Ne^{9+} Lyman α appears when neon gas is bombarded by Ar^{16+} ions, even under single collision conditions! Since undisturbed target atoms have only thermal velocities, recoil broadening and excitation cross sections provide the only limitations on the reduction of the Doppler spread problems to thermal proportions. In more recent experiments in our laboratory,[2] involving production of NeII to NeV excited states in the xuv by foil transmitted S ions of mean charge state ~12+, we have explored the recoil broadening and excitation cross section problem and found neither to be limiting within the resolution available. In particular, instrument limited line widths as low as 7 meV have been observed. Cross sections for production of NeV excited states have been found to be appreciable compared to those for NeII. A detailed description of this method plus some early, representative results for Ne^{q+} ions is provided in the subsequent sections.

Through the use of a second, quite different technique it has proved possible to study symmetric Ne^{q+}-Ne collisions (q = 1-5) in the quasi-molecular (keV energy) regime. Extraction of Ne^{q+} directly from a high power Penning discharge source at ORNL has permitted study of K ionizing collisions in Ne^{q+}-Ne collisions at beam energies ≤ 100 keV. The growth of K x-ray yields has been used to explore the exit channel effect explicitly treated within the framework of a rotational coupling model by Briggs and Macek.[3] Large, mass-dependent isotope effects have been discovered by Peterson, Laubert, Elston, et al.[4] in the threshold region in which the K-hole production cross section rises steeply with beam energy. A striking failure of the equal velocity rule for the two isotopes ^{20}Ne, ^{22}Ne has been observed, using Ne^{+} beams from the NYU Cockroft-Walton accelerator. A description of this second method is also provided, together with a discussion of results on Ne^{q+}-Ne collisions by Peterson et al.[5]

Our discussion of the spectroscopic aspects of the neon work reflects the collective work of the authors in Ref. 2. Our discussion of the collisional aspects reflects the collective work of the authors in Refs. 4 and 5, especially that of Randolph S. Peterson, who until recently has been a graduate research assistant in our laboratory, and is unable to attend this conference because of his present participation in collisions work at the Institut für Kernforschung of the University of Frankfurt (Main).

Target Ion Spectroscopy

As indicated in the introduction, even at the time of the earliest beam-foil spectroscopy experiments[6] it was recognized that Doppler shifts and spreads accompanying emission of light[6] or Auger electrons[7] from fast-moving projectiles ionized and excited in thin foils would severely limit spectroscopic accuracy, and thereby limit the accuracy of precision experiments that could be accomplished. For example, Lamb was characteristically prescient in remarks[8] concerning the first fast beam Lamb shift measurement[9] that problems associated with the high beam velocity might significantly limit accuracy. Indeed, more recent, laser resonance absorption experiments on fast hydrogenic fluorine beams in the 2s state[10] have required moderately heroic efforts to narrow and interpret the asymmetric $2s_{1/2}$-$2p_{3/2}$ line observed as a function of Doppler tuning angle, especially since two strong laser lines were unresolved within the beam Doppler profile. While considerable progress has been made in solving the Doppler problem in the uv to visible region by refocussing techniques, to my knowledge no such methods have been applied in the xuv/x-ray region.

In 1973 it was shown that impact of suitable, highly ionized, foil-transmitted heavy ions generates very high ionization-excitation states. For example, substantial amounts of Lyman α from hydrogenic Ne^{9+} appeared in the target ion excitation spectrum when Ar^{q+} ions from the Oak Ridge Isochronous Cyclotron in the range q ≥ 16 were used as projectiles, even under single collision conditions! It was suggested[11] that precision measurements on target ions in high ionization-excitation states would be feasible if these ions had a more nearly thermal velocity distribution, and if target ionization-excitation cross-sections were suggiciently high.

Estimates of recoil broadening are attractively low for two reasons. First, the long range intense Coulomb field from a highly ionized projectile permits target electron removal and excitation processes to occur at impact parameters larger than the target electron shell radii.[12] Second, the high relative collision velocity (≥ 0.05-0.10 c) provides a short interaction time. For example, a bare 2 MeV/nucleon Ar nucleus passing by a neon atom at an impact parameter of ~ 1/3 Å (a neon L-shell radius) creates a Ne recoil ion travelling at about 89.99 deg with respect to the beam direction at a recoil velocity $v_{REC} \leq 2v_B (M_{REDUCED}/M_{Ne}) \cos\phi_{REC} \cong 3 \times 10^5$ cm/sec $\lesssim 10^{-5}$ c. Hence $v_{REC}/c \ll v_B/c$ by about four orders of magnitude, and both Doppler shifts and spreads should be smaller in target vs. projectile optical or Auger spectra by about the same factor. Moreover, v_{REC} is of the order only of thermal velocities in a hollow cathode discharge.

While such recoil estimates make the method look attractive, there has been up to now no stringent experimental verification of the reduction of Doppler limitations in the xuv/x-ray region at the level of the experiments considered here. Generally, target atom K Auger and x-ray spectra taken with high resolution electron and bent crystal x-ray spectrometers in similar experiments[13] involving impact of highly ionized heavier projectiles on Ne targets have had associated line widths ranging from about 0.3 - 3 eV. In some of our recent experiments, which concern impact of 1.5 MeV/nucleon sulfur ions of mean charge state ~ 12+ on Ne, entirely instrument limited line widths ≤ 0.007 eV have been demonstrated, representing a factor of ~ 50 to 500 improvement (or about an order of magnitude on a fractional Δλ/λ basis). Furthermore, cross-sections ≥ 10^{-19} cm² for production of each of a number of Ne^{q+} L x-rays belonging to charge states q = 2-5 have been demonstrated. An additional feature of considerable interest is that excitation states belonging to a variety of charge states have comparable excitation cross sections. For example, it is found that the cross-section for the production of $2s^2 2p^2$-$2s2p^3$ transitions in Ne V (λ 416.8) is comparable to that for production of $2p^5$-$2p^4(^1D)3s$ transitions in NeII (λ 407.2).

Because the combination of demonstrated small line widths and appreciable excitation cross-sections indicates a bright outlook for the development of precision measurements on target atoms in high ionization-excitation states, it is of interest to describe some relevant experimental details here.

Figure 1 displays a generalized apparatus suitable for performing projectile charge state experiments under approximately single collision conditions. Here a

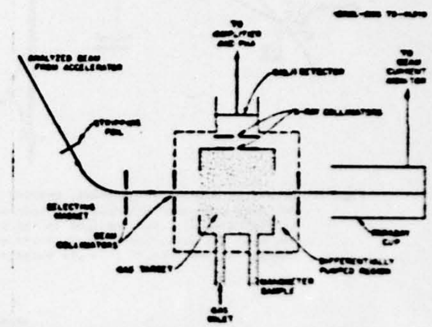

Fig. 1. Apparatus suitable for studying collisional interactions of fast, highly ionized ions in thin gas targets.

stripping foil may be used to prepare an equilibrium mixture of charge states in a high velocity incident, usually lower charge state beam derived from an appropriate accelerator. A selection magnet deflects a pure emergent charge state beam into a collision region viewed by some energy dispersive device which counts energy selected photons or electrons emerging from the collision region. Normalization to incident beam flux is made by integration of collected beam current in a Faraday cup, or alternatively by Rutherford scattering of projectiles in another target foil (not shown) of known thickness. While Fig. 1 shows such an arrangement specific to use of a low resolution Si(Li) surface barrier detection, it is straight forward to replace this detector with a more highly dispersive device such as the 2.2 m grazing incidence xuv spectrometer sketched in Fig. 2.

A typical spectrum for impact of 1.5 MeV/nucleon S ions on a Ne target maintained at 100 mTorr pressure is shown in Fig. 3. To obtain this spectrum, beams of 1.5 MeV/nucleon S ions obtained from the Oak Ridge Tandem accelerator were passed through a carbon stripper foil (mean emergent charge state ~ 12+) located about 2 cm upstream from the vertical entrance slit of a 2.2 m grazing incidence monochromator which dispersed the xuv radiation emitted at 87.5 deg to the beam direction in a horizontal plane. The monochromator viewed an approximately cylindrical interaction region consisting of a 0.3 mm long, 2 mm diameter slice of the beam undergoing collisions in Ne gas maintained at a pressure of 100 mTorr in a differentially pumped target chamber mounted on the entrance slit. The solid angle subtended by the portion of the grating used was typically 4 x 10^{-4} sr.

*Research supported in part by ONR, NSF, and NASA; and by Union Carbide Corporation under contract with ERDA.

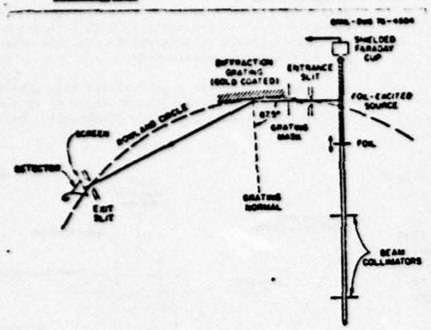

Fig. 2. Layout of extreme ultraviolet, grazing incidence spectrometer suitable for studying decay in flight of foil-excited ions in the xuv, and for studying collisional interactions of fast, highly ionized ions in thin gas targets.

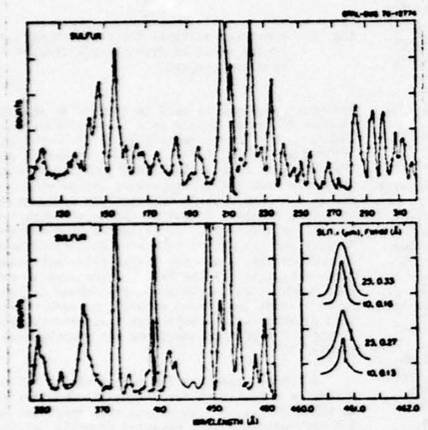

Fig. 3. xuv spectrum from bombardment of Ne gas at 100 μm pressure by foil-stripped sulfur ions at 1.5 MeV/amu. The main body of the spectrum was acquired using symmetric slit widths of 200 μm. The inset spectra were acquired at slit widths of 50 μm. The standard Ne II line at λ 460.7 (lower right) was observed to have an instrument limited width, reaching ≤ 7 MeV at 10 μm. The upper λ 460.7 scan was derived from the hollow cathode source and displays wider lines.

Because equilibrium charge distributions in both gases and solids in this projectile mass range are known to be highly similar, and the beam had been equilibrated 2 cm upstream, it is unlikely that the charge state composition of the beam in the gas deviates appreciably from that expected from straightforward charge equilibration measurements, which indicated that the dominant projectile charge state present at the beam energy used was 12^+. The spectrum between 100 and 500 Å was scanned using integrated beam current (400 nA) to derive equal real time stepping intervals for the monochromator exit slit. A hollow cathode discharge source facing the entrance slit could be turned on at any time to permit on-line wavelength calibration using standard lines of He, Ne, and Ar.

The spectrum in the main body of Fig. 3 obtained at comparatively coarse slit settings of 200 μm, took only about 4h to accumulate under the above conditions. Inset portions of the figure were scanned at higher resolution levels, as indicated in the figure. A great majority of the spectral features observed can be associated with excited states of Ne II, III, IV, and V. As a check, the same region was scanned with gas out, and then with He gas in at about the same pressure. With very few exceptions all of the lines in Fig. 3 are found to be Ne target gas lines.

The inset concerning the well-known $2s^22p^5$-$2s2p^6$ Ne II standard calibration line at λ 460.7 was studied at a variety of slit widths down to 10 μm. At this setting an instrument limited line width ≤ 7 MeV is seen. This width, actually somewhat smaller than the observed width of the same transition excited in the hollow cathode discharge source, is entirely limited by our instrument (2.2 m Rowland circle diameter, 300 line per mm grating).

A short tabulation of prominent, apparently unblended lines and their corresponding assignments and intensities relative to the λ 460.7 line is given in Table I. An approximate excitation cross-section estimate based on the observed normalized intensity of this line and the experimental conditions noted above gives ≥ 4×10^{-19} cm². While this estimate allows for grating reflectivity and astigmatism in addition to the usual geometry factors, it does not allow for light loss due to dispersion into higher diffraction orders nor for notoriously difficult estimates of intensity loss due to possible time-dependent grating surface contaminations or other surface condition losses. Hence the cross-section estimate quoted should be regarded as an approximate lower limit. Corresponding lower limits on excitation cross-sections for the other lines listed in Table I can be inferred from the relative intensities given, provided account is taken of the influence of grating blaze angle and wavelength dependent astigmatism. As the angle of incidence used the combined influence of blaze and astigmatism is such as maximize efficiency near λ 150, at which wavelength the corresponding relative intensities listed in Table I are overstated by a factor of ≤ 2.

Some additional valuable properties of the kind of target ion spectroscopy described here may be noted. First, the excited ions of interest are produced in an environment which is not only cold compared to traditional hollow cathode discharges but also of comparable or lower density. Collision broadening and corresponding lifetime perturbation effects can be further reduced, at the expense of intensity. Second, current technology will easily permit recovery of one of the most valuable features of the beam-foil source, namely the ability to make lifetime measurements. Pulsed beams in the nanosecond regime are standard at numerous accelerator facilities. Delayed coincidence measurements of the time interval between the beam pulse and photon emission are a well-known, standard technique which even now permit lifetime measurements on excited states of

TABLE I

Configurations and relative intensities of various prominent, unblended Ne II-V transitions observed in the present experiment.

λ(Å)	Charge State	Relative Intensity	Configuration
122.5	V	110	$2p^2$-$2p4d$
184.7	V	200	$2p^2$-$2p3s$
212.6	IV	520	$2p^3$-$2p^2(^1D)3s$
301.1	III	310	$2p^4$-$2p^3(^2D)3s$
379.3	III	850	$2s^22p^4$-$2s2p^5$
388.2	IV	80	$2s^22p^3$-$2s2p^4$
405.9	II	440	$2p^5$-$2p^4(^1D)3s$
407.2	II	220	$2p^5$-$2p^4(^1D)3s$
416.8	V	180	$2s^22p^2$-$2s2p^3$
455.3	II	400	$2p^5$-$2p^4(^3P)3s$
460.7	II	1000	$2s^22p^5$-$2s2p^6$
462.4	II	500	$2s^22p^5$-$2s2p^6$

target ions in the nanosecond to hundreds of microsecond regime to accuracies comparable to present beam-foil lifetime measurements. Third, there is a lack of availability of light sources with low thermal and collision broadening for intermediate to high stages of ionization beyond the range of hollow cathode discharge sources which the target ion source may help to fill. Fourth, there is good control over the mean ionization states produced in the target by means of changing the beam energy and thereby altering the projectile equilibrium charge.

It appears that the attractive line widths and excitation cross-sections observed in the experiment illustrated here will have application to many other collision systems. Very high charge states of projectile ions (e.g., Kr^{25+}, Xe^{31+}) are already available[14] at some accelerator facilities (e.g., the Unilac facility at Darmstadt), so that production of highly ionized and excited states of somewhat heavier target atoms should be possible with similarly large excitation cross-sections and small recoil broadening. It should be noted that careful use of refocussing techniques (cf. J. A. Leavitt et al.[15], J. O. Stoner and I. Martinson[16]) has permitted substantial reduction of Doppler spread problems in beam-foil experiments in the uv and visible regions. For the low states of ionization for which hollow cathode discharge sources are useful, careful operation combined with use of higher dispersion spectrometers provides narrower line widths than are demonstrated here. However, in the xuv/x-ray region, where efficient focussing elements are not available, and for the higher ionization-excitation states whose radiative electronic transitions fall in this region, the technique discussed here has advantages inaccessible to these other techniques. Use of the target ion spectroscopy technique may thus permit considerable improvement of the spectroscopic accuracy of conventional beam-foil measurements in the xuv/x-ray region on ions in high ionization-excitation states, and may also permit precision measurements of fundamental atomic quantities pertaining to highly ionized atoms (e.g., the Lamb shift) presently severely hampered by the Doppler spread problem.

Mass-Dependent Symmetric Collision Interactions in keV Energy Ne^{q+}-Ne Collisions

A second method of producing slow, multiply charged ions for use in spectroscopy or collision experiments in the molecular collision regime involves the use of a multiply charged ion source, such as the high power, Penning ion source facility located at the Oak Ridge Isochronous Cyclotron. Originally developed as a test facility for heavy ion cyclotron applications this source produces a beam of highly ionized ions (e.g., B^{4+}, C^{5+}, Ne^{6+}, Ar^{8+}, Fe^{12+}, . . .) by radial extraction of ions from a magnetically confined Penning discharge. The extraction power supply currently available coupled with electrostatic deflector plates and quadrupoles which serve to guide and focus the beam out of the magnetic field region permits preparation of beams of energy ∼ (4-36)q keV, with energy spreads ≤ ½ %. Beam current densities strongly vary with charge state, and range for example from ∼ 1nA of Ne^{5+} per mm² to tens of

microamperes per mm^2 of Ne^{2+} at divergences in the range 1-3 deg. A schematic diagram of the beam layout is shown in Fig. 4. Apparatus suitable for studying keV energy Ne^{q+}-Ne interactions under approximately single collision conditions is shown in Fig. 5, which is very similar to Fig. 1 except for the absence of an upstream stripping foil.

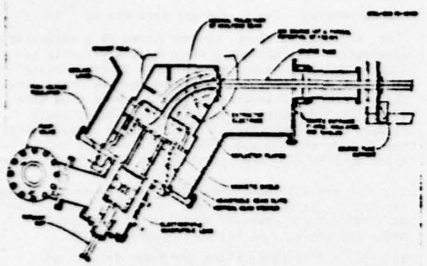

Fig. 4. Layout of the ORNL Penning ion source accelerator facilities for multiply charged ions.

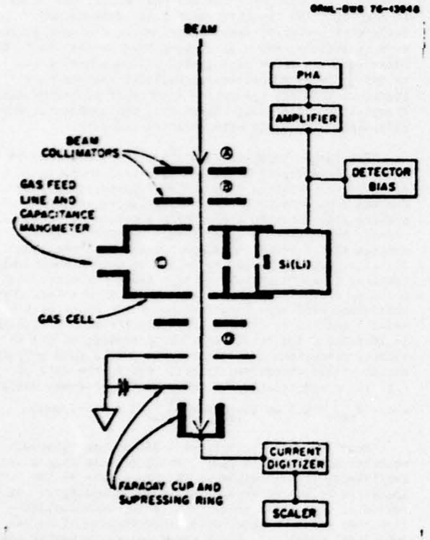

Fig. 5. Apparatus used by Peterson et al. (Refs. 4 and 5) for study of keV energy Ne^{q+} on Ne collisions.

A description of the production of NeK vacancies in symmetric collisions at keV energies (where the internuclear motion is slow compared to K electron velocities) is a principal concern of the Fano-Lichten model[17] of inner shell vacancy production cross sections in this molecular collision regime. In this regime NeK x-ray production in Ne^+-Ne collisions can be qualitatively explained in terms of this molecular promotion model. For two symmetric nuclei a distance R apart, molecular orbitals (MO's) and their energies can be calculated. As the distance R varies from infinity (separated atom limit) to R 0 (united atom limit) during the course of a close collision, these MO energy levels connect and correlate specific separated atom levels with specific united atom levels. Fig. 6 displays an example, for Ne-Ne collisions, kindly lent by J. S. Briggs. Fig. 7 displays a schematic diagram for a slightly asymmetric collision. As R changes, these

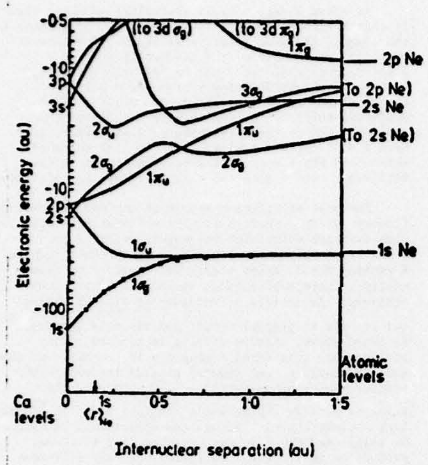

Fig. 6. Ne-Ne diabatic MO correlation diagram, provided by J. S. Briggs (private communication).

MO levels change their separation energies, may cross, *or may undergo pseudo-crossings. Couplings produce* transitions between them--for example, the so-called potential couplings produced by the screened Coulomb field of the nuclei, radial couplings involving transitions caused by changes in the radial internuclear motion, and rotational couplings involving transitions caused by changes in the relative internuclear angular momentum. For symmetric collisions gerade and ungerade reflection symmetry is also preseved in such collisions. Axial symmetry requires that the projection of angular momentum along the incident direction (σ, π, δ, ...) be adiabatically preserved. The speed of the internuclear motion (R) determines the degree of adiabatic behavior of electrons in the corresponding adiabatic MO's. So-called diabatic MO energy level descriptions[17] have been developed which account for deficiencies in the adiabatic approximation, which are especially

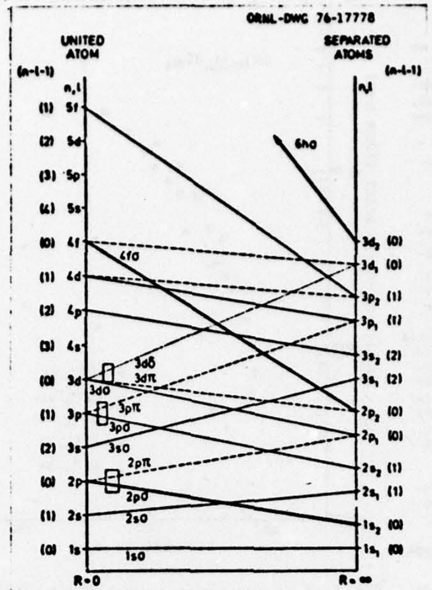

Fig. 7. Asymmetric diabatic MO correlation diagram, for Z_1 slightly greater than Z_2, provided by Q. Kessel (private communication).

serious near crossings (or pseudo-crossings) of molecular levels of the same symmetry. In conformity with standard practice we talk here only in terms of a one-electron version of the MO model, in which a single electron moves in the screened Coulomb fields of the heavy collision partners.

Earlier observations of K-vacancy production in Ne^+-Ne collisions were originally explained by Lichten[18] in terms of the rotational coupling of the $2p\sigma$ and $2p\pi$ MO's in Ne_2^+, starting with an initial neon 2p vacancy that happened to follow the $2p\pi$ MO as the collision approached small R, was transferred to the $2p\sigma$ level by rotational coupling, and thus ended up in the Ne 1s shell as the collision partners separated. *It is also possible for an initial 2p vacancy to* follow, for example, a $3d\sigma$ MO, in which case no $2p\pi$ vacancy will occur. Since the probability of forming a molecule with a $2p\pi$ vacancy is thus < 1, the electron promotion probability never reaches unity for any given impact parameter.

The first quantitative predictions of K vacancy production rates due to rotational coupling of this kind in Ne-Ne collisions were made by Briggs and Macek,[3] who scaled up the molecular energy levels of the H_2^+ molecule, and scaled the collision trajectories in D^+-D collisions (to simulate the same Z/A ratio as in the Ne-Ne case). For Ne^+-Ne collisions, the K-vacancy production rate for a given impact parameter was taken as the product of the probability that the initial 2p vacancy occupied the $2p\pi$ MO and the probability of rotational coupling of the $2p\sigma$ and $2p\pi$ MO's. Isotope effects in the trajectory scaling were considered negligible if the ratio of the nuclear charge to the reduced mass of the collision partners was near unity, and the screened nuclear change was a constant fraction of the bare nuclear charge. As we shall see, the first of these approximations is excellent provided the collision velocity is high enough, but fails badly near threshold, where the K-vacancy production cross section rises nearly vertically with projectile energy.

First we take up the question of the charge state (exit channel) effects. Lichten had predicted that K vacancy production in Ne^{q+} on Ne collisions should be proportional to the number of initial 2p vacancies N. Macek and Briggs[19] calculated the $2p\pi$ ($2p\pi_x$ in their notation) vacancy occupation probability to be N/6 for symmetric collisions and N/3 for asymmetric collisions. The N/6 factor results from statistical distribution of N vacancies over the six molecular orbitals originating in the separated atom 2p levels - $3d\sigma$, $4f\sigma$, two $3d\pi$ projections, and two $2p\pi$ projections (only the $2p\pi_x$ orbital permits K electron promotion). If the collisions were asymmetric, as in Fig. 7 (1 refers to the more strongly bound collision partner), the factor N/3 arises from the 3 MO's corresponding to the $2p_1$ level - one $3d\sigma$ and two $2p\pi$ projections.

A major question is whether Ne^{q+}-Ne collisions are truly symmetric or truly asymmetric. While the nuclear charges and masses of the collision partners may be equal, the energy levels of the more highly charged partner are lower, as in Fig. 7. The 2p level may thus be always associated with the projectile - increasingly so as q grows. Lichten had noted that the use of neutral molecular correlation diagrams might become a poor approximation for higher charge states of the incident ion. Calculations of correlation diagrams for Ne^{q+}-Ne collisions in which the initial charge asymmetry at R=∞ was an explicit boundary condition have very recently been made by Eichler and Wille,[20] who indeed found that the correlation diagrams do become progressively more asymmetric with N. Hence it is of interest to look for a q scaling which grows faster than N/6. This has been one of the goals of our recent experimental work on this subject.

Additional physical effects could complicate the naive picture sketched above. First, the neglect of charge exchange at large distances which would tend to symmetrize the initial charges of the collision partners has not been quantitatively considered, and may be extremely important. Second, Eichler and Wille have modified the rule of Barat and Lichten[21] for constructing diabatic molecular correlation diagrams, n_r (united atom) = n_r (separated atom), where n_r is the number of radial nodes of the wavefunction. The rule neglected certain avoided crossings which violate the rule by assuming such crossings would be very strongly avoided due to subshell splitting effects. The modified rule[20] changes the asymmetric correlation diagram such that the Ne2s level no longer correlates to the 2s united atom level but rather to the 3d level; in doing so it crosses the Ne2p level at large R. Any

mechanism which would permit 2s-2p vacancy transfer at large R would further disturb the initial charge asymmetry.

Because of these numerous unsettled questions, we undertook studies of the q dependence of K vacancy production in Ne^{q+} on Ne collision for q = 2-5, emphasizing the low beam energy region very near threshold, in which the K x-ray decay channel cross-section rises very nearly vertically with beam energy working at such energies serves to suppress additional dynamic complications which further alter the vacancy production rate.[22]

A very difficult experimental problem is caused by the relative sizes of the K x-ray production cross sections (~ 10^{-22} cm²) and the charge exchange cross-sections (~ 10^{-15} cm²). To maintain incident charge state purity, the Ne target must be maintained under approximately single collision conditions for charge exchange, implying pressures ≤ 1 mTorr and target lengths a few cm. The K x-ray data acquisition rates are then very low owing to the 6-7 order of magnitude difference in the cross-sections. Accordingly, these experiments require efficient nondispersive detectors having large solid angle, high beam currents which are difficult to achieve for high charge states, and long data runs. Source melt-down caused by driving the source hard has often been a problem in carrying out these experiments.

Earlier experiments on Ne-Ne collisions in Refs. 17 and 22 on the charge state dependence have tested q scaling for q = 0, 1, and 2. Good agreement with the Fano-Lichten prediction of vacancy production proportional to N was obtained for N=1 and 2. A large discrepancy[23] for N=0 ($Ne^0:Ne^+:Ne^{++}$ ~ 0.6:1:2) may have been caused by difficulties in preparing a ground state neutral Ne beam, as similar tests on other collision systems did not show this anomaly.

Very recently Hoogkamer et al.[24] have published studies of the q dependence in Ne^{q+}-Ne collisions up to q=4 and beam energies up to 1200 keV. The main difference between our experiments and theirs is our concentration on the threshold region (beam energies ~ 45 to 150 keV), thereby supposing additional dynamic effects,[22] and our extension to q=5. Our experiments do in fact give a K x-ray production cross-section which scales appreciably more strongly than N/6, as is clearly indicated in Fig. 8. Fig. 8 displays the measured Ne^{q+}-Ne K x-ray production cross section vs beam energy for q+ = 1,2,3,4, and 5. In Fig. 9 the ratio of the K x-ray production cross section for the q+ = 2,3,4,5 projectile charge states to that for q+ = 1 is plotted as a function of collision energy. In the strict Fano-Lichten description, the ratio data should be beam energy independent, and should correspond to horizontal straight lines at ratio values of 2,3,4, and 5, in the absence of changes in the K shell fluorescence yield ω_K. As is by now very well known[25] the fluorescence yields are charge state dependent. For a statistical distribution of multiplet states, the ratios $\omega_K(q+)/\omega_K(1+)$ go as 1:1.13:1.41:2.22:4.90 for q = 1,2,3,4,5. Accordingly one possible but not very plausible explanation for the ratio data of Fig. 9 is that the linear scaling in the Briggs-Macek description is correct, and that the balance of the $\sigma(q+)/\sigma(1+)$ values are to be attributed to changes in ω_K. This explanation would require $\omega(2+)/\omega(1+) \cong 1$,

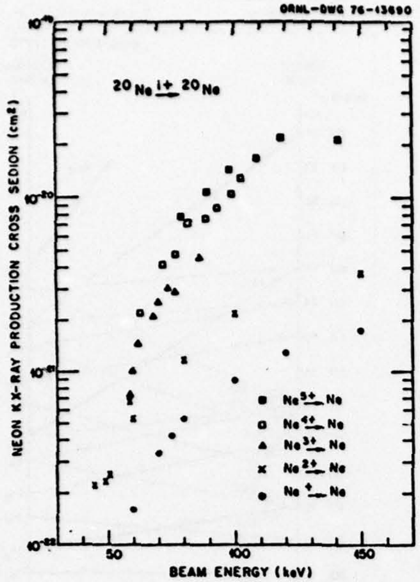

Fig. 8. K x-ray production cross-sections for Ne^{q+} on Ne collisions as a function of beam energy and charge state.

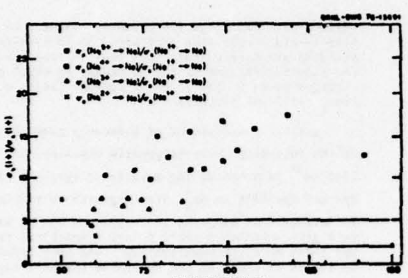

Fig. 9. Ratios of K x-ray production cross-sections for Ne^{q+} on Ne relative to Ne^+ on Ne as a function of beam energy.

$\omega(3+)/\omega(1+) \cong 2.4$, $\omega(4+)/\omega(1+) \cong 2.9$, and $\omega(5+)/\omega(1+) \cong 3.4$. While such ω ratios are within the range of ratio values permitted by the calculations of Chen and Crasemann, the final, post-collision charge state of

the x-ray emitting particle would need to be ≥ 4+ for incident charge q ≥ 3. Inasmuch as the collision energy range is such as to greatly favor electron capture as opposed to electron loss by the incident projectiles, this hypothesis is most unlikely. More likely are the possibilities that the n dependence is gradually changing from N/6 to N/3, or alternatively there is a nonlinear N dependence of $\sigma_K = f(n)\sigma_{ROT}$ beyond the linear term. Which of these alternatives is correct must await direct fluorescence yield measurements $\omega(q)$ as a function of q. When these fluorescence yields are made, the absolute K x-ray production cross sections indicated in Fig. 8 can be translated directly into K vacancy production cross sections.

I wish to return now to the question of the approximate mass dependence of the theory of Briggs and Macek,[3] relating vacancy production in Ne-Ne collisions to D^+-D collisions at an appropriately *scaled beam energy.*

As noted above, a basic approximation of the theory is that K-vacancy production in symmetric collisions is the same at the same relative velocity. The approximation is an example of the frequently applied principle one could call the "equal velocity rule," that for a given collision system where only the masses of the reactants differ, the results of an inelastic collision depend only on the Z's of the reactants and on their relative collision velocity v. Here Z sets the scale size of the Coulomb energies which bind the electrons making transitions in the collisions, and v sets the time scale of the collisions.

The most significant result of our mass dependence (isotope effect) studies is that while at sufficiently high relative velocities the "equal velocity rule" holds very well, for velocities near threshold (where K vacancy yield varies nearly vertically with beam energy), isotope effects as large as 40% have been observed! An article by Peterson et al. describing our results in greater *detail has recently appeared.*[4] As noted above, isotope effects in the trajectory scaling were considered negligible if the ratio of the nuclear charge to the reduced mass of the collision partners was near unity (i.e., $Z/M_r \cong 1$) and the screened nuclear charge was a constant fraction of the bare nuclear charge. Within the approximations used by Briggs and Macek it was expected that K-vacancy production in symmetric collisions between different isotopes of the same element *would be approximately* the same in collisions of the same relative velocity. The present experiments provide the first precise test of this prediction using K x-ray production as a measure of the K-vacancy production. For ${}^ANe^+$-${}^BNe$ collision velocities ≥ 1/2 au we have verified the accuracy of the equal velocity rule, but for velocities ≤ 1/3 au we find a 40% isotope effect in the K-vacancy production rate for equal relative velocities. It is surprising that such sensitive tests of mass dependence can be obtained from relatively simple total cross-section measurements. For $Z_A = Z_B$, and given internuclear separation, isotopic effects on energy levels of the Ne-Ne collision system and on corresponding electronic screening of the nuclei may be neglected. For equal relative velocities isotopic effects on fluorescent yields are also expected to be small. The dominant isotope effects are due to differences in internuclear trajectory, slight variations in which strongly influence the probability of rotational coupling near threshold. Such variations in beam trajectory are a strong function of reduced mass in the threshold region. For this region the cross-section for K x-ray production varies steeply with velocity *due to rapid variation in K-shell interpenetration.*

In the present experiments, Ne^+ beams of masses 20 and 22 from a 400 kV Cockroft-Walton accelerator were directed through a differentially pumped gas cell and collected in a properly biased Faraday cup, whose output was used for normalization, as is sketched in Fig. 5. A collimated lithium-drifted silicon detector counted the Ne K x-rays emitted at right angles to the beam direction. The target gas pressure of ^{20}Ne or ^{22}Ne, typically 3 mTorr, was monitored by a capacitance manometer. This manometer controlled a variable gas leak in order to maintain a constant target density. From such data absolute K x-ray production cross sections could be established, using K x-rays from p-Ne collisions to calibrate the efficiency-solid angle product of the detector. A ratio method of examining the isotope effects was devised to eliminate errors stemming from absolute cross-section measurement errors.

The results for K x-ray yield ratios as a function of relative velocity are shown in Fig. 10. The error bars reflect one standard deviation of the errors mentioned above. At velocities near threshold ($v^2_{rel}/2$ = 4 keV/amu) there are large deviations from simple relative velocity scaling. These deviations are larger for the collision systems with larger reduced masses and center-of-mass collision energies. In the approximation Z/M_r = 1, such an effect is not expected. For a given impact parameter, the available energy in the center of mass system determines the distance of closest approach. The possibility that the yield isotope effects could be accounted for by center-of-mass energy scaling was tested; the results are shown in Fig. 11. The symmetric-mass collisions do not scale with center-of-mass energy, while the asymmetric-mass collisions, shown as open squares in the inset, do scale with center-of-mass energy within experimental errors. The asymmetric-mass collision systems have identical relative velocities when their center-of-mass energies are identical. Therefore, the asymmetric-mass collisions also scale with relative velocity.

For large relative velocities the trajectory in the localized region of large rotational coupling is dominated by relative velocity as opposed to nuclear Coulomb repulsion terms. Hence, relative velocity scaling should become a good approximation at sufficiently high relative velocities. Physically this implies that a rectilinear approximation to the true classical trajectory in the region of strong rotational coupling is approximately valid. Since the rotational coupling of 2pσ - 2pπ molecular orbitals maximizes for collisions with impact parameters of the order of the K-shell radius, as the relative velocity of a collision is increased, the relative velocity scaling of the K-vacancy production cross section becomes a good approximation. This conclusion is borne out by the data of Fig. 10, where relative velocity scaling becomes valid above v_{rel} = 0.5 au ($E_{lab}/M = v^2_{rel}/2$ = 6 keV/amu).

Near threshold velocities ~ 1/3 au the relative velocity scaling fails badly, which implies that a rectilinear approximation to the trajectory in the localized region of strong rotational coupling is not adequate. For these velocities the nuclear Coulomb repulsion prevents penetration into regions of large rotational coupling. For a given impact parameter and relative velocity, the distance of closest approach is smallest for the collision system with the largest

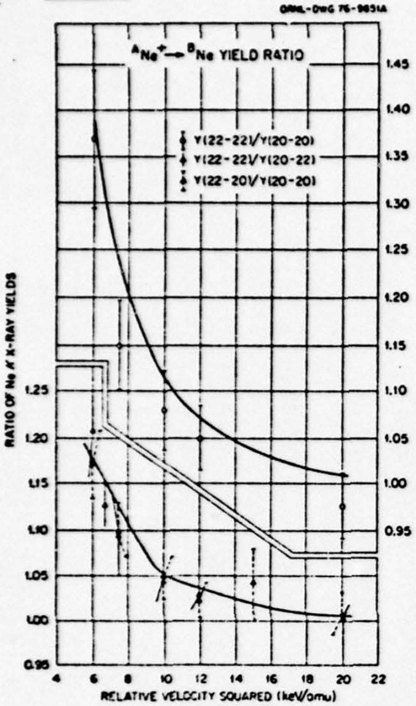

Fig. 10. Ratios of Ne K x-ray yields from $^{A}Ne^{+}$-^{B}Ne collision systems for A,B = 20,22 as a function of relative velocity. The Y(22-22)/Y(20-20) ratios are referenced to the right-hand axis and all other ratios to the left-hand axis. Error bars represent one standard deviation of errors discussed in the text.

center-of-mass energy (and hence with the largest reduced mass). Therefore, the trajectories of collision systems with larger center-of-mass energies will have a larger probability to penetrate into this region of large rotational coupling. These collision systems will have the larger probability to couple the $2p\sigma$ - $2p\pi$ molecular orbitals, which implies large K-vacancy cross-sections. For threshold velocities, the collision system with the largest center-of-mass energy has the largest x-ray yield, as is evident in Fig. 10. The results shown in Fig. 11 indicate that center-of-mass energy scaling is also invalid, even though the difference in distances of closest approach for systems of identical impact parameter and relative velocity is ~ 10%. Yet, the x-ray yields vary as much as 40%. A quantitative explanation of these large deviations from relative velocity scaling for threshold velocities must depend not only on distances of closest approach but also on the internuclear velocities at those distances. If the distance of closest approach did become

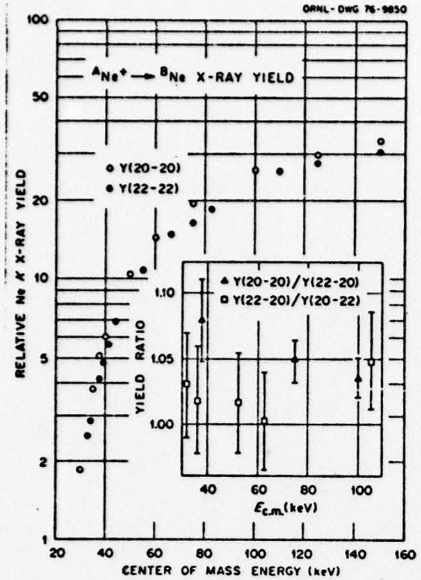

Fig. 11. Plot of Ne K x-ray yields from symmetric-mass collisions, $^{20}Ne^{+}$-^{20}Ne and $^{22}Ne^{+}$-^{22}Ne, as a function of center-of-mass energy. The inset is a plot of ratios of Ne K x-ray yields as a function of center-of-mass energy.

the dominant factor in K-vacancy production near threshold, the center-of-mass energy might be expected to become the valid scaling parameter. It is seen in Fig. 10 that for relative velocities greater than about 0.5 au that relative velocity scaling is good, but that near threshold velocities, neither the relative velocity nor the center-of-mass energy scalings are adequate.

Since completing the Ne^{+} on Ne experiments, Taulbjerg et al.[26] have kindly provided explicit calculation of the isotope effects we have observed for the collision system used in our experiment, based on a mass-dependent refinement of theory to be published in the very near future. The solid curves in Fig. 10 display the results of their mass-dependent treatment. This new mass-dependent treatment of vacancy production in asymmetric collisions by Taulbjerg et al. has thereby been experimentally demonstrated to be excellent. The demonstrated size of such isotope effects even in total cross-section measurements provides a promising experimental tool for use in studying other collision systems.

References

[1] J. R. Mowat, I. A. Sellin, D. J. Pegg, R. S. Peterson, J. R. MacDonald, and M. D. Brown, Phys. Rev. Lett. 30, 1289 (1973).

[2] I. A. Sellin, S. B. Elston, J. P. Forester, P. M. Griffin, K.-O. Groeneveld, D. J. Pegg, R. S. Peterson, R. S. Thoe, and C. R. Vane (to be published).

[3] J. S. Briggs and J. Macek, J. Phys. B5, 579 (1972).

[4] R. S. Peterson, S. B. Elston, I. A. Sellin, R. Laubert, F. K. Chen, and C. A. Peterson, Phys. Rev. Lett. 37, 984 (1976).

[5] R. S. Peterson, I. A. Sellin, S. B. Elston, H. Hayden, and R. S. Thoe (to be published).

[6] S. Bashkin, ed., Beam-Foil Spectroscopy, Vols. 1 and 2 (Gordon and Breach, New York, 1968).

[7] I. A. Sellin, Nucl. Inst. and Meth. 110, 477 (1973); I. A. Sellin, in Topics in Modern Physics: Beam-Foil Spectroscopy, S. Bashkin, ed. (Springer-Verlag, Heidelberg, 1976), Chap. 10.

[8] W. E. Lamb, Jr., private communication.

[9] C. Y. Fan, M. Garcia-Munoz, and I. A. Sellin, Phys. Rev. Lett. 15, 15 (1965).

[10] D. E. Murnick, in Beam-Foil Spectroscopy, Vol. 2, I. A. Sellin and D. J. Pegg, eds. (Plenum, New York, 1967), p. 815; H. W. Kugel, M. Leventhal, D. E. Murnick, C. K. N. Patel, and O. R. Wood, Phys. Rev. Lett. 35, 647 (1975).

[11] I. A. Sellin in Advances in Atomic and Molecular Physics, Vol. 12, D. R. Bates and B. Bederson, eds. (Academic Press, New York, 1976), p. 215.

[12] J. R. Mowat, I. A. Sellin, P. M. Griffin, D. J. Pegg, and R. S. Peterson, Phys. Rev. A9, 655 (1974).

[13] J. R. Mowat, I. A. Sellin, R. Laubert, R. L. Kauffman, M. D. Brown, J. R. MacDonald, and P. Richard, Phys. Rev. A10, 1446 (1974); D. L. Matthews, B. M. Johnson, J. J. Maclay, and C. F. Moore, Phys. Rev. Lett. 31, 1331 (1973); and D. L. Matthews, private communication.

[14] R. Mann, F. Folkmann, K.-O. Groeneveld, to be published (1976).

[15] J. A. Leavitt, J. W. Robson, and J. O. Stoner, Jr., Nucl. Inst. and Meth. 110, 423 (1973).

[16] J. O. Stoner, Jr., and I. Martinson, in Beam-Foil Spectroscopy: Vol. 1, Atomic Structure and Lifetimes, I. A. Sellin and D. J. Pegg, eds. (Plenum, New York, 1976), p. 259.

[17] For a comprehensive review plus numerous bibliographical references to the development of the Fano-Lichten model, see Q. C. Kessel and B. Fastrup, Case Studies in Atomic Physics 3, 139 (1973).

[18] W. Lichten, Phys. Rev. 164, 131 (1967).

[19] J. H. Macek and J. S. Briggs, J. Phys. B7, 1322 (1974).

[20] J. Eichler and U. Wille, in Abstracts of the Fifth International Conference on Atomic Physics, R. Marrus, M. H. Prior, and H. A. Shugart, eds. (Univ. of California, Berkeley, 1976), p. 62.

[21] M. Barat and W. Lichten, Phys. Rev. A6, 211 (1972).

[22] N. Stolterfoht (private communication, and to be published).

[23] B. Fastrup, G. Hermann, and Q. C. Kessel, Phys. Rev. Lett. 27, 71; 1102 (1971).

[24] Th. P. Hoogkamer, P. Woerlee, S. Doorn, F. W. Saris, and H. Tawara, in Abstracts of the Second International Conference on Inner Shell Ionization Phenomena (Univ. of Freiburg, Freiburg, 1976), p. 50.

[25] M. Chen and B. Crasemann, Phys. Rev A12, 959 (1975).

[26] K. Taulbjerg, J. S. Briggs, and J. Vaaben (to be published).

(Submitted to Physical Review A)

CHARGE DEPENDENCE OF K X-RAY PRODUCTION IN NEARLY SYMMETRIC COLLISIONS OF HIGHLY IONIZED S AND Cℓ IONS IN GASES*

J. R. Macdonald, M. D. Brown,+ S. J. Czuchlewski,++ and L. M. Winters+++

Kansas State University, Manhattan, Kansas 66506

and

R. Laubert,# I. A. Sellin, and J. R. Mowat##

University of Tennessee, Knoxville, Tennessee 37916 and

Oak Ridge National Laboratory, Oak Ridge, Tennessee 37830

*Research supported in part by U. S. Energy Research and Development Administration Contract E(11-1)-2753 and ONR; the experiment was carried out at the BNL Tandem Accelerator Laboratory.

+Present Address: Naval Surface Weapons Ctr-223, White Oak, Silver Springs, Maryland 20910.

++Present Address: LASL-Laser Group L1, P. O. Box 1663, Los Alamos New Mexico 87544.

+++Present Address: Dept. of Physics, East Carolina University, Greenville, North Carolina 27834.

#Present Address: Dept. of Physics, New York University, New York, N. Y. 10003.

##Present Address: Dept. of Physics, City College CUNY, New York, N. Y. 10031.

ABSTRACT

Using gas targets K x-ray cross sections have been measured as a function of projectile charge state in nearly symmetric collisions for highly ionized S and Cℓ ions at a velocity comparable to that of the K-shell electrons. For bare nuclei, the projectile cross sections are accurately described by the cross section for capture to excited states calculated in a Brinkman-Kramers approximation and normalized by a single scaling factor. With lower charge state incident ions, the total K-vacancy cross section is in good agreement with the $2p\pi - 2p\sigma$ cross section for rotational coupling.

I. INTRODUCTION

It is well established that the cross section for production of x rays in energetic ion-atom collisions shows a strong monotonic increase with the charge state of the incident projectile,[1] and mechanisms responsible for the phenomenon have been discussed qualitatively. For example, multiple vacancies produced in inner (as well as outer shells) have been shown to depend on projectile configuration giving rise to significant changes in the mean fluorescence yield of ion-excited atoms.[2] In other cases, variations in atomic structure cannot fully account for the charge state dependence but variations in inner-shell vacancy production must also occur.[3] If the mechanism for ionization in a fast collision is predominantly direct Coulomb ionization, one can include variations in nuclear screening or electron binding energy in an explanation of the projectile charge dependence of vacancy production.[4] Estimates of the contribution of electron capture processes[5] have shown that this mechanism can account for the charge dependent trends of vacancy production. For relatively slow collisions, the promotion of inner-shell electrons by the coupling of molecular states[6] has been used to describe successfully the dependence of vacancy production on projectile charge state.

In experimental work that has been reported to date, the measurements of projectile charge dependence have pertained either to asymmetric projectile-target combinations at high energy [>1 MeV/amu][1] or to nearly symmetric collisions at lower energy [<100 keV/amu].[6] In this paper, measurements of the charge dependence of x-ray production cross sections are reported for approximately symmetric collision systems at high energy.

It is obvious that the projectile K x radiation from incident bare nuclei results from electron capture to excited states. For these incident ions the contribution of electron capture of target K electrons is expected to make a significant contribution as well to the target K-vacancy production cross section.[7] The charge dependence of the target x-ray cross sections measured in this work are discussed within this framework. For lower charge state incident ions, the measured cross sections, of both projectile and target K x rays are examined in terms of K vacancy sharing and theoretical cross sections for electron promotion by rotational coupling of molecular states.[8]

II. EXPERIMENTAL METHODS

For this experiment chlorine and sulphur beams of the same velocity (3.77 MeV/amu) and a chlorine beam of lower velocity (3.0 MeV/amu) from the MP tandem Van de Graaff accelerator at Brookhaven National Lab were employed. Following stripping of each momentum-analyzed beam in a thin carbon foil, single incident charge states were magnetically selected and focussed through a thin gas target. The double-differentially-pumped gas cell apparatus that was transported under vacuum from KSU to BNL has been described in detail previously.[9] The target gases used were Ne, SiH_4, H_2S, HCℓ, and Ar. Target and projectile K x rays were counted in a Si(Li) x-ray detector which was mounted within the gas cell so that its field of view did not encompass the target apertures. The detector resolution was 190 eV at 5.9 keV and 174 eV at 2.3 keV. The energy response was calibrated both with standard sources and by proton bombardment of the target gases. Below the peak of an x-ray line, the spectral distribution consisted of a decreasing tail that contained $16 \pm 2\%$ of the line intensity for x rays in the range from 1.7 to 3.0 keV. It was necessary to consider this contribution carefully in obtaining the relative intensities of the target and projectile x rays produced in the nearly symmetric collisions of this experiment.

The low energy spectral tail results from incomplete charge collection in the edges of the detector and the fraction of the peak is constant for x rays from Si K to Ar K. In order to extract the data from the heavy-ion spectra, the response to a single line was investigated in a separate experiment for the spectra produced by proton bombardment of the target gases. A one parameter fitting function composed of a

Gaussian peak with variable width and a straight line tail decreasing from 8% of the peak maximum to zero at the detector noise level was found to give a satisfactory analytic fit to these simple spectra.

With each of the target gases, x-ray spectra were taken at two pressures (approximately 10 and 20 milliTorr) with 3.77 MeV/amu chlorine and sulphur ions incident as bare nuclei, one-, two-, and three-electron ions. Additional spectra were taken with lower charge state S ions and with 3.0 MeV/amu Cℓ ions in all available charge states in SiH_4. The spectra obtained for the various collision systems differ markedly and several examples are shown in Fig. 1. Background spectra were obtained with only residual gas (<0.1 milliTorr) in the cell for each incident ion, and this small contribution was subtracted from each spectrum prior to analysis. For all charge states of S and Cℓ ions incident on Ne and SiH_4 gases, and in some cases with the other gases, the detector resolution was sufficient to use peak-fitting programs[10] to extract peak centroid energies, widths, and relative intensities from each spectrum independently.

Initial fitting of the data at BNL was attempted using a Gaussian fitting routine and treating the low energy tail as a background. For well-separated peaks, such as seen in the upper two spectra of Fig. 1 (for $Cℓ^{+17}$ and $Cℓ^{+14}$ on SiH_4), this was satisfactory as long as the relative intensities were normalized to the total number of x rays in the spectrum. For close peaks, even if well-resolved as in the sixth spectrum in Fig. 1 (for $Cℓ^{+14}$ on H_2S), this was unsatisfactory, giving even relative errors in excess of 25%. Hence, the data was reanalyzed at KSU using a program containing the proper spectral response for each peak. The program converged on three peaks in the spectrum as long as either of the following conditions was met.

The smaller peaks were resolved down to half maximum, as seen in Fig. 1 in the third (for S^{+16} on SiH_4) and the sixth spectrum (for $C\ell^{+14}$ on H_2S). Or, poorly resolved peaks were in order of decreasing intensity with increasing channel number as seen in Fig. 1 for the highest peak in the second spectrum (for S^{+14} on SiH_4) and for all the peaks in the fifth spectrum (for $C\ell^{+14}$ on Ar). For other cases, portions of the spectra did not converge in the fitting program to give separate peaks. For example the program was not adequate to resolve the small, low energy shoulder, arising from target x rays, from the main peak seen in the fourth spectrum of Fig. 4 (for S^{+16} on H_2S). Nor could two peaks be fit to the upper portion of the first spectrum in Fig. 1 (for S^{+14} on Ar). For these and similar cases, some assumptions were required to retrieve all the information from the spectra.

In all cases where the spectra were resolvable the distribution of projectile x rays was found to be independent of target gas for each projectile charge state. To retrieve relative intensity information from partially resolved features in the spectra obtained with H_2S, $HC\ell$, and Ar target gases, this target independence was applied as a general constraint in the analysis. With this assumption, the projectile x-ray distribution and the background distribution for each incident charge state are obtained over the entire spectral range of the detector by forming a composite from the well-resolved portions of the spectra taken with different targets. These distributions were used in a spectral-stripping procedure[11] to extract systematically the relative intensity and distribution of target K x rays produced in the nearly symmetric collisions. In all cases, the distribution obtained with this procedure was a single group of target K x rays.

The possibility of error in the relative intensity of x rays extracted by the peak-stripping technique varies greatly from one collision system to another, and this is reflected in the difference in the uncertainty of the individual cross sections presented in the next section. The centroid energy for the target x-ray group could be determined in some cases but with greater uncertainty than for the projectile groups. For $C\ell$ in $HC\ell$, and S in H_2S, the separation into projectile and target components was possible only because of the presence of a significant resolved $K\beta$ component from projectiles but not for target atoms. The dominance of the projectile radiation over that from the target permitted an accurate determination of the former but resulted in an uncertainty of 30 - 40% in the latter.

Cross sections for x-ray production were determined by normalizing the relative intensities obtained in the spectral analysis to the total number of x rays. Absorption in the 0.025 cm Be window separating the detector from the gas cell introduces a detection efficiency[12] that varies from 0.56 for 1.74 keV Si K x rays to 0.86 for 2.96 keV Ar K x rays. Values of efficiency, accurate to a few percent, were chosen corresponding to the centroid energy for the Si, S, $C\ell$, and Ar K x-ray groups identified in this experiment. A large relative, as well as absolute, uncertainty in the approximately 2.5% efficiency for Ne K x rays, precludes the determination of accurate Ne K x-ray cross sections for this target.

A capacitance manometer was used to monitor the gas target pressure and provided normalization of the target density with a relative precision of 1% and with an absolute uncertainty of 10%. Beam current

normalization was achieved by integrating the total charge collected in a large, suppressed, Faraday cup in the high vacuum region behind the target. Complete transmission through the cell was ensured by geometrical considerations and was confirmed by the measurement of current collected in a removable Faraday cup inside the cell and on the insulated exit apertures of the apparatus.

In the conversion of current normalization to particle normalization, estimates of the effect of charge exchange[13] in the cell were included. In all cases, less than 10% of the beam undergoes charge exchange in the target. For most charge states, beam current in excess of 0.2 na could be obtained through the gas cell. The total uncertainty in particle normalization was less than 5% in these cases. For the highest charge states less beam was obtained and a surface barrier detector replaced the Faraday cup for beam normalization. With this technique the useable beam was limited by the particle counting rate so that statistical uncertainties limited the accuracy of x-ray yields obtained in a reasonable amount of time. In some cases, yields were measured with both methods of normalization and the results agreed within 8%, comparable to the statistical uncertainty obtained with normalization by single particle counting.

The apparatus geometrical factor required to obtain absolute cross sections from the normalized yields was determined by measuring the yield of Ar K x rays produced by 3.77 MeV protons. This yield was normalized to the cross section of $8.0 \pm 0.6 \times 10^{-22}$ cm^2 measured for this radiation in a separate experiment.[14] The absolute uncertainty in the measured cross sections is limited to 8% by this normalization but it makes the results independent of the absolute calibration of the beam integrator, and pressu-

normalization. The relative uncertainty in the cross sections is determined by the spectral analysis, detector efficiency, dead time corrections, corrections for beam transmission through the target, charge exchange in the target, and statistics in some cases. The total uncertainty in the cross sections reported in the next section was obtained by adding the absolute and relative uncertainties in quadrature.

III. RESULTS AND DISCUSSION

A. General Trends of X-ray Cross Sections

In this experiment, the K x rays emitted by the projectiles form the dominant spectral features when the incident ions carry K-shell vacancies into the collision. For lower charge states the total cross sections are reduced by more than an order of magnitude and K radiation from the target is of comparable intensity to that from the projectile. This overall charge state dependence is evident in Fig. 2 in which the K x-ray cross sections for Cℓ incident on SiH_4 at 3.0 and 3.77 MeV/amu are shown for ions carrying n electrons into the collisions. For clarity in the figure, data points for the same incident state are displaced when projectile and target cross sections overlap. The trends of these cross sections are typical of all those measured in this experiment, hence a general discussion of the results will be given before all the results are presented in detail.

The Cℓ K x-ray cross sections for n = 0 and 1, shown in Fig. 2, are almost a factor of two lower for the lower energy than the higher energy collisions while the Si K cross sections are about 10% lower. Such a decrease with energy is characteristic of the general trend of high velocity electron capture cross sections. For example, the energy dependence of the capture cross section to excited states calculated in a Brinkman-Kramers calculation[15] for Cℓ nuclei incident on Si is shown in Fig. 3 by the solid line. Projectile x-ray cross sections from this experiment are also shown in the figure. The calculated cross section has been reduced by an order of magnitude for normalization purposes but reproduces the

general trend of the experimental data.

It is expected that capture is the mechanism for x-ray production for projectiles carrying K vacancies into the collision. However, the observation that the energy dependence for the target cross section is in the same direction to that of the projectile cross section is evidence for a contribution of K-shell capture to the target vacancy production.

When a second electron is present on the incident ion, the projectile cross section is reduced by approximately an order of magnitude but is still a factor of two larger than the cross section with three electron ions. Since it is reasonable to expect a substantial component of $^3S_1$ metastable ions in these incident two-electron beams, with this ion, the observed x rays result from a combination of $^3S_1$ to $^3P_1$ excitation in the collisions as well as inner-shell excitation or ionization concurrent with outer-shell electron capture. These effects will be discussed further in the B part of this section of the paper.

For the ions entering the collision with full K shells, $n > 2$, the cross sections shown in Fig. 2 are comparable for the target and projectile and show no energy dependence. The collision velocities of the experiment match the mean velocity of the K-shell electrons and hence we anticipate that the observed cross sections are near the peak of the excitation function. These cross sections also show a gradual decrease with increasing n. This may reflect a decrease in final state fluorescence yield or a reduction in the K-vacancy production cross section with the addition of L-shell electrons to the projectile.

Results obtained with the other target gases and with sulphur ions show a charge dependence similar to those shown for Cℓ → SiH_4 in Fig. 2

In part B of this section the quantitative results will be discussed for the projectile radiation, and in part C for the target radiation.

B. Projectile K X-Ray Energies and Cross Sections

With the detector resolution of 180 eV the K x rays emitted by the projectiles are separated into two resolvable groups. Even for the thin gas targets used, the lower energy $K\alpha$ group represents several satellite lines making the observed FWHM of this peak range from 260 to 300 eV. The FWHM of the higher energy group ranged from 460 to 520 eV and the designation $K\beta$ is nominal; transitions from higher shells make contributions to the peak also.

Centroid energies for the $K\alpha$ and $K\beta$ projectile groups were obtained with a precision of 9 eV and 27 eV, respectively, from the analysis of the spectra. For a specific incident charge state ion, the centroid energy (and the width) of the $K\alpha$ and $K\beta$ groups, as well as the $K\beta$ to $K\alpha$ intensity ratio, were independent of the target within the precision of the measurements. These parameters were also the same for the two different energy chlorine ions. Values of $K\alpha$ and $K\beta$ centroid energies, averaged for all targets, obtained for incident ions carrying n electrons, are shown in Fig. 4. For comparison, allowed $2p \rightarrow 1s$ transitions[16] for one-, two-, and three-electron sulphur and chlorine ions are shown in the figure as the horizontal lines beside the data points representing the observed $K\alpha$ energies. Similarly, estimates of $3p \rightarrow 1s$ transitions[17] with various numbers of electrons on the ions are shown in the figure.

With incident bare nuclei, $n = 0$, projectile x rays signal the decay of the excited states formed by electron capture. The $K\alpha$ energies, shown in Fig. 4, for this incident state correspond to Lyman α transitions in hydrogen-like ions, and the $K\beta$ centroids are comparable to the Lyman β energy. For the other incident states, the $K\alpha$ centroid is independent of the charge state, at an energy corresponding to $2p \rightarrow 1s$ transitions in helium-like or lithium-like ions. In contrast, there is a monotonic decrease in centroid energy of the $K\beta$ group with additional electrons present on the incident projectile. A similar monotonic decrease is observed in the charge dependence of the $K\beta$ to $K\alpha$ intensity ratio shown in Fig. 5. These features are the same with both S and Cℓ ions incident on all of the targets.

The observation of the $K\beta$ radiation for all incident charge states, initially without M electrons, is indicative of the importance of electron capture to excited states of these highly ionized projectiles. This conclusion is confirmed by the results of calculations, in the Brinkman-Kramers approximation,[15] which show that the dominant capture processes are to projectile excited states. As an illustration of the trend of these calculations, cross sections for capture to projectile states with a given principal quantum number from a particular target shell are shown in Fig. 6 for the case of 3.77 MeV/amu chlorine ions in collision with argon. Results obtained for other projectile-target combinations differ in detail but have the same general trends to those shown in the figure.

Although these calculated results pertain to projectiles with $n = 0$, the presence of inner-shell electrons on the incident ion will screen the nuclear charge and reduce the cross section for capture to excited

states, as calculated in a BK approximation. For the collision systems of this experiment the reduction is small and there is a large probability of capture to outer shells in collisions which produce K vacancies in the lower charge incident ions ($n \geq 2$). Radiative decay of these captured electrons to the ground state is in competition with the filling of K vacancies by the L-shell electrons present on the projectile. The mode of decay of the projectile K-shell vacancies depends sensitively on the L and higher shell populations, and the sharp reduction in Kβ/Kα ratio with increasing n may reflect an increase in K-LL and K-LM Auger decay at the expense of K-M radiative decay. The constancy of the Kα energy for the lower charge state incident ions shows that the stripping of L-shell electrons in these collisions also plays a role and that normally only one or two L-shell electrons are present during the radiative process.

Total cross sections for the production of K x rays from the highly ionized Cℓ and S projectiles of this experiment are listed in Table I. The measured values represent the cross section for collisions with the heavy atoms in the target molecules since the presence of the hydrogen atoms makes a negligible contribution to the total projectile cross section. For example, for low charge state S and Cℓ ions, the x-ray cross section caused by collisions with hydrogen at 3.77 MeV/amu will be comparable to the K x-ray cross section for S and Cℓ excited by 3.77 MeV protons. These cross sections were measured to be 980 and 940 barns, respectively, in conjunction with this experiment. This amounts to a contribution of less than 0.5% of the total projectile cross section. In addition, for incident bare nuclei, the electron capture cross section to excited states of Cℓ or S from hydrogen is calculated to be only 10^{-3} of that from Ne, Si, S, Cℓ, or Ar atoms.[15]

Hence with all charge states we can consider the hydrogen atoms as spectators to the interaction with the heavier atoms in the target.

The trends of cross sections for incident projectiles carrying n electrons are shown in Fig. 7 as a function of the target atomic number. For incident bare nuclei, $n = 0$, the largest x-ray cross sections observed in this experiment are a measure of the cross section for electron capture to excited states, reduced by a factor $f \leq 1$, to account for the fraction of the transitions that do not yield K x rays but lead to 2s final states by either direct capture or cascading. In principle, the factor f can be determined if a complete distribution of angular momentum states populated by electron capture is calculated and then known branching ratios are used to calculate f. In the absence of a theoretical formulation other than the Brinkman-Kramers approximation for calculating these cross sections, such detail is not warranted. In fact, it is well known that a Brinkman-Kramers calculation reproduces the relative trends of cross sections, but grossly overestimates the magnitude of electron capture cross sections by a factor g, that may be a function of velocity and be different for different systems. Hence we can represent the projectile x-ray cross section, σ^0_{px}, by

$$\sigma^0_{px} = fg\,\sigma_{BK}^{*} \qquad (1)$$

where σ_{BK}^{*} is the summation of the Brinkman-Kramers cross section from all shells to all excited states of the projectile. At present, there is no theoretical guidance[18] on how to estimate g. In previous work with fluorine ions, Brown et al.[19] have empirically determined this factor in the range $0.06 \leq g \leq 0.10$ by normalizing the results of a BK calculation to measured total electron capture cross sections. With this normalization a value

f = 0.81 was obtained for the fraction of capture to excited states that result in x-ray decay. Hopkins et al.[7] have normalized x-ray cross section to σ_{BK}^* and have found fg = 0.07 for Cℓ on Kr collisions. For the present set of data with S and Cℓ bare nuclei, each calculated value of σ_{BK}^* was normalized to σ_{px}^0 and a mean value $\langle fg \rangle = 0.098 \pm 0.0005$ was obtained. In Fig. 8 an excellent fit to the σ_{px}^0 data points for the different targets is shown by the broken lines which connect the calculated values of σ_{BK}^* normalized by the single parameter $\langle fg \rangle$. Clearly, the factor of three variation for the electron capture to excited states in these nearly symmetric collisions is accurately reproduced by the calculation. As was shown in Fig. 3, the overall energy dependence of the cross section is reproduced by σ_{BK}^* using the same scaling parameter. The 5% error quoted on the scaling parameter $\langle fg \rangle$ is the standard deviation of the mean of the distribution of the set of fg values and shows that this single factor gives an accurate scaling of the Brinkman-Kramers cross section for these symmetric collision systems. However, this value is 30% larger than that reported for the more asymmetric collisions of Cℓ on Kr.[7]

As discussed previously in the A part of this section, it is quite clear that electron capture to excited states determines the cross section for the one-electron incident ions as well as the bare projectiles. Consistent with this conclusion is the similarity in the target dependence for incident states with n = 0 and 1 apparent in Fig. 7. The experimental cross sections for n = 1 are smaller than those for n = 0 by a factor that averages 2.4 ± 0.1 for this set of data. This factor is in close agreement with results reported for fluorine x-ray cross sections[19] but is considerably smaller than results reported previously for chlorine projectiles.[20] Qualitatively, a factor of 2 reduction can be estimated by assuming a statistical

population of spin states when helium-like P states are formed by electron capture. Then, the six metastable triplet substates $(\Sigma_m {}^3P_{2,0})$ do not decay within the field of view of the detector, while the observed x rays are from the decay of the six short-lived substates $(\Sigma_m {}^{1,3}P_1)$. Since this estimate neglects the metastable S states of both hydrogen-like and helium-like ions, as well as the charge dependence of electron capture, non-statistical populations, and the effects of cascading, it is not definitive but is consistent with the observations of this experiment.

With incident ions carrying two or more electrons into the nearly symmetric collisions with the heavier targets, the projectile cross sections are independent of target atomic number, but for chlorine ions are systematically lower than those for sulphur ions by 18%. In collisions with neon, the cross sections are reduced by 10 to 30% so that the values for both ions are comparable. In all cases, the two-electron ion gives a cross section a factor of two larger than the three-electron ion. As discussed previously, this can be attributed to the large cross sections for capture and excitation of a small $^3S_1$ metastable component that brings K vacancies into the collisions. For example, if we assume that the metastable state has a cross section for x-ray production comparable to that for n = 1 ions, then a 5% metastable fraction gives rise to a factor of two increase in the x-ray yield if the ground state has a cross section comparable to that for the n = 3 ions. Excitation of the metastable $^3S_1$ component to the $^3P_1$ state would contribute to the observed Kα radiation but not to the Kβ peak. The small, but real, decrease in the observed Kβ/Kα intensity ratio for two-electron ions compared to three-electron ions that is evident in Fig. 5 is evidence for metastable excitation.

A further reduction to about 60% of the value for n = 3 ions occurs in the sulphur cross sections when three additional electrons are present on the incident ion. This reduction is caused by the decreasing fluorescence yield of the K-vacancy state with extra electrons present on the ion. The mean fluorescence yield for these ions[21] is very sensitive to the presence of the last two or three L-shell electrons. Since the $K\alpha$ centroid energies shown in Fig. 4 indicate few L-shell electrons present at the time of emission of $K\alpha$ radiation, the bulk of this radiation arises when L-shell stripping is concurrent with K-vacancy production. However, the state is more likely to Auger decay if the L shell remains intact. The $K\beta$ energy, indicating four L electrons present, suggests that the latter event is more probable. Of course, the Auger decay also competes with the $K\beta$ emission making the $K\beta$ to $K\alpha$ ratio continue to fall as seen in Fig. 5 as additional electrons are present on the ion. Because of the difficulty in assessing the fluorescence yield to be used for these ions, any discussion of the processes governing the magnitude of the cross section will be deferred to the discussion of the target cross sections in the next part of this section.

C. Target K X-Ray Energies and Cross Sections

The dominance of the projectile radiation (particularly for high charge states), as well as the limited resolution of the detector, make the determination of the spectral distribution of the K x rays from the target atoms rather uncertain in this experiment. In the data analysis, only single target x-ray groups were identified and centroid energies and intensities were obtained with the use of the data-stripping procedure[11] that removed a normalized spectrum for the projectile radiation from

unresolved spectra. The uncertainty in the centroid energies was ~ 10 eV for Si K, ~ 20 eV for S K excited by Cl ions, ~ 50 eV for Ar K excited by S ions, and greater than this for the other cases. The different targets showed a similar trend in the charge dependence of the centroid energies and as an example the results for Si K are shown in Fig. 9. Estimates of the $2p \rightarrow 1s$ transition energy[22] for silicon ions with a single K vacancy but with various numbers of additional L-shell electrons are shown as the horizontal lines on the figure. Spectator electrons in M or higher shells will not change these energies greatly. Significant multiple L-shell ionization of the target occurs along with K-vacancy production in these violent collisions and in general one or two more electrons are removed by Cl ions than by S ions. Also, on the average one or two more electrons are removed by incident bare nuclei of either ion than by the lower charge states.

Total cross sections for the production of target K x rays by the highly ionized Cl and S projectiles of this experiment are listed in Table II. Trends of the results taken at 3.77 MeV/amu excitation by incident bare nuclei, one-, and three-electron ions are illustrated in Fig. 10. Date for the other incident charge states are comparable to that taken with incident three-electron ions and are omitted from the figure for clarity. To guide the eye, broken lines join the points taken with each incident charge state. The absolute uncertainty on each cross section is given in the table and shown by the error bars in the figure. These uncertainties are dominated by the contribution from the spectral analysis.

In the interpretation of these cross sections, the importance of electron capture of target K-shell electrons, predominantly to the projectile K shell, accounts for the large target cross sections observed with incident bare nuclei (n = 0). However, the mean fluorescence yield that governs the

decay of these highly ionized target atoms depends critically on the unknown configuration of the remaining L-shell electrons.

In the interpretation of the dependence of the target x-ray cross sections on the projectile charge state, the variation of the mean fluorescence yield, $\langle\omega_t\rangle$, of the emitting atoms must be considered. The factor of four increase in cross section that is uniformly observed with the K radiation from all the targets for excitation by bare nuclei over three electron ions, is unlikely to be caused entirely by variations in $\langle\omega_t\rangle$, for these atoms that have neutral atom fluorescence yields that vary only a small amount with the removal of the first four L electrons and by a factor of four only when the L shell is reduced to two electrons.[21] In fact similar conclusions[3] for Ar K radiation excited by F ions have been confirmed by measurements of Auger cross sections.[23] The observed Kα energies indicate that the difference in degree of ionization for excitation by Cℓ and S ions is at least as large as the charge dependent variation. Since the charge dependence in the target x-ray cross sections is similar in the two cases, we conclude that variations in $\langle\omega_t\rangle$ do not dominate the charge dependence, although a gradual variation with charge state may occur, and a value of $\langle\omega_t\rangle$ up to double the neutral atom value may occur even for the low charge state ions.

In the interpretation of the mechanisms that produce the cross section variations, both for the target and for the low charge projectiles, this uncertainty in the fluorescence yield restricts the comparison with theoretical models to general trends. The importance of electron capture of target K-shell electrons accounts for the large target cross sections observed with incident bare nuclei ($n = 0$). However, the trend with target atomic number, seen in Fig. 10, for these cross sections is in opposite directions with Cℓ and S ions. When reasonable estimates of fluorescence yields are considered, the trend with Cℓ ions cannot be described by the

universal scaling of calculated BK capture cross sections, that is successful for all the projectile radiation. For example, if the target K x-ray cross section, σ^0_{tx}, is assumed to originate entirely from K-shell capture with a calculated cross section σ^K_{BK} (assumed to scale in the same way as the projectile cross section σ^0_{px} in equation 1), then the mean fluorescence yield of the target states can be derived as

$$\langle\omega_t\rangle_D = f\,\sigma^0_{tx}\,\sigma^*_{BK} / \sigma^0_{px}\,\sigma^K_{BK} = f\,\sigma^0_{tx} / \langle f_g\rangle\,\sigma^K_{BK} \quad . \qquad (2)$$

where the factor $f \approx 0.8$ accounts for capture and cascading that leads to the projectile 2s state.[19]

For capture by sulphur nuclei, the derived fluorescence yields are about double the neutral atom values, qualitatively consistent with expectations for these highly ionized target atoms. Although the same value is derived for Si for capture by Cℓ values comparable to neutral atom fluorescence yields are obtained for S, Cℓ, and Ar. In fact, the observation of the x-ray energies for the target radiation, as illustrated for Si in Fig. 9, indicates that if any variation exists there should be a higher fluorescence yield for excitation by Cℓ than for S. We are led to the conclusion that assumptions inherent in equation 2 are invalid for these nearly symmetric collisions, even though they have proven valid in previous work with asymmetric collision systems.[1,7,19] The ratio of σ^K_{BK} to σ^*_{BK} ranges from 45% (S on Si) to 18% (Cℓ on Ar) for these collision systems, but amounts to only a few percent in previous work. This strong variation sensitively tests the assumption in equation 2 that the same scaling of the magnitude of Brinkman-Kramers cross sections applies to all target shells for each projectile. The data

indicates that this is invalid in these nearly symmetric collisions, and accurate fluorescence yields cannot be obtained with equation 2. However, with an accuracy of about a factor of two, this scaling of σ_{BK}^{K} accounts for the absolute target cross sections.

Target x-ray cross sections produced by incident one-electron ions are reduced on the average by a factor of 2.2 from the corresponding cross sections produced by bare nuclei. This reduction is comparable to that for the projectile cross sections for these ions. Although the close agreement is surprising, it is somewhat accidental since the projectile data is influenced by the capture of L electrons to excited states, while the target data is influenced by K-shell transfer. Of course, the mean fluorescence yield for target states excited by one-electron ions may also be lower than for the excitation by bare nuclei.

It is interesting to note that a factor of two reduction in the target cross section with one-electron incident ions is predicted using a molecular model for the K-vacancy sharing[24] by radial coupling between $1s\sigma$ and $2p\sigma$ orbitals. This model has been exploited by Meyerhof[24] to explain vacancy production in a heavier collision partner using initial conditions that have a vacancy in the $2p\sigma$ orbital. If the initial vacancy is in the $1s\sigma$ orbital, however, the model provides an alternative to Born approximation calculations of electron transfer from target K shells by incident projectiles containing K vacancies. The occupation of the $1s\sigma$ orbital corresponds to the K-shell electrons in the highly ionized incident projectiles and the transition probability for the $2p\sigma$ electrons from the target K shell will be large in these symmetric collisions giving a sharing probability $W = 1/2$. The target cross section is proportional to the initial $1s\sigma$ occupation

number and hence this model gives a factor of two reduction for incident one-electron ions. The absolute cross section for this mechanism is also proportional to πr_o^2 where r_o is the effective range at which the radial coupling matrix element is large. Detailed investigations of this aspect of the model have not been carried out although the observed cross sections can be accounted for by setting r_o equal to $\sim$ double the target K-shell radius.

For lower charge state incident ions, the target cross sections are about 25% of those for incident bare nuclei. Although K-shell capture is reduced for these systems because of the blocked channel in the projectile K shell, it is by no means negligible. For guidance, examination of Fig. 6 shows that about 50% of the cross section calculated in the BK approximation for capture of argon K electrons by chlorine ions is to excited states of the projectile. Somewhat greater fractions are found for the other collision partners. Electron screening will cause a slight reduction in the K capture to excited states for the lower charge state ions but all the observed target radiation can be accounted for by this process.

An alternate description in terms of electron promotion by rotational coupling between filled $2p\sigma$ orbitals and vacant $2p\pi_x$ orbitals can also be used to account for the K-vacancy production by the incident ions with filled K shells.[8] Of course, this process must include vacancy sharing by $2p\sigma - 1s\sigma$ radial coupling on the outgoing part of the trajectory, as well, so that the total cross section for both target and projectile K vacancies should be included in this discussion. Again, a knowledge of the fluorescence yield for both target and projectile states is necessary to make comparison with the predictions of the model. Through vacancy sharing

in these symmetric collisions, the K vacancies are expected to be equally divided between target and projectile, however the x-ray cross section for the former is only about 1/3 of the latter. Since the incident three electron projectiles for both S and Cℓ are expected to have a fluorescence yield of about 0.6 (if the two L-shell electrons remain on the ion but are distributed in the L shell by 2s-2p excitation[25]), a value of 0.2 for the target states excited by these ions is assumed. With these gross simplifications the total K-vacancy cross sections estimated from the measured x-ray cross sections with incident three electron ions have been obtained and are listed in Table III.

Also shown in Table III are the $2p\sigma - 2p\pi_x$ rotational coupling cross sections calculated using the universal scaling for this process recently published by Taulbjerg et al.[8] The close agreement between the experimental and theoretical cross sections is somewhat fortuitous considering the assumptions used in estimating the fluorescence yields. However, that the molecular model correctly describes these cross sections at a scaled velocity near unity, gives us evidence that the simple universal scaling of the $2p\pi - 2p\sigma$ cross section is valid over a wide velocity range.

IV. CONCLUSION

K x-ray energies and cross sections have been measured, under single collision conditions for charge transfer, as a function of the incident charge state of highly ionized S and Cℓ ions. For incident bare nuclei, the dependence of the projectile cross sections on the target atomic number are accurately reproduced for both ions by scaling cross sections for capture to excited states calculated in a Brinkman-Kramers approximation by a single normalization constant. The magnitude of the target cross section is also reproduced by the same scaling of calculated cross sections for capture of K-shell electrons. However, the details of the cross section for different targets is inconsistent with the trends of the calculated results.

With one-electron ions incident, the cross sections are reduced by factors of 2.4 and 2.2 for the projectile and target, respectively. The reason for this reduction is different in the two cases, being qualitatively explained by lifetime arguments in the former case but by the $1s\sigma$ occupation number in the latter.

For the lower charge state ions, the mean fluorescence yield of the emitting states is estimated using vacancy-sharing arguments. Total K-vacancy production cross sections are found to be in excellent agreement with the values calculated using the rotational coupling of $2p\pi - 2p\sigma$ orbitals even at a scaled velocity near unity.

V. ACKNOWLEDGMENTS

We thank the most able and co-operative BNL Tandem Accelerator staff for their help in conducting this experiment. One of us, JRM, acknowledges computational assistance of J. A. Guffey and C. P. Bhalla, useful discussions with C. L. Cocke, and the secretarial assistance of Dea Richard, during the data analysis and preparation of this paper.

REFERENCES

1. J. R. Macdonald, L. M. Winters, M. D. Brown, T. Chiao, and L. D. Ellsworth, Phys. Rev. Letters 29, 1291 (1972); J. R. Mowat, D. J. Pegg, R. S. Peterson, P. M. Griffin, and I. A. Sellin, Phys. Rev. Letters 29, 1577 (1972); F. Hopkins, R. Brenn, A. R. Whittemore, N. Cue, V. Dutkiewicz and R. P. Chaturvedi, Phys. Rev. A 13, 74 (1976).
2. D. Burch, N. Stolterfoht, D. Schneider, E. Wieman, and J. S. Risley, Phys. Rev. Letters 32, 1151 (1974).
3. L. M. Winters, J. R. Macdonald, M. D. Brown, T. Chiao, L. D. Ellsworth, and E. W. Pettus, Phys. Rev. A 8, 1835 (1973); C. W. Woods, R. L. Kauffman, K. A. Jamison, C. L. Cocke, and P. Richard, J. Phys. B 7, L474 (1974).
4. R. L. Kauffman, C. W. Woods, K. A. Jamison, and P. Richard, Phys. Letters 50A, 75 (1974).
5. A. M. Halpern and J. Law, Phys. Rev. Letters 31, 4 (1973).
6. B. Fastrup, E. Bøving, G. A. Larsen, and P. Dahl, J. Phys. B 7, L206 (1974); N. Stolterfoht, D. Schneider, D. Burch, B. Aagaard, E. Bøving, and B. Fastrup, Phys. Rev. A 12, 1313 (1975).
7. F. Hopkins, N. Cue, and V. Dutkiewicz, Phys. Rev. A 12, 1710 (1975).
8. K. Taulbjerg, J. S. Briggs, and J. Vaaben, J. Phys. B 9, 1351 (1976).
9. L. M. Winters, M. D. Brown, L. D. Ellsworth, T. Chiao, E. W. Pettus, and J. R. Macdonald, Phys. Rev. A 11, 174 (1975).
10. All the spectra were printed digitally, plotted graphically, and stored on magnetic tape at BNL. At KSU the data were analytically fit using the graphical output for guidance, and normalized absolutely to the number of counts in the digital output after subtracting the number of counts in the background spectra.

11. The composite spectrum for each projectile charge state was normalized by peak height prior to subtraction from the spectrum to be stripped.

12. The detector window is removable and the transmission function has been measured. The results are consistent with the absorption curve calculated for this window and shown in L. M. Winters, J. R. Macdonald, M. D. Brown, L. D. Ellsworth, and T. Chiao, Phys. Rev. A 7, 1276 (1973).

13. Charge exchange cross sections have not been reported for these highly ionized ions, but were estimated from the measured projectile x-ray cross sections of this experiment.

14. J. R. Macdonald, E. Salzborn, L. D. Ellsworth, and J. A. Guffey, to be published; and E. Salzborn, J. A. Guffey, L. D. Ellsworth, and J. R. Macdonald, BAPS 20, 639 (1975).

15. The calculation uses hydrogen-like wave functions for closed target shells and give total cross sections from a particular target shell to all angular momentum states of a given principal quantum number in the projectile. The closed form expression for the cross section is given by V. S. Nikolaev, Sov. Phys. J.E.T.P. 24, 847 (1967).

16. C. L. Cocke, B. Curnutte, J. R. Macdonald, and R. Randall, Phys. Rev. A 9, 57 (1974); C. L. Cocke, B. Curnutte, and R. Randall, Phys. Rev. A 9, 1823 (1974). The energies shown are the mean energy of the multiplets formed with each charge state.

17. C. P. Bhalla, private communication.

18. For example, see the conclusions drawn by A. M. Halpern and J. Law, Phys. Rev. A 12, 1776 (1975).

19. M. D. Brown, L. D. Ellsworth, J. A. Guffey, T. Chiao, E. W. Pettus, L. M. Winters, and J. R. Macdonald, Phys. Rev. A 10, 1255 (1974).

20. J. R. Mowat, I. A. Sellin, P. M. Griffin, D. J. Pegg, and R. S. Peterson, Phys. Rev. A 9, 644 (1974).

21. C. P. Bhalla, Phys. Rev. A 8, 2877 (1973).

22. L. L. House, Astrophys. J. Suppl. Ser. 18, 21 (1969).

23. C. L. Cocke, R. R. Randall and B. Curnutte, IX ICPEAC Abstracts Vol. 2, 933-34 (1975), edited by R. Geballe and J. S. Risley.

24. J. S. Briggs and K. Taulbjerg, J. Phys. B 8, 1919 (1975); W. E. Meyerhof, Phys. Rev. Letters 31, 1341 (1973).

25. J. R. Macdonald and E. H. Pedersen, BAPS 20, 674 (1975).

TABLE I

PROJECTILE K X-RAY CROSS SECTIONS (10^{-19} cm^2)

Incident State n=Z-q \ Target	Chlorine Ions 105 MeV SiH_4	Chlorine Ions 132 MeV Ne	SiH_4	H_2S	HCℓ	Ar	Sulphur Ions 120.7 MeV Ne	SiH_4	H_2S	HCℓ	Ar
0	257±20	95±8	148±13	165±17	199±22	232±25	72±6	105±9	153±16	155±17	178±18
1	103±9	54±4	57±4	79±8	82±9	98±11	31±2	41±3	53±6	60±7	69±7
2	7.2±0.7	7.0±0.5	8.0±0.5	8.8±1.0	8.0±1.6	8.6±1.0	6.7±0.5	9.8±0.7	10.1±1.4	11.1±1.3	11.3±1.2
3	3.4±0.3	3.1±0.2	3.9±0.3	5.0±0.6	4.4±0.6	4.8±0.6	3.7±0.2	4.8±0.3	4.9±0.7	5.6±0.7	5.6±0.6
4	2.9±0.3						-	-	-	-	-
5	2.4±0.2						-	-	-	-	-
6	-						2.2±0.2	2.9±0.2	3.1±0.4	3.3±0.4	3.6±0.4
7	-										
8	1.8±0.2										

TABLE II

TARGET K X-RAY CROSS SECTIONS (10^{-19} cm^2)

Incident State n=Z-q \ Target x ray	Chlorine Ions 105 MeV Si K	Chlorine Ions 132 MeV Si K	S K	Cℓ K	Ar K	Sulphur Ions 120.7 MeV Si K	S K	Cℓ K	Ar K
0	14±1.6	13.0±1.6	8.0±1.2	6.3±2	6.6^{+2}_{-3}	8.9±1.1	13±4	14±4	14±2
1	8.1±0.8	6.7±0.6	4.1±0.6	3.3±1	2.4±1	4.8±0.4	4.9±2	5.3±1.5	6.1±0.8
2	4.2±0.4	4.3±0.3	1.9±0.2	1.7±0.6	1.3±0.4	2.9±0.3	2.0±0.6	1.2±0.3	1.8±0.2
3	3.3±0.3	3.3±0.3	1.6±0.2	1.4±0.5	1.6±0.4	2.3±0.2	1.6±0.5	1.3±0.3	1.4±0.2
4	2.9±0.3					-	-	-	-
5	2.5±0.2					-	-	-	-
6	-					1.7±0.2	1.3±0.2	1.2±0.2	1.2±0.2
7	-								
8	1.8±0.2								

TABLE III

Total K-vacancy cross sections, σ_v (expt) for three electron incident ions at 3.77 MeV/amu. Mean fluorescence yields of 0.6 and 0.2 were assumed for projectile and target radiation, respectively. Cross sections σ_v (calc) were calculated using the rotational coupling of $2p\pi_x \leftharpoondown 2p\sigma$ orbitals.

Projectile	Cℓ				S			
Target	Si	S	Cℓ	Ar	Si	S	Cℓ	Ar
σ_v (expt) (10^{-19} cm^2)	23	16	14	16	18	16	16	16
σ_v (calc)	24	20	18	17	26	22	20	18

FIGURE CAPTIONS

Fig. 1. Typical spectra.

Fig. 2 Target and projectile K x-ray production cross sections as a function of the number of electrons on the incident projectile.

Fig. 3 Projectile x-ray cross section for bare nuclei of Cℓ incident on SiH_4 at 3.77 MeV/amu. The solid line shows the energy dependence of the cross section for capture to excited states calculated in a Brinkman-Kramers approximation and reduced by an order of magnitude.

Fig. 4 Projectile K x-ray energies observed in this experiment as a function of the number of electrons on the incident projectile. The horizontal lines are theoretical x-ray energies determined for the lowest configuration containing an initial K vacancy and the indicated number of electrons.

Fig. 5 Kβ to Kα intensity ratio for the projectile radiation observed as a function of the number of electrons on the incident ions.

Fig. 6 Cross sections for electron capture by bare nuclei of Cℓ from particular shells of Ar to all final states with a particular principal quantum number. The calculations are made in a Brinkman-Kramers approximation.

Fig. 7 Projectile K x-ray cross sections as a function of the target atomic number for incident ions carrying n electrons into the collision. (a) for Cℓ ions (b) for S ions.

Fig. 8 Projectile K x-ray cross sections for incident bare nuclei at

3.77 MeV/amu as a function of the target atomic number. The broken lines join cross sections for electron capture to all excited states calculated in a Brinkman-Kramers calculation scaled by 0.098.

Fig. 9 Observed Si K x-ray energies excited by Cℓ and S ions carrying n electrons into the collisions. The horizontal lines are theoretical estimates of the Si Kα x-ray energy for initial states containing one K-shell vacancy and the indicated number of electrons in the lowest configuration.

Fig. 10 Target K x-ray cross sections as a function of target atomic number for excitation at 3.77 MeV/amu for incident ions carrying n electrons into the collision. (a) Excitation by Cℓ ions, (b) by S ions.

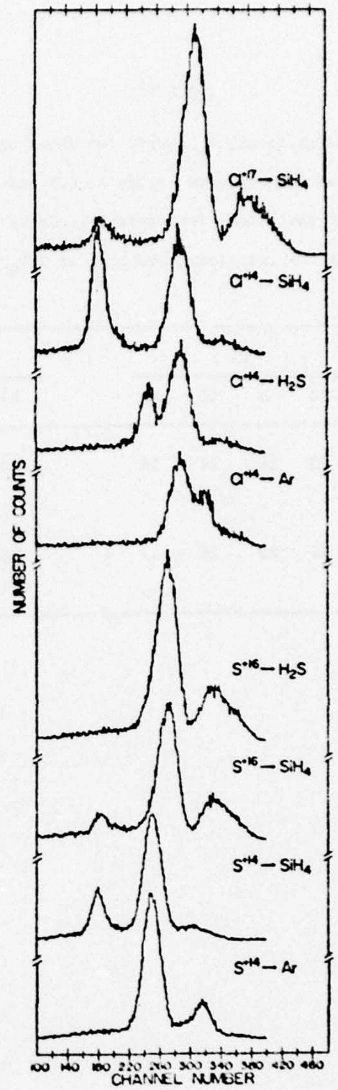

Fig. 1

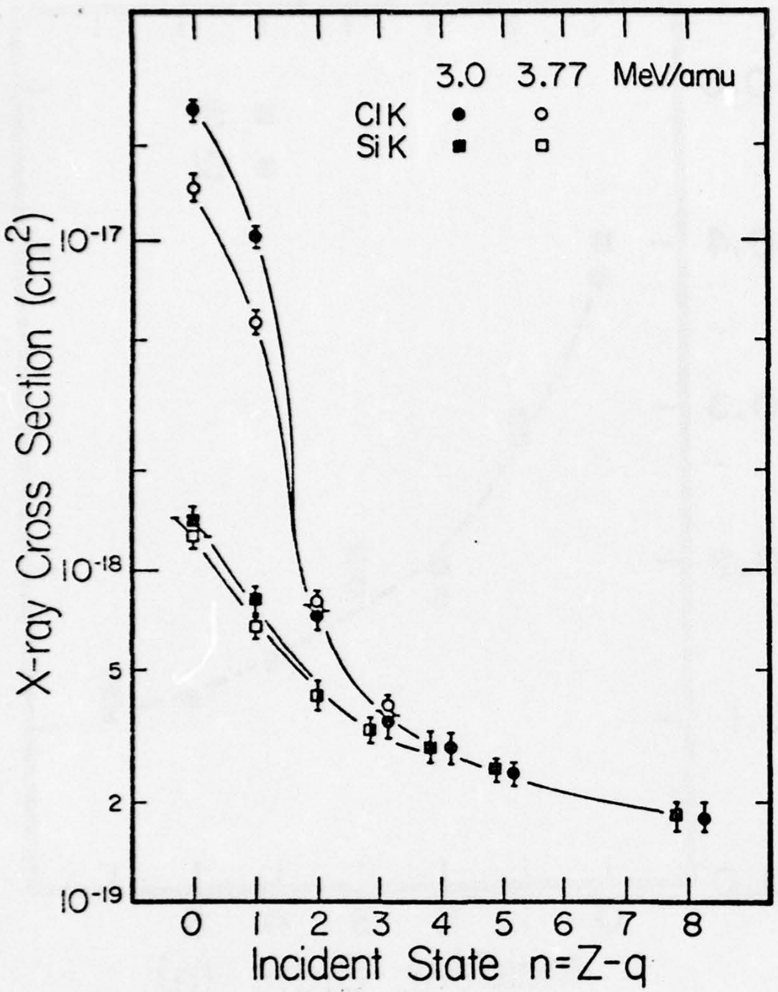
3.0 3.77 MeV/amu
Cl K
Si K
X-ray Cross Section (cm^2)
10^{-17}
10^{-18}
5
2
10^{-19}
0 1 2 3 4 5 6 7 8
Incident State n=Z-q

Fig. 2

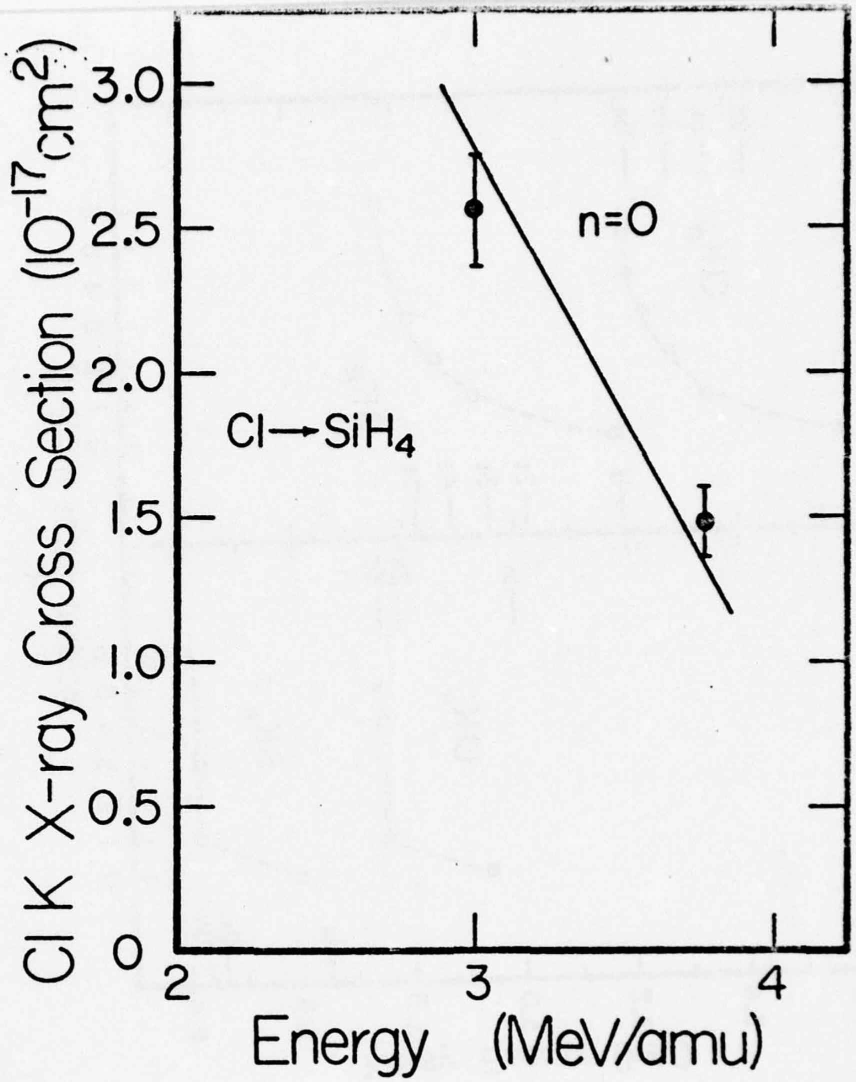
Cl K X-ray Cross Section (10^{-17}cm^2)
3.0
2.5
2.0
1.5
1.0
0.5
0
2 3 4
Energy (MeV/amu)
Cl → SiH$_4$
n=0

Fig. 3

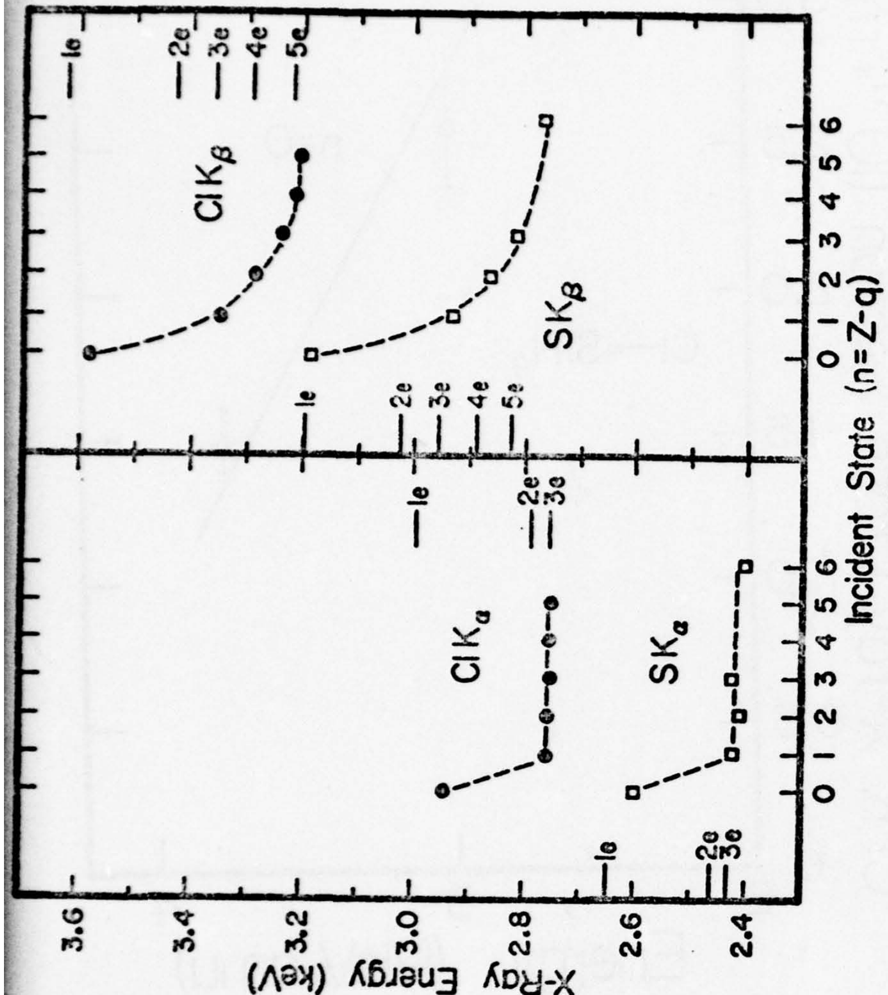
Cl K_β
S K_β
Cl K_α
S K_α
1e
2e
3e
4e
5e
X-Ray Energy (keV)
3.6
3.4
3.2
3.0
2.8
2.6
2.4
Incident State (n=Z-q)
0 1 2 3 4 5 6

Fig. 4

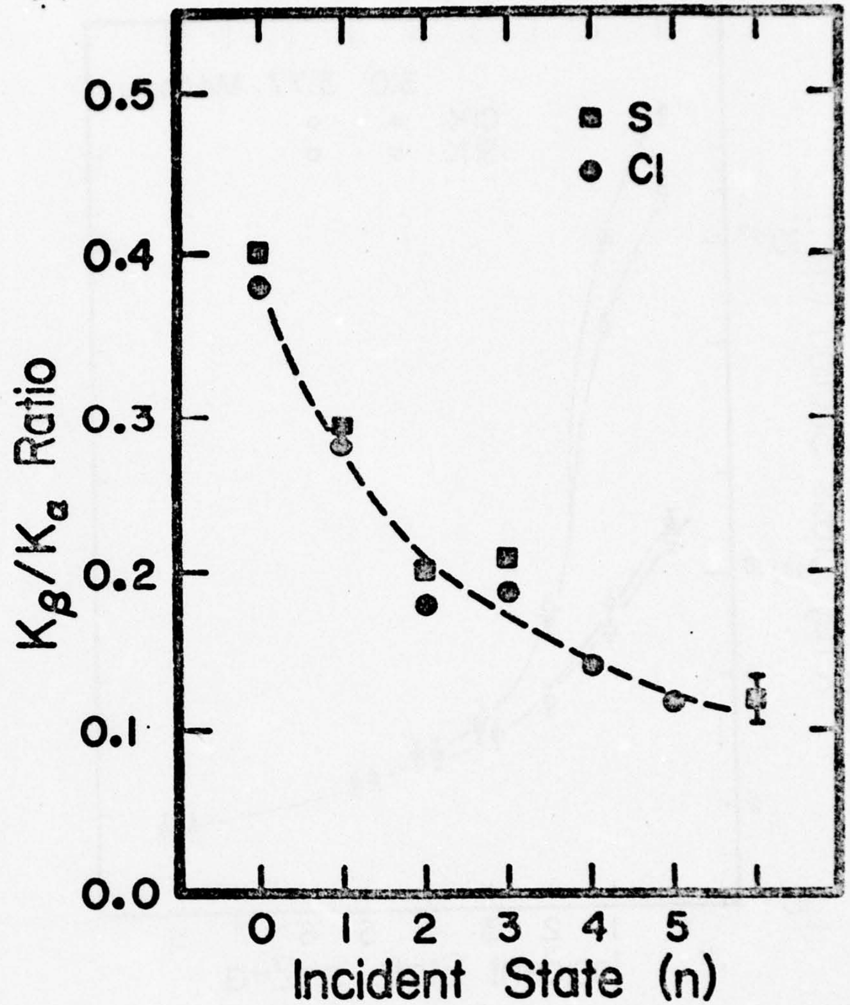
S
Cl
K_β/K_α Ratio
0.0
0.1
0.2
0.3
0.4
0.5
0 1 2 3 4 5
Incident State (n)

Fig. 5

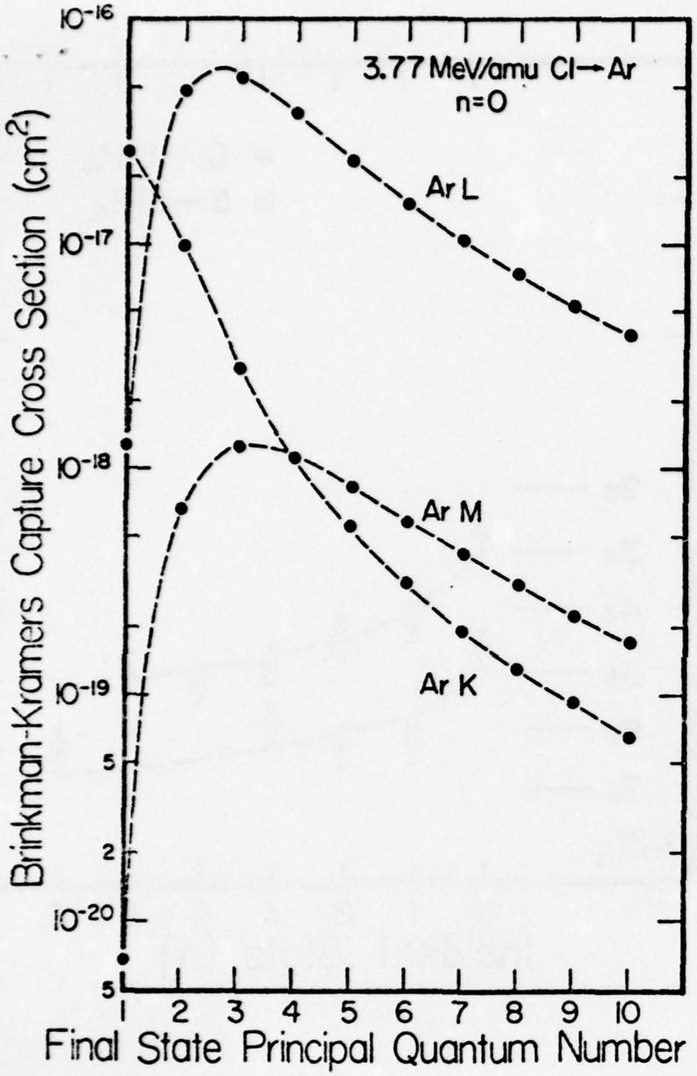
3.77 MeV/amu Cl→Ar
n=0
Ar L
Ar M
Ar K
Brinkman-Kramers Capture Cross Section (cm²)
Final State Principal Quantum Number

Fig. 6

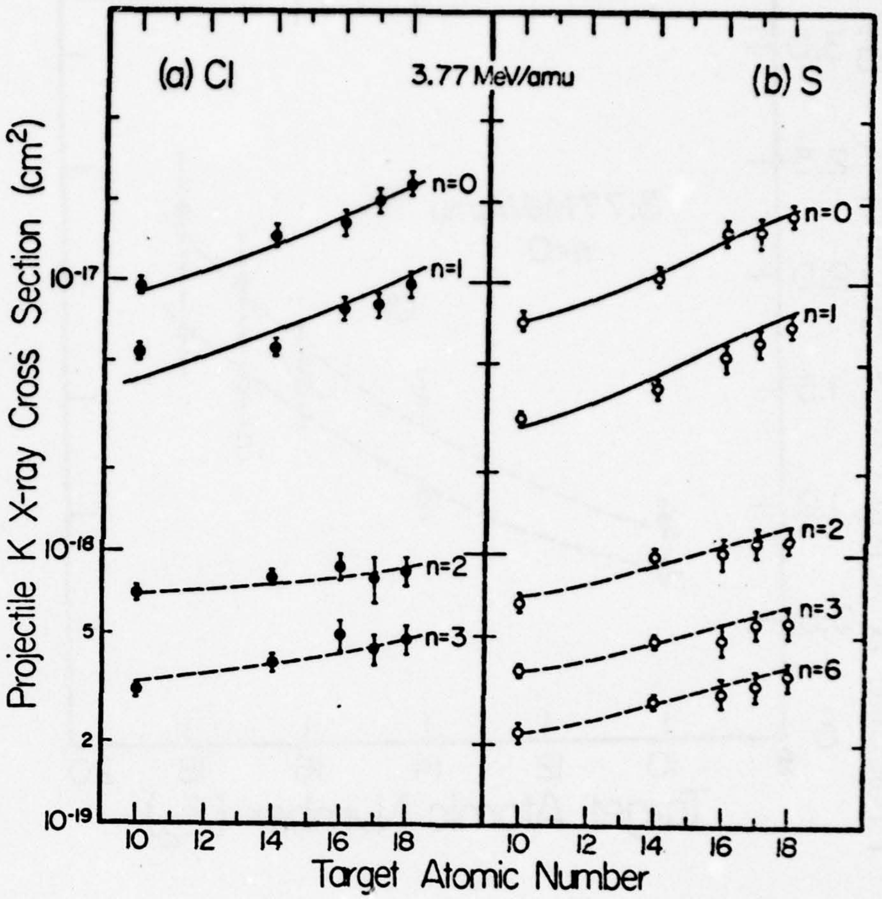
(a) Cl
3.77 MeV/amu
(b) S
n=0
n=1
n=2
n=3
n=6
Projectile K X-ray Cross Section (cm²)
Target Atomic Number

Fig. 7

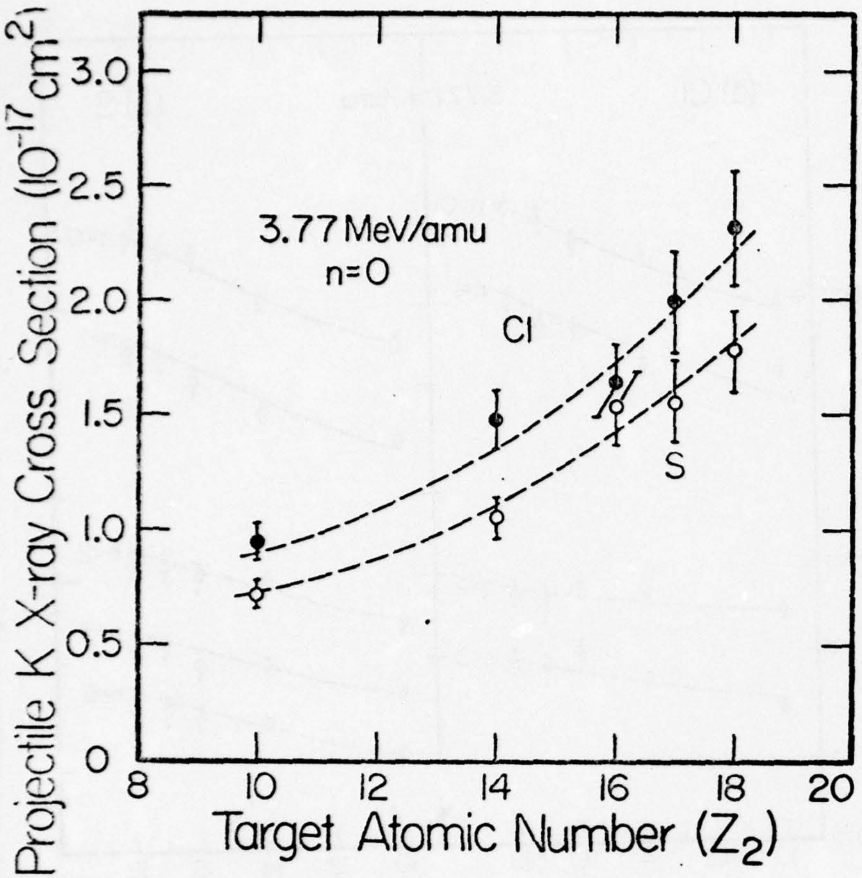
3.77 MeV/amu
n=0
Cl
S
Projectile K X-ray Cross Section (10^{-17} cm^2)
Target Atomic Number (Z_2)
Fig. 8

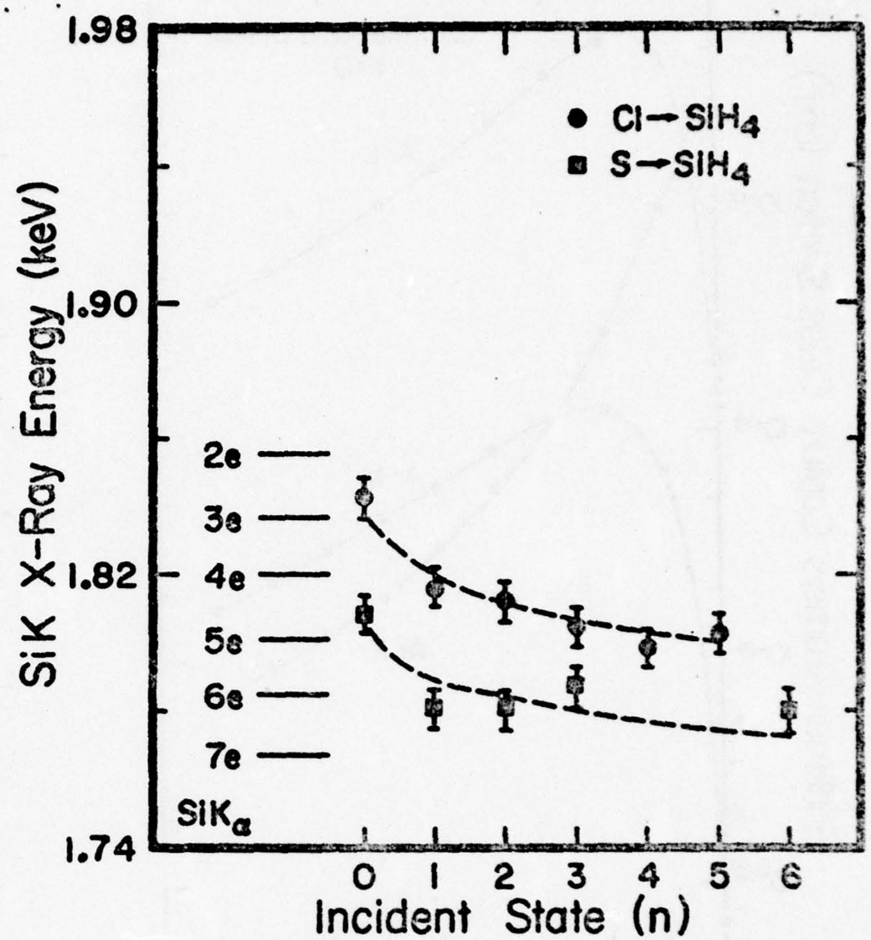
Cl→SiH$_4$
S→SiH$_4$
2e
3e
4e
5e
6e
7e
SiK$_\alpha$
SiK X-Ray Energy (keV)
Incident State (n)
Fig. 9

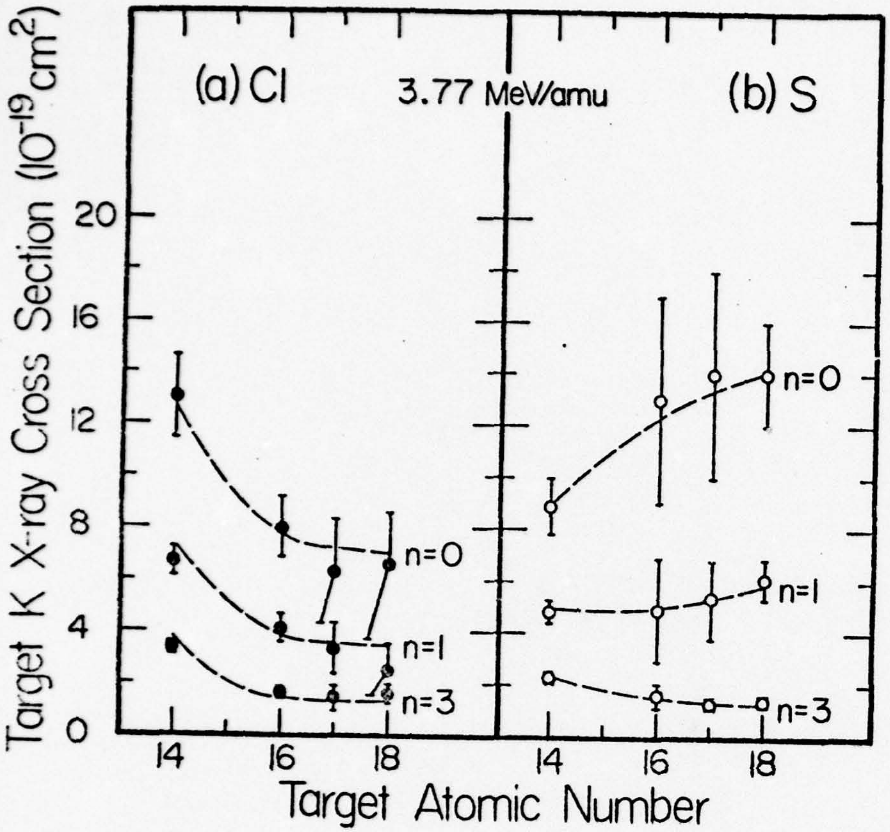

(a) Cl
3.77 MeV/amu
(b) S
n=0
n=1
n=3
Target K X-ray Cross Section (10^{-19} cm^2)
Target Atomic Number

Fig. 10

Projectile Charge-State Dependence in K-Shell Ionization of Neon, Silicon, and Argon Gases by Lithium Projectiles*

F. K. Chen, G. Lapicki, and R. Laubert
New York University
New York, NY 10003

and

S. B. Elston, R. S. Peterson, and I. A. Sellin
University of Tennessee
Knoxville, Tenn. 37916
and
Oak Ridge National Laboratory
Oak Ridge, Tenn. 37830

The ratios of x-ray yields from the K shells of gaseous $_{10}$Ne, $_{14}$Si, and $_{18}$Ar by $^{6}_{3}Li^{+3,2,1}$ and protons were measured at projectile velocities comparable to the orbital velocities of the target K shells. Projectile charge-state dependence is accounted for in a theory which considers electron capture by the projectile and screening by its electrons.

It is assumed in Coulomb ionization theories[1,2] that the projectile acts as a bare particle in creation of an inner shell vacancy by removing the electron to the continuum of the target atom; ionization is projectile charge-state independent. To test this assumption for K-shell ionization, we measure the target x-yields produced by lithium ions (atomic number $Z_1 = 3$) in all its charge states ($q = 3,2,1$), $Y(Z_1^{+q})$, and by protons, $Y(1^{+1})$. Ratios of these yields are found to depend on the projectile charge state in systematic ways. We explain this dependence through inclusion in the theory[2] of: (i) electron capture to unoccupied projectile states[3] and (ii) screening by bound projectile electrons.

The experiments were performed utilizing the Brookhaven National Laboratory Tandem Van de Graaf accelerator which supplied ion beams of protons and $^{6}_{3}Li^{+q}$ ($q = 3,2,1$) in the velocity range of 2 to 4 MeV/amu. Gaseous $_{10}$Ne, $_{14}$Si (in the form of SiH_4), and $_{18}$Ar targets were prepared in a differentially pumped gas cell, so that the projectile charge state could be well defined. The interaction region was ~2 cm in length and the target pressure, mantained through a servo-mechanical valve driven by a capicitance manometer, was typically 3-10 mTorr. A collimated lithium-drifted silicon detector counted the target x rays emitted at right angles to the beam direction. After transmission through the gas cell the ion beam was collected in a biased Faraday cup. At each

energy and projectile charge state the x-ray yield was measured as a function of target pressure. The experiment was constrained to pressures for which this function was linear and could be extrapolated to the origin at zero pressure. Under such conditions only a negligible fraction of the ion beam equilibrates, so that the incident projectile charge state is a well defined quantity in these collisions.

From a knowledge of the target-detector geometry and the x-ray yield per incident projectile, the absolute x-ray production cross sections were determined and found to agree with measurements[4] for K-shell ionization by protons. Rather than to compare the absolute cross sections with the predictions of inner shell ionization theories, we analyze the ratios of x-ray yields produced by lithium ions and protons. Many systematic uncertainties cancel in such ratios so that one can test theory to about 10-20%. On the other hand, absolute ionization cross sections are uncertain to about 30-40% (or even more than 50% for neon due to the window transmission and background signal), not including possible errors in the fluorescence yiled. We assume that fluorescence yields are the same for protons and lithium ions, and, therefore, our measured ratios can be directly compared with various inner-shell ionization theories. According to the plane-wave Born approximation (PWBA)[1], the ratio $Y(Z_1^{+q})/Z_1^2 Y(1^{+1})$ should be unity for projectiles of equal velocity. As shown in Fig. 1, the perturbed-stationary-state (PSS) theory[2] gives a single curve (x marked curve) for each target atom. An increase in the ratio is obtained (solid curves) when electron capture[3] is added to the predictions of the PSS theory. However, the data for not fully stripped $Li^{+2,1}$ ions lie significantly below such predictions. The inclusion of screening in the PSS theory (dashed curves) further improves the agreement with our experiments. Besides screening of the projectile as calculated[5] in the PWBA, this screening decreases the polarization effect in the PSS theory.

We find similar agreement and trends for the yield ratios measured with carbon (Z_1=6) projectiles of q = 6,5, and 4. These data, as well as the detailed manner in which electron capture and screening are included in the theory, will be reported in a separate publication.

We would like to acknowledge the assistance of Carl Peterson and the BNL Tandem staff. We benefited from discussions with Werner Brandt and William Losonsky.

* Work supported in part by ERDA, NSF, and ONR.

References

(1) E. Merzbacher and H. W. Lewis, in Handbuch der Physik, edited by S. Flügge (Springer, Berlin, 1958) Vol. 34, p.166.

(2) G. Basbas, W. Brandt, and R. Laubert, Phys. Rev. A7 (1973) 783, Bull. Am. Phys. Soc. 18 (1973) 103, and to be published.

(3) G. Lapicki and W. Losonsky, Bull. Am. Phys. Soc. 20 (1975) 638, 21 (1976) 32, and to be published.

(4) K. G. Harrison, H. Tawara, and F. J. de Heer, Physica 66 (1973) 16, L. H. Toburen, in Proc. Inter. Conf. on Inner-Shell Ionization Phenomena, Atlanta, 1972, edited by R. W. Fink et al. (U.S. AEC, Oak Ridge, 1973) 979, L. M. Winters et al., Phys. Rev. A7 (1973) 1276, D. Burch et al., Phys. Rev. Lett. 32 (1974) 1151, N. Stolterfoht and D. Schneider, Phys. Rev. A11 (1975) 721, H. Tawara et al., Phys. Rev. A13 (1976) 572, C. W. Woods et al., Phys. Rev. A13 (1976) 1358, and N. Kobayashi et al., J. Phys. Soc. Jap. 40 (1976) 1421.

(5) G. Basbas, in Abstracts of Papers, 9th Inter. Conf. on the Physics of Electronic and Atomic Collisions, edited by J. R. Risley and R. Geballe (Univ. of Washington Press, Seattle, 1975), p.502.

Figure Caption

Figure 1 Ratios $Y(Z_1^{+q})/Z_1^2\, Y(1^{+1})$ for $_3Li^{+q}$ projectiles in K-shell ionization of $_{10}Ne$, $_{14}Si$, and $_{18}Ar$. The open, half-filled, and filled circles represent the measured ratios for the lithium ions in the q=3,2, and 1 charge states, respectively. According to the PWBA (Ref. 1) these ratios should be equal to unity. The PSS theory for direct ionization (Ref. 2) (x marked curves) also predicts that the ratios are projectile charge-state independent. The solid curves are obtained when electron capture (Ref. 3) is added; the dashed curves show the additional charge-state dependence due to the screening by the electrons of the lithium ions in the q = 2 and 1 charge states.

Fig. 1

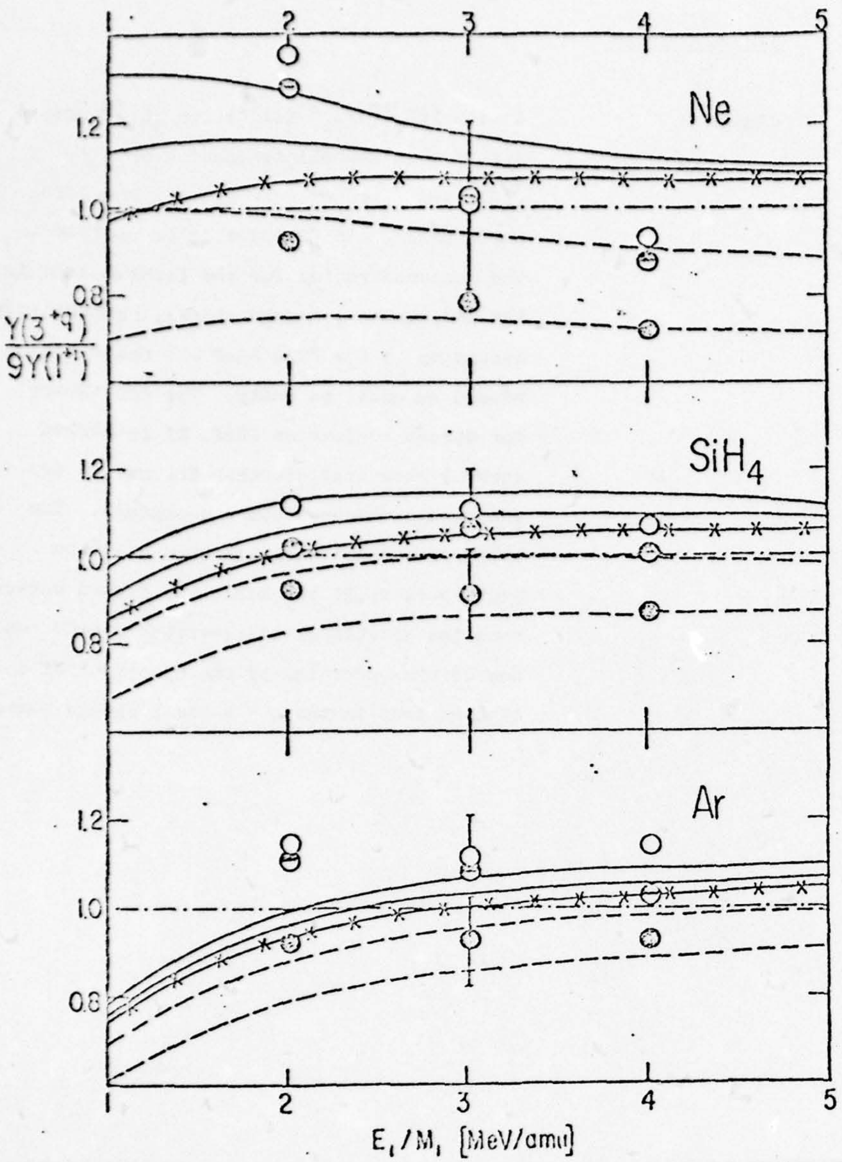

Lifetime Measurements in Si IX-Si XII using Beam-Foil Excitation*

D. J. Pisano† and K. W. Jones

Brookhaven National Laboratory, Upton, New York 11973

and

P. M. Griffin, D. J. Pegg and I. A. Sellin

University of Tennessee, Knoxville, Tennessee 37916

and

Oak Ridge National Laboratory, Oak Ridge, Tennessee 37830

and

T. H. Kruse

Rutgers University, New Brunswick, New Jersey 08903

and

S. Bashkin

University of Arizona, Tucson, Arizona 85721

Abstract

The beam-foil excitation method has been used to study the radiative lifetimes and E1 transition rates for $\Delta n = 0$ transitions in highly ionized silicon.

*Research supported in part by NSF, ONR, NASA, ERDA, and Union Carbide Corporation under contract with ERDA.

†Present address: EMI Medical Inc., Northbrook, Illinois 60062

I. Introduction

The value of the beam-foil technique in measuring the lifetimes of excited states of highly stripped ions is well known. The recent advent of a "universal" negative ion source (UNIS)[1] has, however, extended the range of available species that can be accelerated to MeV/a.m.u. energies using tandem accelerators.

We report here on the measurement of some radiative lifetimes in Si IX - Si XII ions using the beam-foil time-of-flight method. We have previously reported[2] on the foil-excited spectra of highly stripped silicon ions in the wavelength range ~ 100-400 Å. Most of the decay studies reported here involve $\Delta n = 0$ E1 transitions of the type $2s^2 2p^k - 2s2p^{k+1}$ or $2s2p^k - 2p^{k+1}$. Whenever possible, we have extracted atomic transition probabilities from the lifetime results. These "in-shell" transitions in highly ionized silicon have considerable astrophysical significance since they are responsible for many of the prominent features of the total solar corona extreme-ultraviolet (EUV) spectrum.

II. Experimental Technique

A silicon ion beam from the Oak Ridge National Laboratory EN tandem Van de Graaff accelerator was passed through a thin ($\sim 5\ \mu g/cm^2$) carbon foil target which served to both further strip and excite the ions of the beam. The incident beam energies of 20 and 42 MeV were chosen to maximize particular charge states in the post-foil source. EUV radiation from the foil-excited source was dispersed by a 2.2 meter, vacuum-ultraviolet grazing-incidence spectrometer equipped with a 300 lines/mm gold-coated grating and was detected by a continuous dynode, spiral electron multiplier located behind the exit slit

of the spectrometer. The detector had an ~ 90% transmission wire mesh screen (biased to -800 v) in front of it to keep out stray electrons. An angle of incidence of 87.5° was used in the present work. For spectral studies the signal strength was normalized to the radiation diffracted and scattered into a second photon counter located on the normal to the grating. For lifetime measurements the data was normalized to a fixed amount of accumulated beam charge in a well-shielded Faraday cup. The decay curves were obtained in the usual manner by measuring the yield of a given line as a function of the distance downstream from the point of excitation, i.e., the surface of the foil. All data was taken with an instrumental bandpass of from ~ 0.4 - 0.8 Å. Prior to measuring a decay curve of a new line a spectral scan was made in the immediate vicinity of the line in order to locate its centroid. A more detailed description of the experimental arrangement is reported by Pegg et al.[4] who made studies of analogous transitions in highly stripped sulfur ions.

III. Results

Figure 1 shows spectra of foil-excited silicon ions taken at two different incident beam energies, 20 and 42 MeV. Identification of lines was made by a comparison to the wavelength tables of Fawcett[5] and Kelly and Palumbo.[6] Decay-in-flight lifetime measurements were made on the most prominent features of the spectra. Figures 2 and 3 show typical decay curves. In all cases possible the intensity decay was studied to at least three decay lengths in order to search for possible long-lived decay components due to cascading and/or line blending. Similarly a careful study was made close to the foil ($x = 0$) in an attempt to observe very short-lived components

of the same origin. The decay curves were found to be well represented over several decay lengths by single exponentials for most of the transitions studied in this experiment. In order to determine mean decay lengths (and hence lifetimes) the experimental points were fit using a least squares technique to an exponential function plus a background. The background to each experimental point is from two sources (1) the dark current in the electron multiplier which is proportional to the time it takes to measure that point and (2) scattered radiation which is proportional to the total beam, i.e., the total integrated charge for each point. The functional form for the background was, therefore, taken to be $B = b_1 \cdot \text{time} + b_2$, where b_1 and b_2 are constants to be determined by a fit to the experimental points.

The lifetime results are shown in Table I, and the resulting transition probabilities derived from these lifetimes are compared to theoretical predictions in Table II. As can be seen from Table II, the present transition rates are consistently lower than predicted by current theory, even when rather sophisticated many-particle models such as that used by Sinanoglu[9] are employed. Relativistic effects on the transition rates should be quite small for these ions. It appears that $\Delta n = 0$ transitions can be particularly correlation sensitive even at relatively high Z. For example, there exists an ~ 30% discrepancy between the present experimental result and theory for the $(2s^2 2p)^2P^o - (2s2p^2)^2P$ transition in the boron-like silicon ion (Si^{9+}) which is similar in magnitude to the discrepancy quoted by Pegg et al.[4] in their recent work on boron-like sulfur (S^{11+}). Furthermore, this discrepancy continues to lower Z members of the boron-like sequence for this same transition.

The question of cascades interfering with the measurement of a lifetime always arises when the beam-foil technique is used. In the present case, the $\Delta n \neq 0$ transitions from the higher excited states are generally too fast to influence our data measurably. There are $\Delta n = 0$ transition, however, feeding states of interest that could possibly cause problems. There were several checks that were made to determine the degree of interference by cascades. Where the cascading transition was of a wavelength close to the desired transition, their relative intensities could be compared. A weak cascade has a minimal effect. More importantly, deviations of the data from a linear fit provide the strongest evidence for cascades. No strong evidence was seen in the data for the presence of cascades.

IV. Conclusions

Decay curves of several transitions of the type $2s^2 2p^k - 2s2p^{k+1}$ and $2s2p^k - 2p^{k+1}$ in Si IX-Si XII were measured using the beam-foil excitation technique. Lifetimes and, where possible, oscillator strengths were extracted by least-squares fitting of exponential plus background functions to the data. Most of the lifetimes measured in the present experiment are found to be longer than those predicted by current theories.

References

1. R. Middleton and C. T. Adams, Nucl. Instr. and Meth. 118, 329 (1974).
2. P. M. Griffin, D. J. Pegg, I. A. Sellin, K. W. Jones, D. J. Pisano, T. H. Kruse and S. Bashkin, Beam-Foil Spectroscopy, I. A. Sellin and D. J. Pegg eds. (Plenum Press, New York, 1976) Vol. 1, p. 321.
3. For example, M. Malinovsky and L. Heroux, Astrophys. J. 181, 1009 (1973).
4. D. J. Pegg, S. B. Elston, P. M. Griffin, H. C. Hayden, J. P. Forester, R. S. Thoe, R. S. Peterson and I. A. Sellin, to be published in Phys. Rev. A.(Sept. 1976).
5. B. C. Fawcett, Atomic Data and Nuclear Data Tables 16, 135 (1975).
6. R. L. Kelly and L. J. Palumbo, Atomic and Ionic Emission Lines Below 2000 Angstroms, NRL7599, Naval Research Laboratory, Washington, D. C., 1973.
7. M. W. Smith and W. L. Wiese, Astrophys. J. Sup. No. 196, 23, 103 (1971).
8. U. I. Safronova, A. N. Iranova, and V. N. Kharitonova, Th. and Expt. Chem. (USSR) 5, 209 (1969).
9. O. Sinanoğlu, Nucl. Instr. and Meth. 110, 193 (1973).
10. E. H. Pinnington, A. E. Livingston, and J. A. Kernahan, Phys. Rev. A 9, 1004 (1974).

Table I. Lifetimes in highly ionized silicon.

Number of Electrons	Wavelength (Å)	Upper Level	Lifetime (10^{-12} sec)
3	129.9	$(4f)^2F^o{}_{5/2}$	39 ± 8
4	358.3	$(2p^2)^1S_o$	112 ± 15
5	253.7, 256.4, 258.4	$(2s2p^2)^2P_{1/2,3/2}$	80 ± 8
5	272.0	$(2s2p^2)^2S_{1/2}$	149 ± 15
5	356.1	$(2s2p^2)^2D_{5/2}$	600 ± 70
5	347.7	$(2p^3)^2D^o{}_{5/2}$	250 ± 30
6	227.3	$(2s2p^3)^1P^o{}_1$	47 ± 5
6	350.0	$(2s2p^3)^3D^o{}_3$	540 ± 50

Table II. Transition probabilities in highly ionized silicon.

Number of Electrons	Transition	Transition Probability (10^9 sec^{-1})	
		Present	Theory
3	$(3d)^2D - (4f)^2F^o$	25.6 ± 5.3	28.2[a]
4	$(2s2p)^1P^o - (2p^2)^1S$	8.93 ± 1.20	10.0[a], 9.3[b]
5	$(2s^22p)^2P^o - (2s2p^2)^2P$	12.50 ± 1.25	18.0[a], 16.8[c]
5	$(2s^22p)^2P^o - (2s2p^2)^2S$	6.71 ± 0.67	9.7[a], 8.5[c]
5	$(2s^22p)^2P^o - (2s2p^2)^2D$	1.67 ± 0.20	2.3[a], 2.1[c]
5	$(2s2p^2)^2D - (2p^3)^2D^o$	4.00 ± 0.48	4.8[a], 5.3[b]
6	$(2s^22p^2)^3P - (2s2p^3)^3D^o$	1.85 ± 0.17	2.8[a], 2.2[c]

[a]Reference 7

[b]Reference 8

[c]Reference 9

Figure Captions

Fig. 1 Portion of EUV spectral scan of foil-excited silicon ions from ~ 345 - 375 Å. Two different incident beam energies are shown, 20 MeV (upper spectrum) and 42 MeV (lower spectrum).

Fig. 2 Intensity decay curve for the $(2s^2 2p^2)^3P - (2s2p^3)^3D^o$ transition in the carbon-like silicon ion (Si^{8+}).

Fig. 3 A typical time-of-flight decay curve for the $(2s^2 2p)\ ^2P^o - (2s2p^2)^2P$ transition in boron-like silicon (Si^{9+}) taken with a 20 MeV silicon beam. The points are plotted with the background subtracted from them and are normalized to the D = 0 point. The line is the result of a least squares fit to the data.

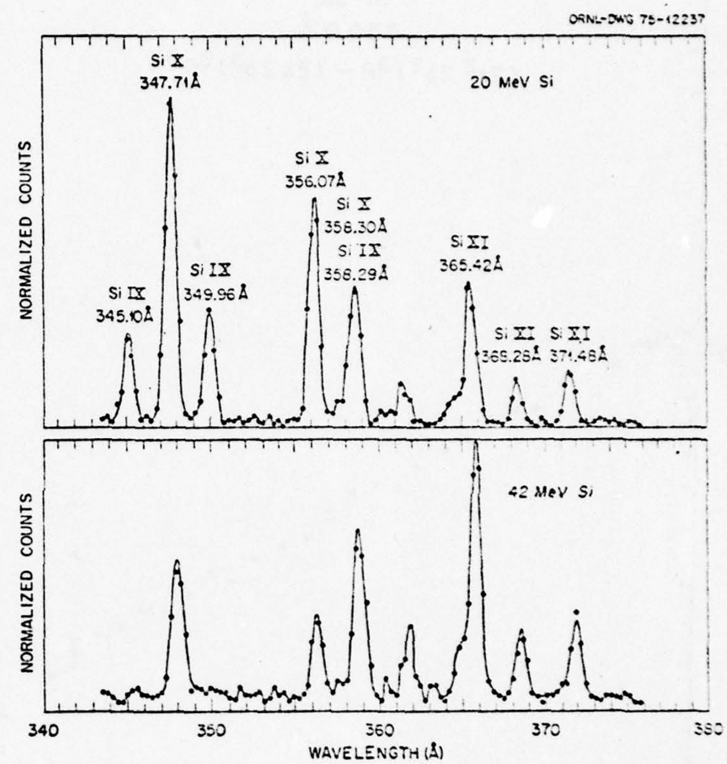

Figure 1

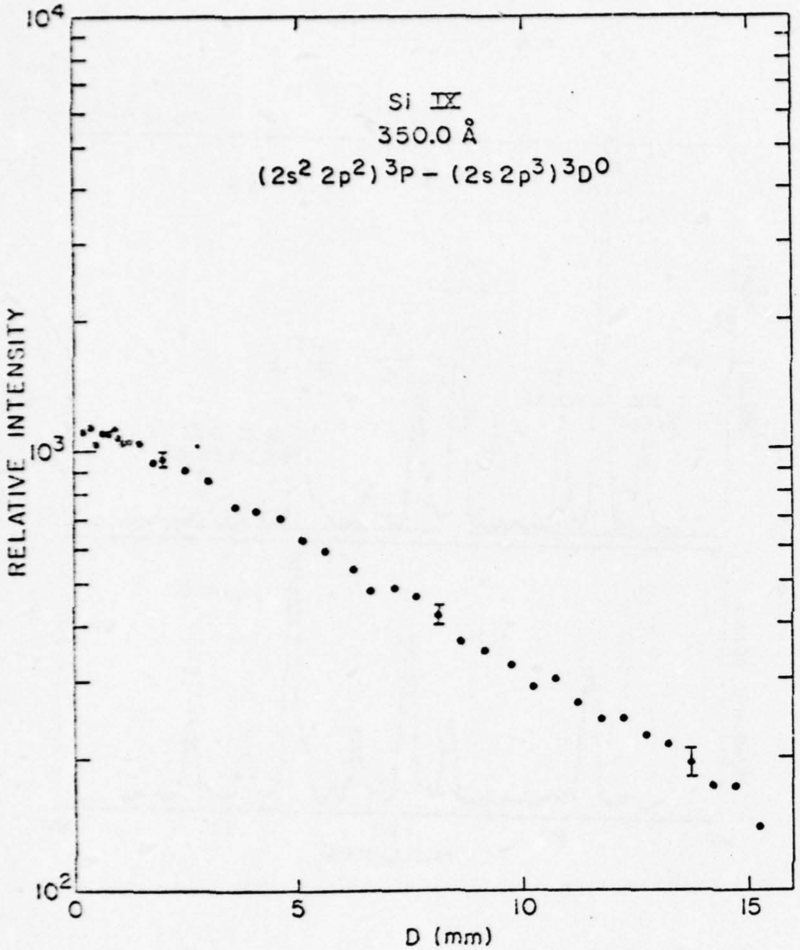

Figure 2

Neg. #9-342-76

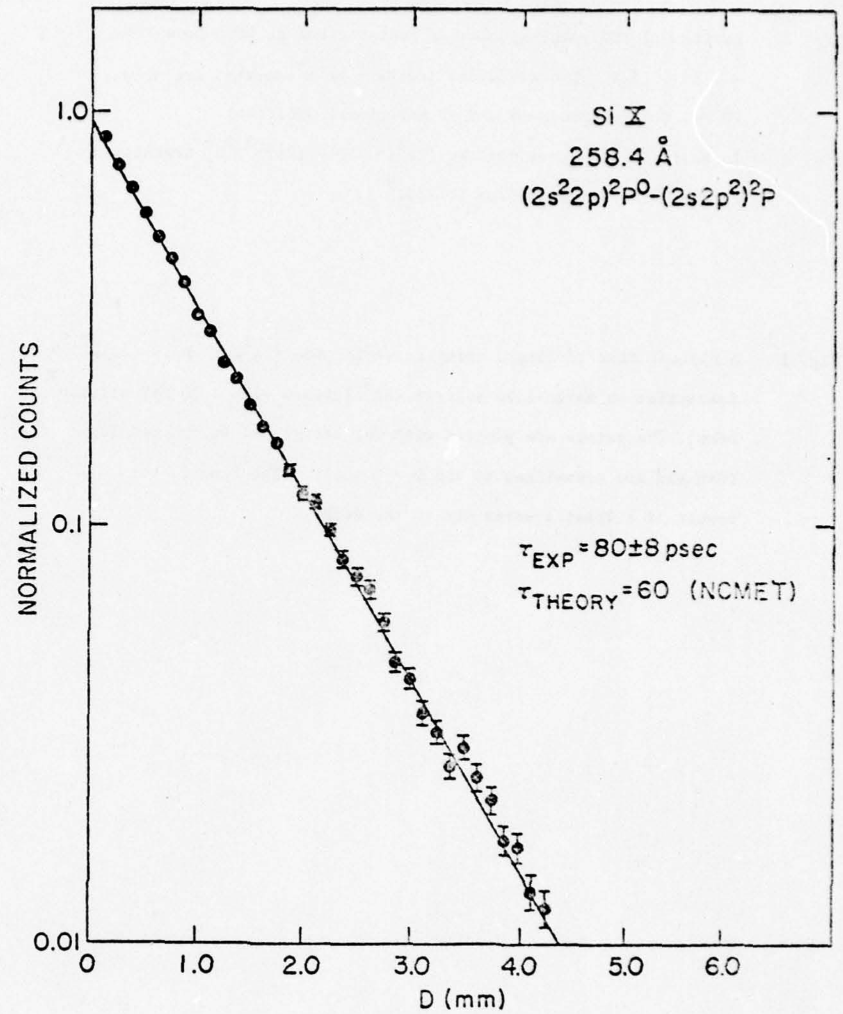

Figure 3

Neg. #6-941-76

(submitted for publication in Astrophysical Journal Letters '76) (6)

THE SPLITTING AND OSCILLATOR STRENGTHS FOR THE $2s^2S$ - $2p^2P°$ DOUBLET IN LITHIUMLIKE SULFUR*

D. J. Pegg, J. P. Forester, S. B. Elston, P. M. Griffin, K-O. Groeneveld+, R. S. Peterson, R. S. Thoe, C. R. Vane, I. A. Sellin

University of Tennessee, Knoxville, Tennessee 37916
and
Oak Ridge National Laboratory, Oak Ridge, Tennessee 37830

ABSTRACT

The beam-foil technique has been used to study the $2s^2S$ - $2p^2P°$ doublet in SXIV. The results confirm the doublet splitting measured aboard Skylab during solar flare events. In addition, the oscillator strengths for the resonance transitions comprising this doublet have been measured and found to agree well with recent relativistic f-value calculations.

*Research supported in part by NSF, ONR, NASA, and Union Carbide Corporation under contract with ERDA.

+Permanent address: Inst. für Kernphysik, Universität Frankfurt/M. W. Germany.

I. Introduction

Recently both Widing and Purcell (1976) and Sandlin et al. (1976) reported in this journal on observations of the $2s^2S$ - $2p^2P°$ doublet in highly stripped lithiumlike ions made aboard Skylab during solar flare events. This doublet was among the strongest of the high temperature lines observed and was used as a diagnostic of the plasma temperature. The doublet splittings derived from these astrophysical measurements, however, appear to be in some disagreement with the results of earlier laboratory investigations (Fawcett 1970, 1975) for several ions of the lithium isoelectronic sequence.

In the present letter we report on a recent beam-foil study made in our laboratory on the $2s^2S$ - $2p^2P°$ doublet in SXIV. These lines from highly ionized sulfur are prominent in the reported solar flare spectra. In addition, we have used the beam-foil time-of-flight method to measure the lifetimes of the upper levels of these resonance transitions thus enabling us to derive oscillator strengths for the two electric dipole decay channels comprising the doublet.

II. Experimental Arrangement

A detailed description of the experimental arrangement used in this work has been reported elsewhere (Pegg, 1976). A 46 MeV sulfur ion from the Oak Ridge tandem accelerator was passed through a thin ($\sim 5 \mu g/cm^2$) carbon foil which served to further ionize and excite the ions of the beam. Extreme ultraviolet (EUV) radiation emitted in a direction approximately perpendicular to the foil-excited source was collected and dispersed by a 2.2m grazing incidence spectrometer and detected by a channel electron multiplier. This

signal has normalized to the beam charge collected in a well-shielded faraday cup. The foil target could be translated parallel to the beam direction be means of a precision screw to facilitate time-of-flight lifetime measurements. For spectral studies, a hollow cathode source, which was situated directly opposite the entrance slit of the spectrometer, was used to calibrate the instrument in the spectral region of interest. For example, in the present work we used several NeII standard lines (Kelly and Palumbo, 1973) to establish the wavelengths of the doppler-shifted beam lines, i.e., the $2s^2S$ - $2p^2P°$ doublet in SXIV. A foil-excited spectrum is shown in Fig. 1. The magnitude of the doppler shift associated with each line of this doublet was obtained experimentally by finding the doppler shift associated with the $2s^{2\,1}S_0$ -$2s2p^1P^\circ_1$ line in SXIII whose rest frame wavelength is very well established (Behring et al., 1976) and which was also prominent in the same beam-foil source. The Lyβ line in HeII from the hollow cathode source was used to calibrate the wavelength scale of the spectrometer in the spectral region of this berylliumlike sulfur (SXIII) resonance line. Table 1 summarizes our results for the measured wavelengths and doublet splitting in SXIV along with other laboratory and astrophysical determinations. It can be seen that we confirm the recent Skylab solar flare measurements.

The usual beam-foil time-of-flight technique was employed to measure the radiative lifetimes of the $2p^2P^\circ_{1/2,3/2}$ levels. A typical decay curve for the decay in flight of the $2p^2P^\circ_{3/2}$ level in SXIV is shown in Fig. 2. All such decay curves were found to be well fitted to a single exponential over several decay lengths indicating that cascading effects are negligible for these transitions. The present lifetime and derived oscillator strength results are shown in Table 2 along with the theoretical predictions of Kim and Desclaux (1976). It can be seen in the table that there exists a lifetime difference between the J=3/2 and 1/2 levels of the $2p^2P°$ term in SXIV as predicted by the relativistic multiconfigurational Hartree-Fock calculations of Kim and Desclaux (1976).

REFERENCES

Behring, W. E., Cohen, L., Feldman, U., Doschek, G. A., 1976, Ap. J., 203, 521.

Fawcett, B. C., 1970, J. Phys. B. 3, 1152.

Fawcett, B. C., 1975, Atomic and Nuclear Data Tables, 16, 135.

Kelly, R. L., and Palumbo, L. J., 1973, NRL Rept., No. 7599.

Kim, Y-K., and Desclaux, J. P., 1976, Phys. Rev. Letters, 36, 139.

Pegg. D. J., Elston, S. B., Griffin, P. M., Hayden, H. C., Forester, J. P., Thoe, R. S., Peterson, R. S., and Sellin, I. A., 1976, Phys. Rev. A (Sept. 1976).

Sandlin, G. D., Brueckner, G. E., Scherrer, V. E., and Tousey, R., 1976, Ap. J. (Letters), 205, L47.

Widing, K. G., and Purcell, J. D., 1976, Ap. J. (Letters), 204, L151.

Table 1. The Transition $2s^2S$ - $2p^2P°$ in SXIV.

Source	Wavelength (Å) 1/2-3/2	1/2-1/2	Doublet Splitting (cm^{-1}) $\sigma(^2P^o_{3/2} - {}^2P^o_{1/2})$
a	417.69	445.72	15,056
b	417.60	445.78	15,138
c	417.67	445.71	15,061
d	417.65	445.71	15,074

[a] Present work: (Absolute wavelength uncertainty ±0.03Å).
[b] Fawcett (1970): (Absolute wavelength uncertainty ± 0.03Å).
[c] Widing and Purcell (1976): (Absolute wavelength uncertaingy ±0.02Å).
[d] Average over 4 flares = 15,054 cm^{-1}.
Sandlin et al. (1976): (Absolute wavelength uncertainty ±0.03Å).

Table 2. Radiative Lifetimes and Oscillator Strengths in SXIV.

Wavelength (Å)	Transition	Lifetime of Upper Level (psec)	Oscillator Strength Present	Oscillator Strength Theory
417.69	$2s^2S_{1/2}-2p^2P^\circ_{3/2}$	767±39	0.068	0.064*
445.72	$2s^2S_{1/2}-2p^2P^\circ_{1/2}$	918±92	0.032	0.030*

*Kim and Desclaux (1976).

FIGURE CAPTIONS

Fig. 1 Portion of the beam-foil spectrum of a highly ionized sulfur beam (45.7 MeV) showing the $2s^2S$ - $2p^2P^\circ$ doublet in SXIV. The wavelengths of these doppler-shifted lines are corrected by making an independent wavelength measurement on the $2s^{2\,1}S$ - $2s2p\,^1P^\circ_1$ line in SXIII whose rest frame wavelength is well established.

Fig. 2 Typical spatial decay curve for the $2p^2P^\circ_{3/2}$ level in SXIV. Spatial coordinates are converted to temporal co-ordinates by dividing by the constant velocity of the post-foil beam.

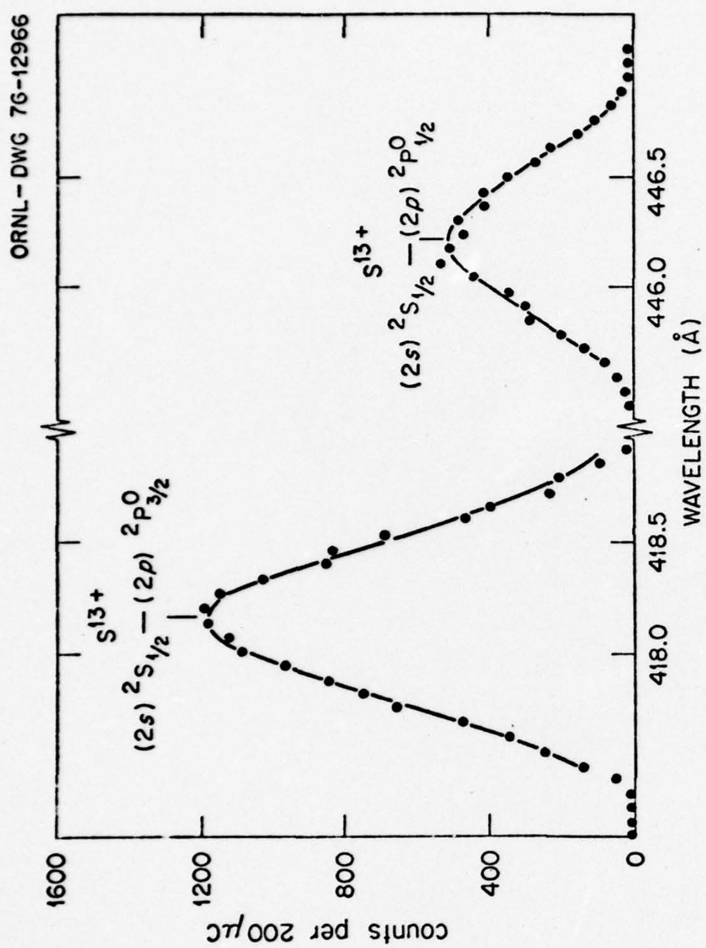
ORNL-DWG 76-12966
S^{13+}
$(2s)\ ^2S_{1/2} - (2p)\ ^2P^0_{3/2}$
S^{13+}
$(2s)\ ^2S_{1/2} - (2p)\ ^2P^0_{1/2}$
1600
1200
800
400
0
counts per 200 μC
418.0
418.5
446.0
446.5
WAVELENGTH (Å)

Fig. 1

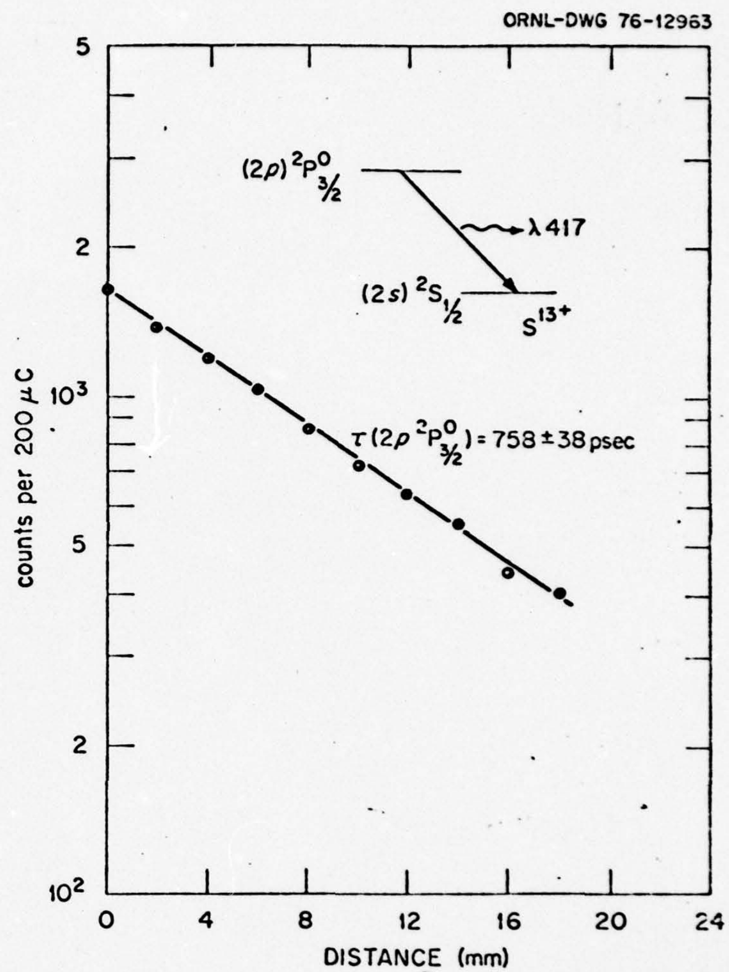
ORNL-DWG 76-12963
$(2p)\ ^2P^0_{3/2}$
λ417
$(2s)\ ^2S_{1/2}$
S^{13+}
$\tau(2p\ ^2P^0_{3/2}) = 758 \pm 38$ psec
5
2
10^3
5
2
10^2
counts per 200 μC
0
4
8
12
16
20
24
DISTANCE (mm)

Fig. 2

Radiative lifetimes and transition probabilities for electric-dipole $\Delta n = 0$ transitions in highly stripped sulfur ions*

D. J. Pegg, S. B. Elston, P. M. Griffin, H. C. Hayden,† J. P. Forester, R. S. Thoe, R. S. Peterson, and I. A. Sellin

University of Tennessee, Department of Physics, Knoxville, Tennessee 37916 and Oak Ridge National Laboratory, Oak Ridge, Tennessee 37830

(Received 27 May 1976)

The beam-foil time-of-flight method has been used to investigate radiative lifetimes and transition rates involving $\Delta n = 0$ allowed transitions within the L shell of highly ionized sulfur. The results for these transitions, which can be particularly correlation sensitive, are compared to current calculations based upon multiconfigurational models.

INTRODUCTION

Transition probabilities or, equivalently, absorption oscillator strengths (f values) for atoms and ions are fundamentally important atomic quantities which find frequent practical application in many areas of research, e.g., astrophysics, laser physics, and plasma physics. For example, there exists an urgent need at the present time for f values of resonance transitions of high-Z heavy ions which form impurities in magnetically confined thermonuclear plasmas.[1] These impurities, although only believed to be present in small concentrations, are thought to contribute strongly to radiative energy losses from the plasma.

Recent studies[2] of the systematic trends of dipole ($E1$) f values along isoelectronic sequences, which are based upon the nonrelativistic perturbation expansion of f values in terms of the inverse nuclear charge, have proven to be extremely valuable for low-to-intermediate-Z ions. Beam-foil results in this region have been very instrumental in the establishment of such trends along many sequences including the detection of certain f-value anomalies brought about by configurational level crossings or cancellations of transition integrands. It is in this region of low to intermediate Z that electron correlation effects can become important particularly for transitions in which the principal quantum number of the active electron does not change in the transition, i.e., $\Delta n = 0$ (intrashell) transitions. These intrashell or "shell-equivalent" transitions are particularly correlation sensitive owing to the interpenetration of the electrons of the same principal quantum number, and many-particle atomic models which include configuration mixing effects are used to replace the simple independent-particle picture. Correlation effects, although usually most important for low-Z ions, are not entirely negligible for such intermediate-Z ions as sulfur, which is being studied here. For some transitions, however, limited mixing with adjacent configurations of the same shell is found to be sufficient but this may not be the case for other transitions studied. The present work on $\Delta n = 0$ transitions within the L shell of sulfur ions represents a considerable extrapolation in nuclear charge along the isoelectronic sequences of all the transitions studied. Results for even higher-Z ions will be necessary in order that one may confidently extrapolate the existing nonrelativistic systematic curves into the very-high-Z region where relativistic effects on f values, such as orbital shrinkage and configurational effects involving the breakdown of the LS coupling scheme, become appreciable. Recent relativistic f-value calculations by Kim and Desclaux,[3] Weiss,[4] and Lin and Armstrong[5] indicate that in the cases of the Li and Be sequence, for example, the calculated f value for the resonance lines begins to depart significantly from the nonrelativistic value around $Z \sim 25$. A selected number of experimental beam-foil results in this uncharted relativistic regime could greatly serve to guide theoretical progress.

Comparisons of accurately measured electric dipole transition probabilities or f values with calculations of such quantities afford sensitive tests of the correctness of the wave functions in the upper and lower states of the transition. Two distinct types of allowed radiative processes can be distinguished. "Out-of-shell," intershell or $\Delta n \neq 0$ transitions, whose rates scale as Z^4 along an isoelectronic sequence and "in-shell," intrashell or $\Delta n = 0$ transitions, which scale linearly with Z. The $\Delta n \neq 0$ transitions become too rapid for the beam-foil time-of-flight method for large-Z low-N ions (N is the number of electrons) but $\Delta n = 0$ transitions remain accessible to beam-foil studies to surprisingly high Z owing, of course, to the considerably weaker Z-scaling dependence. It is these $\Delta n = 0$ transitions of the type $2s^2 2p^n$-$2s2p^{n+1}$ and $2p^n$-$2p^{n+1}$, within the L shell of sulfur, that are studied in the present work. Figure 1

shows a partial energy-level diagram of the $n=2$ manifold of states associated with the carbonlike ion S^{10+} to illustrate this type of transition.

Such $\Delta n = 0$ transitions are particularly important since they constitute, for example, the strong resonance lines of atoms and ions of the first and second rows of the Periodic Table. Many of the transitions studied in the present work are also prominent in the solar spectrum[6] and thus could find practical application in sulfur-abundance determinations, for example.

EXPERIMENTAL METHOD

The Oak Ridge National Laboratory tandem accelerator was used to obtain a magnetically analyzed 38-MeV sulfur-ion beam. The beam was collimated and sent through a thin carbon foil (~5 $\mu g/cm^2$ thickness) which served to both further strip and excite the beam ions. In this method, the beam-foil-excitation technique, the post-foil beam emerges in a distribution of charge states whose mean is determined by the incident beam energy. The charge state distribution for 38-MeV sulfur ions incident on a thin carbon foil is shown, as given by Wittkower and Betz,[7] in Fig. 2. Extreme ultraviolet (EUV) radiation emitted in flight by the decaying foil-excited ions was collected perpendicular to the beam direction and dispersed with the 2.2-m grazing-incidence spectrometer shown schematically in Fig. 3. The gold-coated (300 grooves/mm) concave grating used in the instrument has a blaze angle of 2°4′ (blaze wavelength of 191 Å at an angle of incidence of 87.5°). A hollow cathode discharge source, which is not shown in the figure, is situated directly opposite the entrance slit of the spectrometer. This source can be used to periodically calibrate the instrument during a run using, for example, the well-established resonance lines of He and He^+. A low-noise (~0.08 Hz) electron channel multiplier (channeltron) is positioned behind the exit slits of the spectrometer and a 90% transmission grid is used to bias out stray electrons. The spectrometer could be stepped in discrete and variable wavelength intervals and the detector output, which was normalized to a fixed amount of beam charge collected in a well-shielded Faraday cup, could be stored in a multichannel scaler that was synchronized with the stepping process. Examples of EUV spectra, taken at a fixed distance behind the foil, are shown in Figs. 4 and 5. The linewidths [full width at half-maximum (FWHM)] in these spectra, mostly instrumental in origin, are 0.75 Å. Doppler broadening of the lines due to the finite

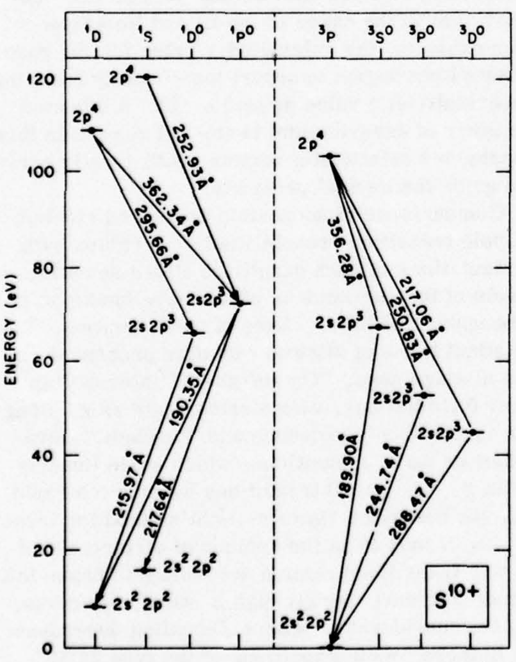

FIG. 1. Partial energy-level diagram showing $\Delta n = 0$ transition within the $n=2$ manifold of states in the carbonlike ion S^{10+}. The wavelengths shown are multiplet averages derived from Ref. 8.

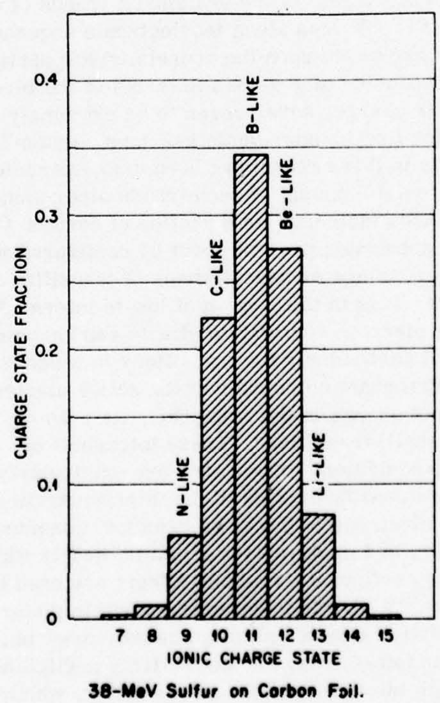

FIG. 2. Post-foil charge state distributions following the transmission of a 38-MeV sulfur-ion beam through a thin carbon foil.

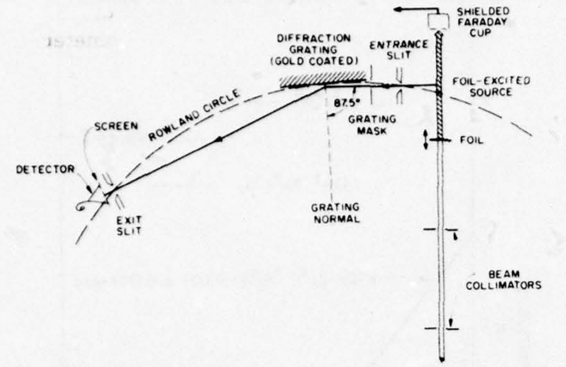

FIG. 3. Schematic diagram of the essential experimental arrangement used in the present work (not to scale).

but small entrance aperture was negligible in this spectral region. The spatial resolution along the beam, which is determined by the beam-spectrometer geometries, was 300 μm in this experimental arrangement. This corresponds to a temporal resolution of ~20 psec for a 38-MeV sulfur-ion beam.

Time-of-flight lifetime measurements were made on the most intense and unblended features by observing (photoelectrically) the intensity of a wavelength-selected line as a function of the spatial distance between the point of initial excitation, i.e., the back surface of the foil, and the viewing region of the spectrometer. The spatial decay can be converted to a temporal decay via the constant velocity of the beam. For transitions involving unity branching ratios, such lifetime measurements can be used to obtain the fundamentally important quantities, atomic transition probabilities (A_{ij}) or, equivalently, the multiplet oscillator strengths (f_{ji}), via the well-known relationships

$$A_{ij}=1/\tau_i$$

and

$$f_{ji}=1.4992\times10^{-16}\bar{\lambda}^2_{ij}(g_i/g_j)(1/\tau_i),$$

where τ_i is the lifetime of the upper state (sec), g_i, g_j are the statistical weights of the upper and lower states, respectively, and $\bar{\lambda}_{ij}$ is the average

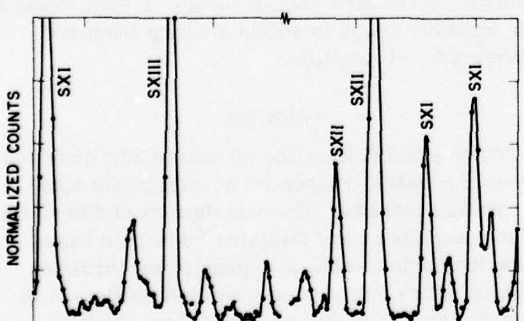

FIG. 4. Portion of an EUV spectral scan of the foil-excited sulfur source from ~250–300 Å. The incident beam energy is 38 MeV. The charge states of the most prominent features are shown. The linewidth of ~0.75 Å (FWHM) is almost entirely instrumental.

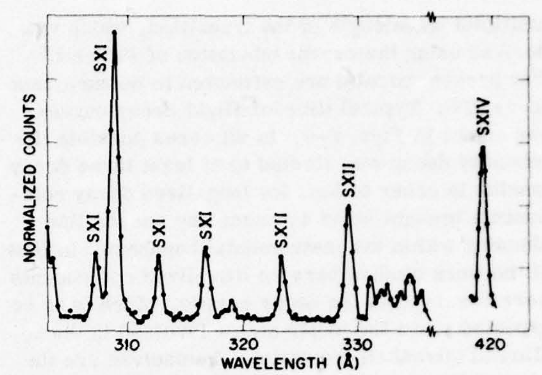

FIG. 5. Same as in Fig. 4 except wavelength interval from 300–420 Å.

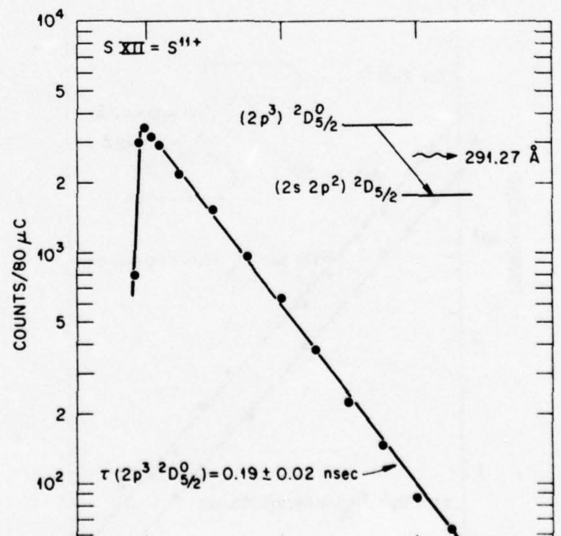

FIG. 6. Typical time-of-flight decay curve for an allowed $\Delta n=0$ transition in boronlike sulfur. The $x=0$ or foil surface position occurs at the intensity maximum. The spatial distance of 0.2 in. corresponds to a temporal delay of 336 psec using a 38-MeV sulfur beam. The semilog plot of this decay is seen to be linear over more than three decay lengths.

multiplet wavelength of the transition, which was derived using the recent tabulation of Fawcett.[8] The present results are estimated to be uncertain to ~ ±10%. Typical time-of-flight decay curves are shown in Figs. 6–8. In all cases possible the intensity decay was studied to at least three decay lengths in order to look for long-lived decay components brought about by cascading and/or line blending within the instrumental bandpass. In most of the work studied here no long-lived components were observed in the decay curves, which is to be expected since the upper states involved in these allowed intrashell transitions themselves are the longest-lived excited states of the ion. "Out-of-shell" cascade transitions, whose rates scale as a factor of Z^3 faster than the "in-shell" rates, are expected to "dump" their population very close to the foil. We were very careful in defining the point of excitation, i.e., $x = 0$, in these studies in order to try to observe very-short-lived cascade components but again, in most cases, cascading is not found to be a problem. Cascades, when present, are in-shell processes. Figure 6 indicates how the $x = 0$ position is defined by translating the foil slowly into the viewing region and recording the initial build-up in intensity to a maximum. This maximum corresponds to the viewing region being completely filled by the foil-excited beam source. In the other decay curves of Figs. 7 and 8 the intensity decay is shown starting from the measured $x = 0$ position.

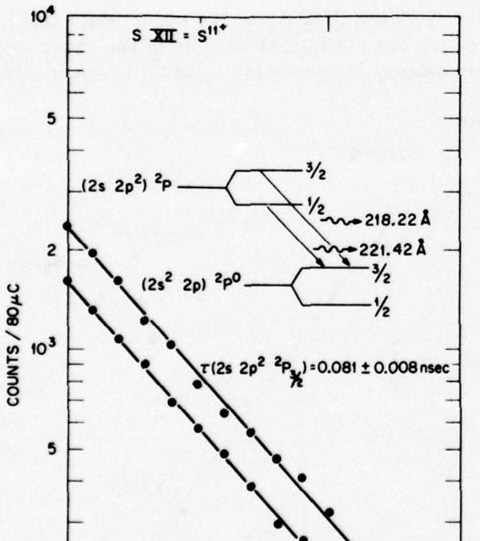

FIG. 7. Spatial decay-in-flight curves for resonance transitions in the boronlike sulfur ion, S^{11+}. The upper and lower decay curves represent the decay of the $J = \frac{3}{2}$ and $J = \frac{1}{2}$ levels, respectively. The semilog plots of the decays are both linear over more than three decay lengths.

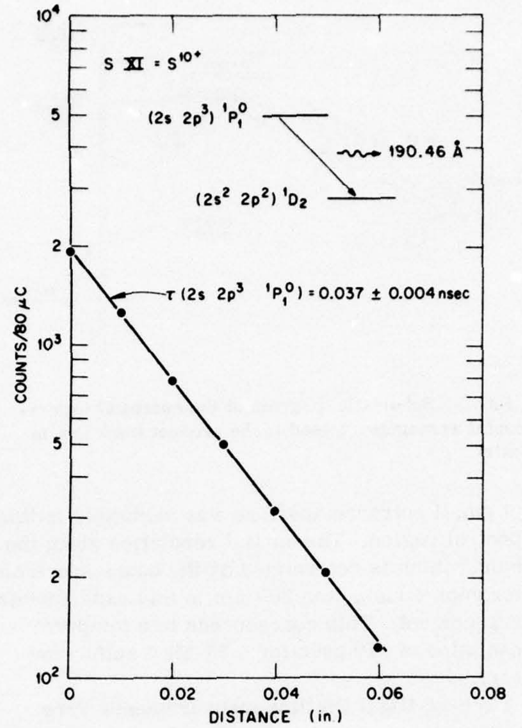

FIG. 8. Spatial decay-in-flight curve for the transition indicated in carbonlike sulfur, S^{10+}. The semilog plot of the decay is seen to be linear for ~ 100 psec which is equivalent to approximately three decay lengths.

RESULTS

Tables I and II show the measured lifetimes and transition rates, respectively, along with some theoretical results. The calculations of Safronova *et al.*[9] and Cohen and Dalgarno[10] are both based upon the nuclear-charge expansion perturbation method which includes only limited configuration interaction. For intermediate-Z ions such as sulfur, however, there appears little difference for most transitions between the results of Safronova *et al.*[9] and those of Sinanoğlu.[11] The latter results represent a more sophisticated electron correlation treatment (the results for sulfur ions are derived from a linear extrapolation of the f value that is quoted by Sinanoğlu[11] for isoelec-

TABLE I. Lifetimes in highly ionized sulfur.

Number of electrons	Wavelength (Å)	Upper level	Lifetimes (10^{-12} sec) Present [a]	Theory [b]
4	256.70	$(2s,2p)^1P_1^o$	160	135,[c] 129 [d]
4	308.95	$(2p^2)^3P_2$	168	168,[c] 156 [d]
5	288.39, 299.64	$(2s2p^2)^2D_{3/2,5/2}$	410	383,[c] 344,[d] 385 [e]
5	291.27	$(2p^3)^2D_{5/2}$	190	146 [c]
5	218.23, 221.44	$(2s2p^2)^2P_{3/2,1/2}$	81	50,[c] 46,[d] 48 [e]
5	243.00	$(2p^3)^4S_{3/2}^o$	90	54,[c] 49 [d]
6	190.46	$(2s2p^3)^1P_1^o$	39	29,[c] 32 [e]
6	216.00	$(2s2p^3)^1D_2^o$	73	47,[c] 41,[d] 77 [e]
6	188.69	$(2s2p^3)^3S_1^o$	35	23,[c] 21,[d] 22 [e]
6	247.10	$(2s2p^3)^3P_1^o$	150	136,[c] 114,[d] 133 [e]
6	295.59	$(2p^4)^1D_2$	70	72,[c] 67 [d]
7	180.77	$(2s2p^4)^2P_{3/2}$	23	20,[c] 19 [e]

[a] Estimated uncertainty, ±10%.
[b] Average wavelengths used in conversion from Ref. 8.
[c] Reference 9.
[d] Reference 10.
[e] Reference 11.

tronic silicon ions). It can be seen from the tables that, in general, the measured lifetimes are longer than predicted by current theory by up to 40%. Of course, transition probabilities, where derivable, are lower than corresponding theoretical predictions by the same amount. Since cascading and/or blending do not in general appear to be a major problem in the present experiments, it is suspected that insufficient mixing effects have been taken into account in the multiconfigurational calculations. In cases such as the $(2s2p)^3P^o$-$(2p^2)^3P$ transition in the Be sequence (S^{12+}), where configuration mixing is expected to be very small, there exists excellent agreement between theory and the present result. In contrast, however, the measured transition probability for the $(2s^22p)^2P^o$-$(2s2p^2)^2P$ transition in the B sequence (S^{11+}) is found to be ~40% lower than the current theoretical values. In addition, this difference between theory and beam-foil measurements appears to continue, by roughly the same amount, to lower-Z members of the sequence for this particular transition. Strong mixing effects between the ground-state $2s^22p^n$ and the excited-state configurations $2p^{n+2}$ (same parity and within the same shell) will occur, particularly for the low-Z end of the sequences. Mixings between L-shell configurations and higher-shell configurations are expected to be small especially for intermediate-Z ions such as sulfur.

TABLE II. Transition probabilities for some allowed $\Delta n = 0$ transitions of highly ionized sulfur.

Number of electrons	Transition	Transition probability (10^9 sec^{-1}) Present [a]	Theory [b]
4	$(2s^2)^1S$-$(2s2p)^1P^o$	6.25	7.42,[c] 7.77 [d]
4	$(2s2p)^3P^o$-$(2p^2)^3P$	5.95	5.96,[c] 6.40 [d]
5	$(2s^22p)^2P^o$-$(2s2p^2)^2D$	2.44	2.61,[c] 2.90,[d] 2.60 [e]
5	$(2s^22p)^2P^o$-$(2s2p^2)^2P$	12.35	19.80,[c] 21.65,[d] 20.79 [e]
5	$(2s2p^2)^4P$-$(2p^3)^4S^o$	11.11	18.45,[c] 20.35 [d]
6	$(2s^22p^2)^1D$-$(2s2p^3)^1D^o$	13.70	21.45,[c] 24.64,[d] 13.01 [e]
6	$(2s^22p^2)^3P$-$(2s2p^3)^3S^o$	28.57	44.39,[c] 47.79,[d] 45.21 [e]
6	$(2s^22p^2)^3P$-$(2s2p^3)^3P^o$	6.67	7.35,[c] 8.74,[d] 7.51 [e]

[a] Estimated uncertainty, ±10%.
[b] Average wavelengths used in conversion from Ref. 8.
[c] Reference 9.
[d] Reference 10.
[e] Reference 11.

*Research supported in part by the National Science Foundation, by the Office of Naval Research, by the National Aeronautics and Space Administration, and by Union Carbide Corporation under contract with the U. S. Energy Research and Development Agency.

†Permanent address: Dept. of Physics, Univ. of Connecticut, Storrs, Conn. 06268.

[1]E. Hinnov, Princeton University Report No. MATT-1022, 1974 (unpublished).

[2]W. L. Wiese and A. W. Weiss, Phys. Rev. 175, 50 (1968); M. W. Smith and W. L. Wiese, Astrophys. J. Suppl. No. 196, 23, 103 (1971).

[3]Y. K. Kim and J. P. Desclaux, Phys. Rev. Lett. 36, 139 (1976).

[4]A. W. Weiss, in *Beam-Foil Spectroscopy*, edited by I. A. Sellin and D. J. Pegg (Plenum, New York, 1976), Vol. I.

[5]D. L. Lin and L. Armstrong, Jr., Bull. Am. Phys. Soc. 21, 626 (1976).

[6]M. Malinovsky and L. Heroux, Astrophys. J. 181, 1009 (1973).

[7]A. B. Wittkower and H. D. Betz, At. Data Tables 5, 113 (1973).

[8]B. C. Fawcett, At. Data Nucl. Data Tables 16, 135 (1975).

[9]U. I. Safronova, A. N. Iranova, and V. N. Kharitonova, Theor. Exp. Chem. (USSR) 5, 209 (1969).

[10]M. Cohen and A. Dalgarno, Proc. R. Soc. A 280, 258 (1964).

[11]O. Sinanoğlu, Nucl. Instrum. Methods 110, 193 (1973).

AN EXPERIMENTAL SURVEY OF ELECTRON TRANSFER IN keV COLLISIONS OF MULTIPLY CHARGED IONS WITH ATOMIC HYDROGEN

J.E. Bayfield, P.M. Koch and L.D. Gardner*

Physics Dept., Yale University, New Haven, Conn. 06520

I.A. Sellin, D.J. Pegg and R.S. Peterson**

Physics Dept., University of Tenn., Knoxville, Tenn. 37916

D.H. Crandall***

Oak Ridge National Laboratory, Oak Ridge, Tennessee 37830

The ORNL Penning Ion Source Facility[1] has been coupled with a new apparatus containing the Yale atomic hydrogen scattering target[2] to measure various kilovolt energy electron transfer cross sections. The extension of earlier measurements with proton and helium ion beams[3] to heavier multiply charged species is of fundamental interest as a further test of theoretical calculations. Cross sections for multiply charged C, N and O ions are also needed for the assessment of impurity problems in thermonuclear fusion devices. As the electron transfer is expected to be primarily into excited states, future X-ray laser applications may arise.[4]

The basic procedures for making the measurements follow those previously developed.[2,5] The charge-selected ion beam was initially brought into 10^{-8} Torr vacuum, then magnetically reanalyzed, collimated to an angular spread of 1 mrad, and passed through the target at a pressure of 10^{-5} Torr. Cross sections for cold H_2, cold Ar and hot Ar targets were measured in addition to (hot) H. Dissociation fraction values of nominally 90% were routinely measured using a variation of the double electron capture technique[2,5], employing B^{3+} incident ions. A large parallel plate electrostatic analyzer was used to separate scattered and incident charge states. Ion-counting detection involved a Johnston MMI particle multiplier. The absolute target thickness was determined by a number of calibration runs on He^{++} + Ar, $He^{++} + H_2$, B^{3+} + He and $B^{3+} + H_2$, processes where previous independent absolute measurements exist. The present absolute cross section values are believed accurate to better than ±30%.

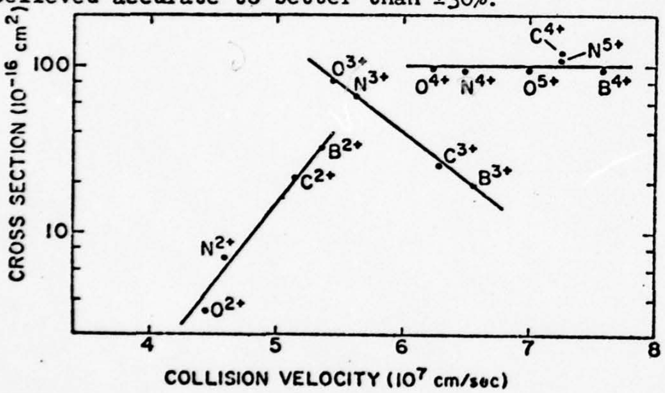

Figure 1.

Figure 1 shows values of the cross sections for fourteen incident ions, obtained at a single Penning Facility accelerator voltage. The energy dependences for $B^{2+,3+,4+}$ have also been obtained. The interesting features of the data shown are first that the cross sections for ion charges >3 are 10^{-14} cm^2, quite large. Second, the 2+, 3+ and 4+ points each lie on curves, suggesting that a simple theoretical model for these electron transfer processes might be found. As the electron transfer for incident 3+, 4+ and 5+ is expected to be into unfilled shells of the final state ion, one-electron initial and final states should make these processes amenable to calculation.

This research is supported by *The Physical Research Division of ERDA, **NSF and ***ERDA under contract with Union Carbide Corp.

1. M.L. Mallory and D.H. Crandall, to be published.

2. J.E. Bayfield, Rev. Sci. Instr. 40, 869 (1969).

3. J.E. Bayfield, in Atomic Physics IV, G. zu Putlitz et al., editors, Plenum Press, 1975, pages 397-434.

4. W.H. Louisell, M.O. Scully and W.B. McKnight, Phys. Rev. A11, 729 (1975).

5. J.E. Bayfield, Phys. Rev. 185, 105 (1969).

10

LIFETIMES AND TRANSITION RATES FOR ALLOWED "IN-SHELL" TRANSITIONS IN HIGHLY STRIPPED SULFUR*

D. J. Pegg, S. B. Elston, J. P. Forester, P. M. Griffin,
H. C. Hayden†, R. S. Peterson, I. A. Sellin and R. S. Thoe

University of Tennessee, Knoxville, Tennessee
and
Oak Ridge National Laboratory, Oak Ridge, Tennessee

An experimental study of allowed "in-shell" ($\Delta n=0$) transitions of the type $2s^22p^n$-$2s2p^{n+1}$ and $2p^n$-$2p^{n+1}$ has been made on highly stripped ions of sulfur containing 4, 5, 6 and 7 electrons. The present oscillator strength (f-values) results represent a considerable extension in nuclear charge over previous work for all the isoelectronic sequences studied. Accurately measured f-values for these "in-shell" transitions provide an excellent testing ground for many-particle atomic structure calculations since such calculated values are sensitively dependent upon the amount of configuration mixing included in the wavefunctions of the upper and lower state of the transition. For high Z, highly stripped ions, however, this configuration interaction is usually limited to configurations within the same shell. In addition, the present results should find application in solar physics since many of the transitions studied produce prominent lines in the "quiet-sun" spectra of the solar corona.

The Oak Ridge National Laboratory tandem accelerator was used to produce a high energy ($\sim$ 38 MeV) sulfur beam which was further stripped and foil-excited for time-of-flight lifetime measurements. Transition probabilities and f-values were obtained from the lifetime results wherever possible. The present results are in good agreement with many-particle calculations where limited configuration interaction effects are expected. However, in other cases, for example, the $(2s^22p)^2P^0$-$(2s2p^2)^2P$ transition in boron-like sulfur, the difference between the measured f-value and current theoretical calculations incorporating some configuration interaction is as much as 40%, a trend which appears to be present throughout the isoelectronic sequence for this transition.

*Research supported in part by the National Science Foundation, Office of Naval Research, National Aeronautics and Space Administration and by Union Carbide Corporation under contract with the Energy Research and Development Agency.

†Permanent address, Department of Physics, University of Connecticut, Storrs, Connecticut.

LIFETIME MEASUREMENT OF THE S
ULTRAVIOLET LASER EXCITATIO

A. Arnesen, A. Bengtson, L.
C. Nordling and T. Noreland

Institute of Physics, Univer
S-751 21 Uppsala 1, Sweden

The possibility to make
lifetime measurements of at
excitation of a fast ion be
H. J. Andrä et al. in Berlin
tuning have been used in thi
tuning of fixed frequency la
dye lasers.[2,3]

The work reported here is
tuning method. A 45 KeV Sc^+
ground state to the z $^3F^o_2$ le
The 363.8 nm laser line was
transition by setting the in
two beams at 22.7° as is sho
intensity as a function of d
excitation region was measur
system, movable parallel to
curve is shown in fig. 2. Th
fitting the experimental dat
$A + B\exp(-t/\tau)$, where A repr
The final result, including
velocity uncertainties, is pr
with other measurements and t

Table 1. Experimental and the
lifetime, τ(ns) of the 3d 4p

This work	Other experi
6.2 ± 0.2	5.5 ± 0.6
	6.5[b]

a) Buchta et al. (ref.4) bea
b) Corliss and Bozman (ref.5
c) Weiss (ref.6) SOC and Kur
d) Warner (ref.8) Coulomb ap

§ on leave from University of

NUCLEAR INSTRUMENTS AND METHODS 132 (1976) 397–404; © NORTH-HOLLAND PUBLISHING CO.

Part VII. Photon emission

APPLICATIONS OF BEAM-FOIL SPECTROSCOPY TO ATOMIC COLLISIONS IN SOLIDS*

I. A. SELLIN

The University of Tennessee, Knoxville, Tennessee, U.S.A.
and
Oak Ridge National Laboratory, Oak Ridge, Tennessee, U.S.A.

An account of some highlights of the Fourth International Conference on Beam-Foil Spectroscopy of particular pertinence to ionic collision phenomena in solids is given.

The overlap between the sciences of beam-foil spectroscopy and of atomic collisions in solids primarily arises in the description of excitation states, decay modes, scattering, and energy losses of projectile ions created during passage through or upon emergence from thin foil targets. The present article will mainly summarize results presented at the Fourth International Conference on Beam-Foil Spectroscopy[1]) (held September 15–19, 1975 in Gatlinburg, Tennessee) which seem of particular pertinence to the community of scientists interest in ionic collision phenomena in solids, but which have not already been discussed in the papers of Datz[2]) and Betz[3]) at the present conference. Time limitation necessitates the omission of much pertinent material in favor of a detailed discussion of a small number of topics.

Before passing on to such selected topics, it is well to note the larger number and diversity of papers presented in Gatlinburg, which are of interest to students of atomic collisions in solids. We list several examples, details concerning which will appear in the conference proceedings[1]).

Sørensen discussed a number of solid target effects which complicate the measurement of excited projectile ion lifetimes for low energy heavy element ions, and how to surmount them[4]). In particular, foils lasting at best but a few seconds under impact of microampere beam of ≈ 50 keV heavy elements can be made to last substantially longer, even with an order of magnitude increase in current, by using a continuously sliding foil technique described in his talk. In such experiments, the energy loss is appreciable (often $\gtrsim 25\%$) compared to the beam energy itself, a phenomenon whose effect on lifetime measurements is complicated by dose-dependent foil thickening of the irradiated portion of the foil. Such energy loss and thickening phenomena are now studied by comparing the Doppler shift of a foil-excited spectral line with that of a line excited in a gas cell, also in the spectrometer viewing region. In a study with similar technical motivations, Astner et al.[5]) reported using a two-spectrometer, quantum beat technique to calibrate the time scale after foil excitation to a known fine-structure separation in the $3p\,^3P$ state of neutral helium. The second spectrometer can then be tuned to another transition of interest, whose decay length or quantum beat intensity fluctuation vs length periodicity can then be measured relatively. Forester et al.[6]) noted that relative Doppler shifts are significantly larger fractionally in the case of Auger spectroscopy of electrons emitted by projectile ions because the ratio of beam velocity v_p to electron velocity is $\gg v_p/c$, leading to yet a third method of measuring dose-dependent energy loss and foil thickening phenomena.

The extension of lifetime measurements by direct decay in flight measurements to ≈ 1 ps with accuracies ≈ 20–30% was reported at the conference by scientists from the Université Laval[7]) and from the Kansas State University[8]). In the Laval experiments, revised placement of defining entrance slits to a grazing incidence xuv spectrometer of width $\gtrsim 10\,\mu$m combined with the careful use of flat foils permitted lifetime measurements in xuv emitting states of highly ionized ions ranging from B to F. In experiments on the lifetime of the $1s2p\,2^3P_1$ state of heliumlike sulfur (which decays by a spin-forbidden E1 transition to the 1^1S_0 state), a Doppler tuned spectrometer with $20\,\mu$m spatial resolution was used by Varghese et al.[8]) to measure a lifetime of (1.7 ± 0.3) ps. The dynamic range of beam-foil lifetime measurements has thus been extended to a full six decades, ranging from $\approx 1\,\mu$s to 1 ps. The short lifetime end of this range thus adjoins the range of

* Work supported in part by the Office of Naval Research; by the National Science Foundation; by the National Aeronautics and Space Administration; and by the Energy Research and Development Administration under contract with Union Carbide Corporation.

the foil thickness dependence, lifetime measurement technique described by Betz[3]).

In another area of interest to participants at this conference, Beauchemin and Drouin[9]) presented data on the angular behavior of stopping powers of carbon foils for argon ions between 40 and 240 keV. The dependence of dE/dx vs θ upon foil thickness (4–14 $\mu g/cm^2$) and on beam energy was studied in detail. Among the principal conclusions is that the bulk of the discrepancies with the total stopping power values given by the theory of Lindhard, Scharff, and Schiøtt[10]) (which does not refer to a particular angle of emergence) disappears if an average over θ is carried out, although serious discrepancies remain at beam energies below 100 keV.

In other stopping power measurements, Wehring and Bucher[11]) reported the energy loss of fission fragments as a function of atomic number Z_1, using K X-ray detection as a fragment signature, and compared their results to earlier theoretical and experimental data.

Electron emission accompanying the passage of heavy particles through solid targets was discussed by Groeneveld[12]) and by Meckbach[13]). Groeneveld reviewed electron emission from solid targets under bombardment with projectiles ranging from $Z = 1$ to $\bar{Z} \approx 55$ (fission fragments) having energies between about 1 MeV and 70 MeV. The number N of emitted electrons per projectile, integrated over all electron energies and angles, is found to be roughly proportional to dE/dx, and to depend on both target thickness and work function of the target surface. Typical emergent electron energy distributions are found to exhibit monotonic decrease with electron energy, a sharp drop in N at electron velocities equal to the projectile velocity ($E_{e_1} = E_0$), dependence of the slope $N(E_{el} > E_0)$ on target electron binding energies, and superposed Auger electrons characteristic of both projectile and target ions. In general, the binary encounter model, taking into account the energy loss of the electrons inside the target material, seems to provide satisfactory agreement with the experimental data for light projectiles.

Emergent electron number and energy distributions for projectiles below 1 MeV incident on thin solid targets was reviewed by Meckbach[13]), with particular attention to the total number of electrons per unit energy emitted into the forward vs backward hemisphere subsequent to passage of ≈ 100 keV protons through carbon foils. In fig. 1, the differential secondary electron emission coefficient for forward emitted electrons (eV^{-1}) as measured by Meckbach et al.[13]) is plotted vs secondary electron energy for incident proton energies of 41.5 keV (curve A) and 257 keV (curve B). Curve C gives the differential distribution in the backward hemisphere, also for 257 keV protons. As can be seen, the forward emitted electrons appear to obey a $\sim E_{el}^{-\frac{3}{2}}$ power law dependence on electron

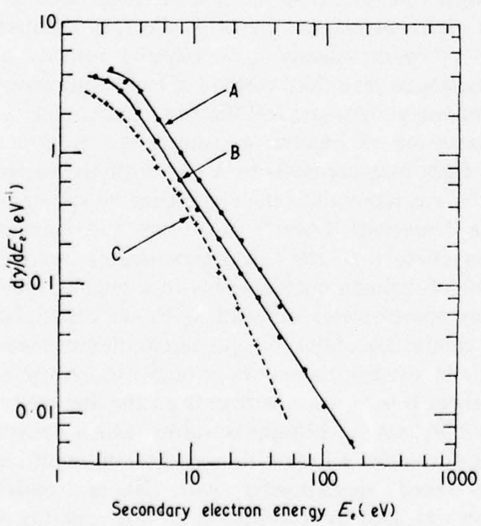

Fig. 1. Differential secondary electron emission coefficient for protons in C foils incident at 41.5 keV (curve A), and 257 keV (curves B and C). Curves A and B refer to the forward hemisphere, and C to the backward hemisphere. From ref. 13.

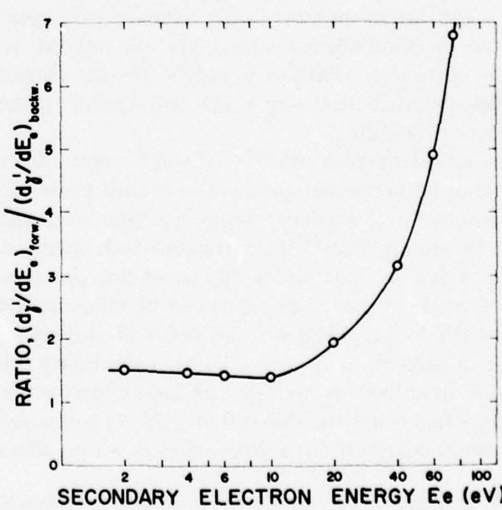

Fig. 2. Ratio of forward to backward differential secondary electron emission coefficients as a function of emitted electron energy. From ref. 13.

energy over much of the range of electron energies studied. Interestingly, the electrons emitted in the backward hemisphere exhibit a similar electron energy dependence. The ratio (>1) of forward to backward emitted electron fluxes has been in part successfully interpreted by Meckbach in terms of electron capture into continuum states, as is well known to occur in gas targets. Fig. 2 shows the rapid rise in the ratio of forward to backward differential coefficients beginning at about 10 eV. This onset matches a similar rise in estimates of total stopping power for secondary electrons traversing solid materials at about the same electron energy. Secondary electron emission studies subsequent to H^+ and H_2^+ passage through thin carbon foils was also discussed by Menendez and Duncan[14]) for beam energies between 350 keV and 1 MeV and foils between 5 and 50 $\mu g/cm^2$ in thickness. Particular attention was paid to the narrow angular distribution of electrons emerging from the foil at velocities $\sim v_p$.

Both the energy loss and yield accompanying the passage of fast molecular clusters in solid targets was reviewed by Laubert[15]). The extent to which projectiles moving as clusters through solid targets lose energy more rapidly than isolated particles of the same velocity was quantitatively discussed, together with very recent work on the yield of beam molecules after penetration through carbon foils.

Models for excited state distributions and for

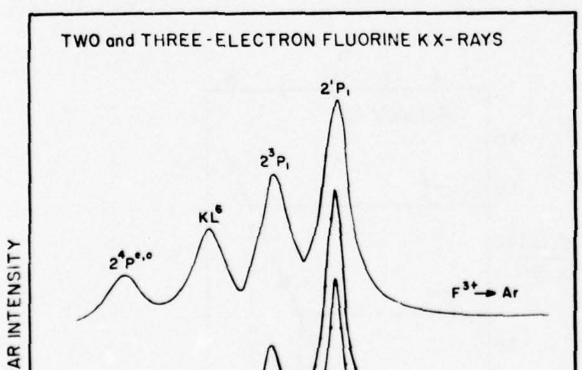

Fig. 3. Heliumlike and lithiumlike fluorine K X-ray line intensities from F^{3+} projectiles in gaseous Ar, C foil, and solid graphite, respectively, at energy ≈ 1 MeV per nucleon. From ref. 20.

consequent effective lifetimes for highly excited ions emergent from foils were discussed by Bukow et al.[16]) and by Hopkins and von Brentano[17]), the latter of which authors paid particular attention to the form of the so-called slow, non-exponential, $\sim t^{-\frac{3}{2}}$ decay feeding from high n, y-rast levels ($l \sim n-1$) into faster-decaying excited states whose delayed decays then mimic a $\sim t^{-\frac{3}{2}}$ dependence. In the limit of high principal quantum number n, a relative population $\propto n^{-5}$ is estimated by Hopkins and von Bretano for systems such as hydrogenic oxygen and fluorine, whereas an excited state population dependence nearer n^{-3} for foil excited, low-lying He states was described by Bukow et al[16]).

Variations in the ratio of intensities of lines from forbidden vis a vis allowed transitions between the same electron configurations are much used in astrophysical interpretations of collisional quenching of metastable excited states [cf. the review article by Jordan[18])]. Similarly, the variation in ratios can be used to infer excited state collision quenching cross-sections in beam experiments with either gaseous or solid targets. A particularly useful pair of lines is the $1s^2\,{}^1S_0$–$1s2p\,{}^{1,3}P_1$ transitions in heliumlike ions like F^{7+}, which can easily be excited by passing fluorine ions through carbon foils at energies ≈ 1 MeV/nucleon. The ${}^1P_1$ lifetime of 1.8×10^{-13} s is well known from standard tables, and the ${}^3P_1$ intercombination line lifetime of (0.56 ± 0.03) ns is well established from the work of Mowat et al.[19]). Studies reported in Gatlinburg by Matthews and Fortner of the variation with pressure of the ratios of the ${}^{3,1}P_1$ line intensities excited in an argon gas target led to a measured quenching cross-sections for ${}^3P_1$ states in argon of $\sigma_Q^T \cong 1\times10^{-16}\,cm^2$. Comparison of line intensity ratios in solid vs gas targets leads to a number of interesting further conclusions, some of which are depicted in fig. 3. Relative intensities of ${}^{1,3}P_1$ transitions as presented by Matthews and Fortner[20]) are seen to be quite different for C foils and thick graphite targets (for graphite the ${}^3P_1$ transition is very weak). Interpretation of such data led the authors to estimate a quenching cross-section for the singlet state in C foil targets of $\sigma_Q^S \cong 8\times10^{-18}$ cm. While the fluorescence yields of both ${}^{1,3}P_1$ states are essentially unity in vacuo, a simple definition of a so-called "dynamic fluorescence yield", $\omega_D = (1/\tau_R)/[(1/\tau_R)+N\sigma_Q v]$, where τ_R is the normal radiative lifetime, N the target number density, and v the beam velocity, permits extraction of a value for $\omega_D({}^3P_1)$ for solid targets of $\cong 10^{-6}$, and of $\omega({}^1P_1)$ of ≈ 0.07. A more complete spectrum obtained by these authors is given in fig. 4, which exhibits spectra obtain-

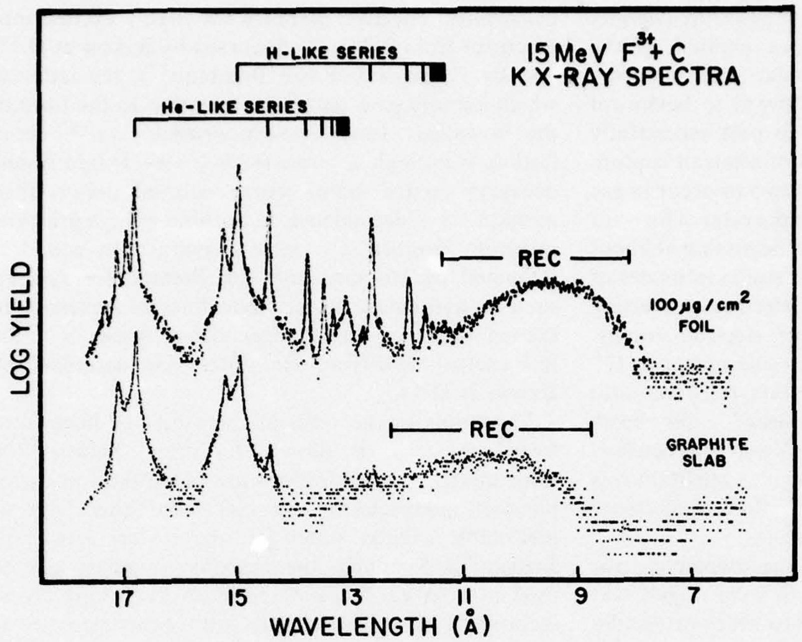

Fig. 4. Comparative yields of projectile K X-rays from 15 MeV F^{3+} projectiles in 100 $\mu g/cm^2$ C foils and a solid graphite target, respectively. From ref. 20.

ed with 15 MeV F^{3+} beams incident on 100 $\mu g/cm^2$ C foils and thick graphite targets, respectively. A number of hydrogenic and heliumlike spectral lines are observed. In comparing foil yields with those of thick targets, a reduction in 1s–3p line strength relative to 1s–2p line strength by more than a factor of three was observed, and no higher Rydberg states above $n = 3$ were apparent with the thick target. Hence line strength ratios for various states as a function of target thickness promise to be a useful tool in studying excited state collision kinetics in solids.

In similar experiments but at lower beam energies, Fortner et al[21]) reported studies of collision broadening of X-rays emitted from ≈ 100 keV ions moving in solids. High resolution K X-ray spectral measurements for boron and neon projectiles moving in gas and solid targets were reported. Comparisons of the spectra indicated little or no structure when solid targets were used. This lack of structure in the solid target spectra was attributed to collisional broadening which results from multiple collisions taking place within the lifetime of the inner shell vacancy. The collisional broadening was studied as a function of target density by using both graphite and diamond targets. The amount of broadening was found to be very sensitive to target density. K X-ray spectra were also reported for a neon gas target and a neon target implanted in

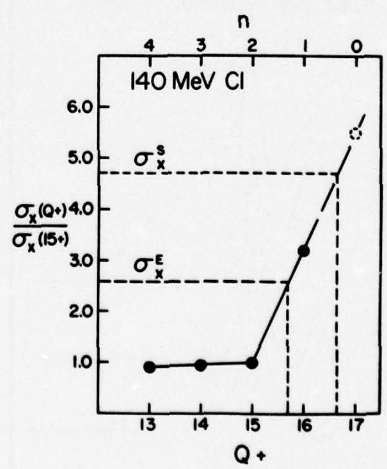

Fig. 5. Cu K X-ray yields from 140 MeV Cl ions on ≈ 1 $\mu g/cm^2$ Cu targets as a function of incident ion charge state. The Cu K yield from ions emergent from a C "pre-foil" 24 cm upstream is indicated by σ_x^E, and the Cu K yield from ions emergent from a ≈ 200 $\mu g/cm^2$ carbon foil directly on to a 1 $\mu g/cm^2$ Cu target is indicated by σ_x^S. From ref. 22.

graphite. Although no collisional broadening was observed, the binomial intensity distribution of X-ray lines from different charge states often observed for such spectra was not seen in the implanted target spectra.

Recent results of Hopkins[22]) concerning residual K-shell excitation in chlorine ions penetrating carbon received informal discussion at the conference. Some results are included here, as they are related to the matter of projectile charge state-increase upon emergence from solid targets as discussed by Datz[2]) and in fact suggest a projectile charge state increase of ≈ 0.5 to 1 unit. In fig. 5, Cu K X-ray yields subsequent to impact of 140 MeV Cl ions in various charge states on $\approx 1\ \mu g/cm^2$ Cu targets are shown. The Cu K-yields are seen to be sensitive only to K vacancies in the incident Cl ions, and only weakly to L vacancies. When an upstream "pre-foil" target is used as in the experiment of Datz et al.[23]), yields characteristic of an emergent charge state distribution with $\bar{q} \cong 15.7$ are obtained, and are labelled σ_x^E. When a $\approx 200\ \mu g/cm^2$ carbon foil is directly upstream of the Cu and in contact with it, a large increase in yield occurs and is attributed to steady state K vacancies in the Cl beams as is indicated by the level labelled σ_x^S. The ratio σ_x^S/σ_x^E is plotted in fig. 6 for two different Cl beam energies as a function of upstream carbon layer thickness, as well as for 78 MeV F beams (for which there is a null effect). The corresponding K-vacancy fractions Y as a function of carbon thickness are estimated in parts (b) and (c) of fig. 6, and reach values $\approx 80\%$ for 140 MeV incident beam energy. Depending on assumptions concerning fluorescence yields, a charge increase upon emergence of $\gtrsim \frac{1}{2}$ unit can be inferred from the 70 MeV data, and perhaps a larger increase for the 140 MeV data. In fig. 7, the summed yields of the 1s2s2p ^4P lithiumlike and the 1s2p 2^3P_2 heliumlike X-ray decays at 70 MeV, which are the dominant K X-ray yields over the 1–3 cm distance range of intensity integration downstream of the foil, are seen to exhibit a relative yield which is well described by the K-vacancy equilibrium curve seen in fig. 6. Hence the metastable X-ray emitting levels emergent from the foil seem to be indicative of the corresponding inner shell vacancy distribution while the ion is inside the target. An interesting variation of equilibrium K-vacancy fraction with upstream target material is seen in fig. 8. As yet, no detailed explanation of this dependence is available.

The X-ray spectrum of quasi molecules[24]), which arises from the radiative filling of a K vacancy during a close collision, is intimately linked to study of collisions in solids. Whether a double collision mechanism is required[25]), in which a vacancy created

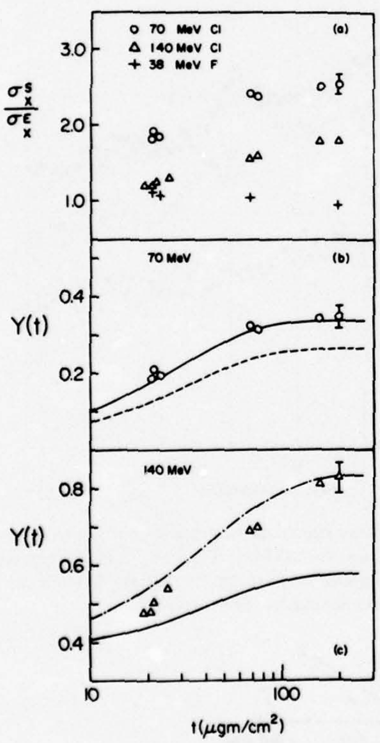

Fig. 6. Ratios σ_x^S/σ_x^E (a) at 70 and 140 MeV for incident Cl, and at 38 MeV for incident F, as a function of carbon layer thickness. (b) and (c) describe conversions of the data in (a) to estimated K-vacancy yields. The theoretical curves indicated are described in ref. 22.

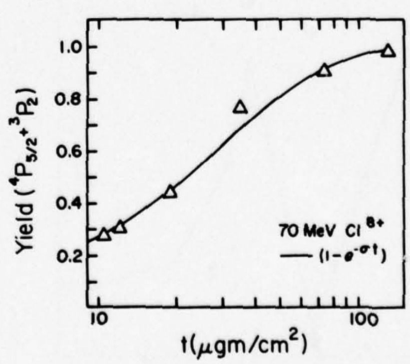

Fig. 7. Relative yields for 70 MeV Cl beams traversing C foils of the sum of the projectile K X-rays resulting from lithiumlike $^4P_{5/2}$ and heliumlike $^3P_2$ decays between 1 and 3 cm downstream of the foils. The relative yield is fairly well described by the K-vacancy yields in fig. 6. From ref. 22.

in a prior collision is brought into a second close collision within a K-hole lifetime during which radiative filling occurs, is a much debated issue. Recently, Bell et al.[26]) have published evidence for single collision production in which the vacancy production and radiative filling occur during the same collision, for 48 MeV S on Ne encounters. Comparison of the intensity of MO tails for 48 MeV S on Ne at ≈ 1 torr vs 55 MeV S on 100 $\mu g/cm^2$ Al foils, normalized to the strength of the S characteristic K radiation in each case, led to the conclusion (because of the equally intense tails) that single collision production was an important consideration in both cases.

At the Gatlinburg conference, however, Peterson et al.[27]) presented comparisons of 40 MeV Si on gaseous SiH_4 targets at 300 mtorr with 40 MeV Si on Al, again normalizing to the projectile characteristic line strength. Fig. 9 shows the region of the continuum X-ray spectrum near the united atom limits indicated by the corresponding arrows. (The small peaks are thought to arise from Coulomb excitation of trace impurities some five orders of magnitude less intense than the characteristic lines of projectile and target.) As can be seen, there is at least one order of magnitude difference in intensity, leading to a supposition of double collision processes being dominant in this case. Because of the similarity or projectile Z and beam energy, it is difficult to reconcile the dissimilar results.

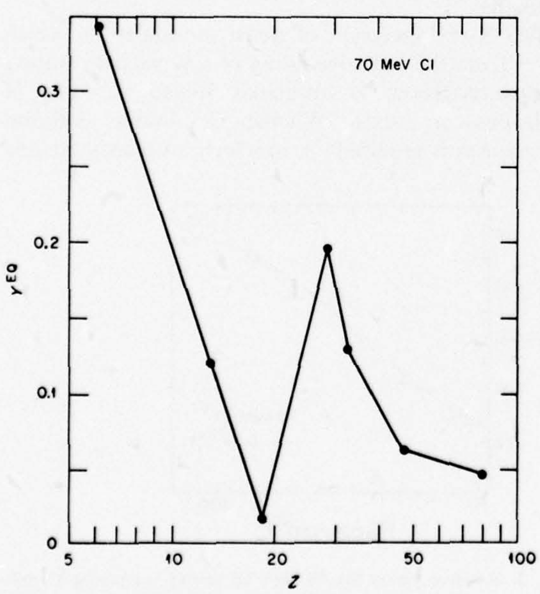

Fig. 8. Equilibrium K-vacancy yields for C, Al, KCl, Ni, Ge, Ag, and Au targets as determined in 1 $\mu g/cm^2$ Cu layers evaporated on their downstream side. From ref. 22.

Normalization to the characteristic line strengths in both experiments may be tricky because of significant differences in the fluorescence yields of the solid vs gas data. Until the differences can be resolved, it seems unlikely that any firm conclusions relative to one-vs-two-collision process dominance for similar collisions can be reached.

The emergent surface interaction in beam-foil spectroscopy is the final subject discussed at the Gatlinburg conference to be treated here. It first became clear from the work of Sellin et al.[28]) following a suggestion of Eck[29]) that atoms emergent from foils (in this case H atoms on C) do not emerge in eigenstates of definite parity but rather in mixed parity states. Electric dipole oscillations of the electronic

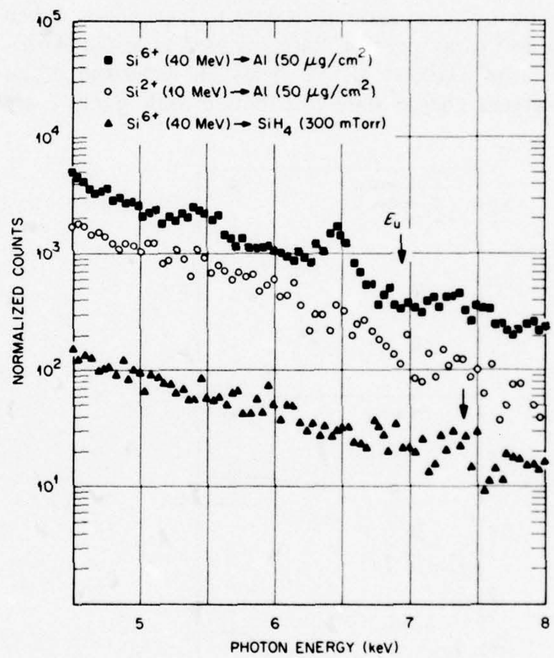

Fig. 9. Continuum X-ray spectrum near the united atom limits (indicated by the arrows) for 40 MeV Si ions in SiH_4 targets at 300 mtorr and in 50 $\mu g/cm^2$ Al targets, normalized in each case to the characteristic line strengths. From ref. 27.

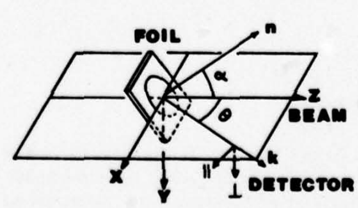

Fig. 10. Geometry of tilted-foil experiments. From ref. 33.

charge distributions of the emergent atoms along the beam direction were found to occur, and the surface interaction was found not to have reflection symmetry in the plane of the foil. Another way of characterizing the situation is to speak of an oscillating electronic linear momentum distribution asymmetry along the beam direction. At the Gatlinburg conference, Schectman et al.[30]) reported the discovery and properties of a number of similar mixed parity coherences in the $n = 3$ levels of H and in the $n=4$ levels of He^+ emergent from foils. In the He^+ data, oscillation frequencies corresponding to SP, PD and DF mixing were manifest. Schectman also reviewed the subject of mixed parity beats in general.

Angular momentum asymmetries (alignment) in which the emergent atomic orbital angular momentum tends to be preferentially parallel or anti-parallel to the beam, depending on the nature of the projectile and its speed, have been known for some time (see refs. 31 and 32). It is to be emphasized that to date, foils exposed to air beforehand and situated in practical vacuums have been used in such experiments, and in the more recent tilted foil experiments which Berry[33]) reviewed at the Gatlinburg meeting.

The geometry characterizing such tilted foil experiments is shown in fig. 10. The Z direction is taken as the axis of the incident beam, the polar angle θ specifies the direction of view of emitted photons, and the angle α specifies the direction of the unit normal to the foil surface. The polarization properties of light emitted by emergent atoms may be specified by four parameters called the Stokes parameters, one of which is the total intensity I. A second, called M, is related to the alignment, and for the special case of viewing along the x direction, M/I becomes simply $\langle L_y^2 - L_z^2\rangle / \langle L_x^2\rangle$. Another parameter, S/I, is proportional to $-\langle L_x\rangle / \langle L_x^2\rangle$, and cannot be other than 0 for cylindrical symmetry ($\alpha = 0$). Observation of a finite value of S for non-zero alpha implies that a net torque causes rotation of the electronic charge distribution of an emergent atom in either a clockwise or counter clockwise direction (depending upon sign). Such non-zero values have now been found for a number of emergent projectile excited states, and the α-dependence of the Stokes parameters tested. Berry reviewed both available experimental data as well as yet incomplete theoretical attempts to explain the α-dependence of such data by a number authors[33]). To illustrate the surprising character of the data, we may cite some of the results of Berry et al.[33]): (1) for the 2s–3p singlet transitions in He at 130 keV beam energy, both M and S have been found to be positive, but at 286 keV, $M>0$ and $S<0$. For 2p–4d singlet transitions in He, on the other hand, $M<0$ but $S>0$. $|S/I|$ has been found to vary quite rapidly with α, and has been observed to reach values $\approx 20\%$ in some cases. A preliminary account of experiments with similar motivation, but involving ions incident on polished bulk metal surfaces in practical vacuums inclined at $\approx 89^\circ$ to the beam, was presented at the meeting by Silver[34]). Values of $S/I \approx 20$–30% were reported for 300 keV Ar^+ beams incident on such surfaces. As measurements of S/I are made by studying the circular polarization of the emitted light, intensities of left hand as appeared to right hand circularly polarized light are therefore found to be very different. In some of the data presented by Silver[34]), values of $(I_{RH} - I_{LH})/(I_{RH} + I_{LH})$ approaching 50% were found, where the sense of positive polarization corresponded to $\hat{\boldsymbol{n}} \times \boldsymbol{v}$, where $\hat{\boldsymbol{n}}$ specifies the direction of the surface and $\boldsymbol{v}$ the beam velocity.

This partial listing of contributions to the Fourth International Conference on Beam Foil Spectroscopy which appeared to me to be of direct interest to participants in the present conference is necessarily both sketchy and incomplete. I hope I have, however, been able to communicate my opinion that the overlap of interests between the two disciplines is a strong one, and that scientists involved in the two fields have much to learn from each other.

References

1) *Beam-foil spectroscopy: heavy ion atomic physics*, Vols. 1 and 2 (eds. I. A. Sellin and D. J. Pegg; Plenum Press, New York, 1976).
2) S. Datz, these proceedings, p. 7.
3) H.-D. Betz, these proceedings, p. 19.
4) G. Sørensen, in ref. 1.
5) G. Astner, L. Liljeby, I. Martinson and J. O. Stoner, Jr., in ref. 1.
6) J. P. Forester, R. S. Peterson, P. M. Griffin, H. Haselton, K.-H. Liao, J. R. Mowat, D. J. Pegg, I. A. Sellin and R. S. Thoe, in ref. 1.
7) D. J. G. Irwin, E. J. Knystautas and R. Drouin, in ref. 1.
8) S. L. Varghese, C. L. Cocke, B. Curnutte and R. R. Randall, in ref. 1.
9) G. Beauchemin and R. Drouin, in ref. 1.
10) J. Lindhard, M. Scharff and H. E. Schiøtt, Kgl. Dan. Vid. Selsk. Matt.-Fys. Medd. **33**, no. 14 (1963).
11) B. Wehring and R. Bucher, in ref. 1.
12) K. O. Groeneveld, in ref. 1.
13) W. Meckbach, in ref. 1.
14) M. Menendez and M. Duncan, in ref. 1.
15) R. Laubert, in ref. 1.
16) H. H. Bukow, H. v. Buttlar, G. Heiner and M. Reinke, in ref. 1.
17) F. Hopkins and P. von Brentano, in ref. 1.
18) C. Jordan, Nucl. Instr. and Meth. **110** (1973) 373.
19) J. R. Mowat, I. A. Sellin, R. S. Peterson, D. J. Pegg, M. D. Brown and J. R. Macdonald, Phys. Rev. **A8** (1973) 145.

[20]) D. L. Matthews and R. J. Fortner, in ref. 1.
[21]) R. J. Fortner, D. C. Matthews, J. D. Garcia and H. Oona, in ref. 1.
[22]) F. Hopkins, in ref. 1; and in Phys. Rev. Lett. **35** (1975) 270.
[23]) S. Datz, B. R. Appleton, J. R. Mowat, R. Laubert, R. S. Peterson, R. S. Thoe and I. A. Sellin, Phys. Rev. Lett. **33** (1974) 733.
[24]) F. W. Saris, W. F. van der Weg, H. Tawara and R. Laubert, Phys. Rev. Lett. **78** (1972) 717.
[25]) F. W. Saris, C. Fortner, A. Langenberg and J. van Eck, J. Phys. B. **7** (1974) 1494.
[26]) F. Bell, H.-D-. Betz, H. Panke, E. Spindler, W. Stehling and M. Kleber, Phys. Rev. Lett. **35** (1975) 841.
[27]) R. S. Peterson, R. Laubert, R. S. Thoe, H. Hayden, S. Elston, J. Forester, K.-H. Liao, P. M. Griffin, D. J. Pegg and I. A. Sellin, in ref. 1.
[28]) I. A. Sellin, J. R. Mowat, R. S. Peterson, P. M. Griffin, R. Laubert and H. H. Haselton, Phys. Rev. Lett. **31** (1973) 1335.
[29]) T. G. Eck, Phys. Rev. Lett. **31** (1973) 270.
[30]) R. M. Schectman, H. G. Berry, G. Gabrielse, P. O. Berge, L. J. Curtis and R. Hight, in ref. 1.
[31]) ed. S. Bashkin, Nucl. Instr. and Meth. **110** (1973).
[32]) eds. I. Martinson, J. Bromander and H. G. Berry, Nucl. Instr. and Meth. **90** (1970).
[33]) H. G. Berry, in ref. 1.
[34]) J. D. Silver, in ref. 1.

Reprinted from: BEAM-FOIL SPECTROSCOPY, VOL. 2 (1976)
Edited by Ivan A. Sellin and David J. Pegg
Book available from: Plenum Publishing Corporation
227 West 17th Street, New York, New York 10011

DIFFERENCES IN THE PRODUCTION OF NONCHARACTERISTIC RADIATION IN SOLID AND GAS TARGETS*

R. S. Peterson, R. S. Thoe, H. Hayden, S. B. Elston, J. P. Forester, K.-H. Liao, P. M. Griffin, D. J. Pegg, and I. A. Sellin

University of Tennessee
Knoxville, Tennessee 37919
and Oak Ridge National Laboratory
Oak Ridge, Tennessee 37830

and

R. Laubert

New York University
New York, New York

Recent experimental results of Bell et al. [1] for 55 MeV S → Al and 48 MeV S → Ne collisions indicated that the production of noncharacteristic radiation (NCR) was similar for gas or solid targets when normalized to the characteristic line of the projectile ion. Such a result would indicate that a one-collision mechanism for NCR production, in which a vacancy in the K shell is produced and filled during the collision, is as important as the two-collision model proposed by Saris et al. [2]. Experiments have been completed using more nearly symmetric collision partners, and it is found that the yield of x rays near the combined-atom K x-ray limit (E_u) for 40 MeV $Si^{6+} \rightarrow SiH_4$ is significantly smaller than the yield of NCR for 40 MeV $Si^{6+} \rightarrow Al$.

Beams of silicon ions from the Oak Ridge National Laboratory 6.5 MV tandem Van de Graaff were passed through a gas target cell, shown in Figure 1, and the x rays produced in the resulting collisions

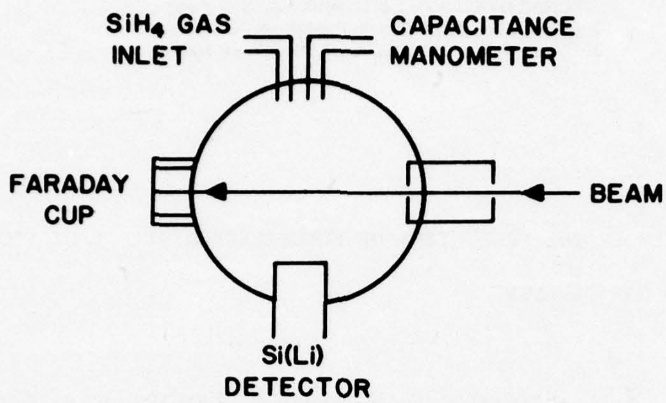

Figure 1. Gas Target Schematic. Ion beams of various energies entered the gas cell through collimators and were collected in the Faraday cup. A capacitance manometer was used to measure the gas pressure and to control the gas flow, maintaining the target gas pressure at 300 mTorr. A Si(Li) detector was used to observe the x-ray spectrum at 90 degrees to the ion beam.

were viewed at 90^o by a Si(Li) detector with FWHM of 160 eV at 5 keV. A two mil Mylar window was used with the Si(Li) detector to preferentially absorb the Si and Al characteristic K x rays with respect to the higher energy x rays. The beam current, which was collected in a Faraday cup, was kept low enough that pulse pile-up was avoided.

The gas pressure was monitored by a capacitance manometer which also controlled the gas flow valve, keeping the target pressure constant at 300 mTorr. When thin foils were used, no gas was admitted to the chamber and a foil was inserted in the beam path.

X-ray spectra were recorded for 10 - 40 MeV Si^{q+} on Al (50 $\mu g/cm^2$) foils and 40 MeV Si^{6+} on SiH_4 (300 mTorr). The spectra for 40 MeV Si^{6+} on SiH_4 and Al are shown in Figure 2, where the spectra were normalized to the gas target K x-ray characteristic lines. Even though no corrections for absorption were made in this figure, it is obvious that the x-ray yield near the combined-atom limit (E_u) is greater for the solid target (Al) than for the gas target (SiH_4).

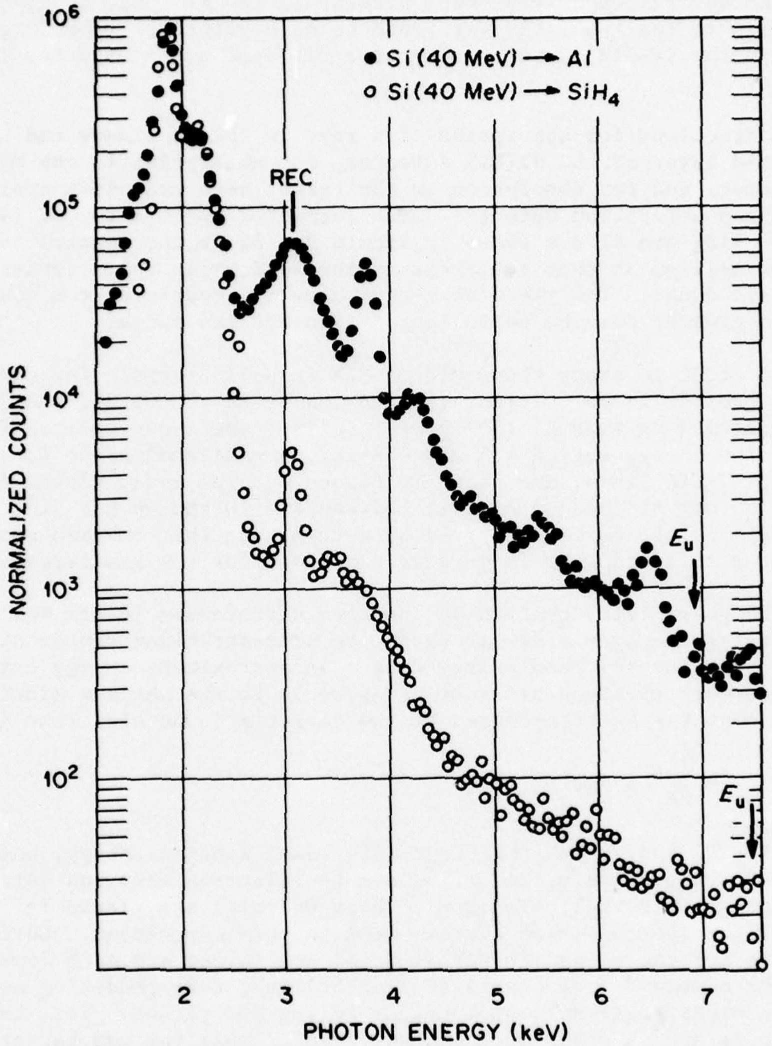

Figure 2. X-ray spectra for Si^{6+} (40 MeV) on Al and SiH_4. The x-ray spectra have been normalized to the Si K x-ray lines. Impurity peaks at 3.7 keV, 5.4 keV, and 6.4 keV in the solid Al target are probably due to K x-rays of calcium, chromium, and iron. The peak at 3.1 keV is due to REC in the solid target and argon K x rays in the gas target.

Although several impurities were present in the Al foil, their contribution to the NCR yield was found to be negligible. The large peaks in the Si-SiH_4 data are due to a residual argon impurity in the gas.

Corrections for absorption of x rays in the Be window and silicon dead layer of the Si(Li) detector, for absorption in the Mylar attenuator, and for absorption in the target were made from available x-ray absorption data [3]. The corrected spectra for Si (40 MeV) on SiH_4 and Al are shown in Figure 3. Again the spectra have been normalized so that the areas of the Si K x-ray characteristic lines are equal. The yield of x-rays near the combined atom limit (E_u) is greater for the solid target than the gas target.

In order to study the yield of NCR in solid targets for different projectile velocities, silicon ion beams at 10, 20, and 30 MeV were used on thin Al (50 $\mu g/cm^2$) foils. The x-ray spectra for the photon energy region 4.5 keV - 8 keV, normalized to the Si characteristic lines, are shown in Figure 4. The x-ray yields for 20 and 30 MeV Si ions on Al fall between the 10 and 40 MeV Si^{q+} on Al data. In all cases the yield of x-rays near the combined atom limit for solid targets is greater than that for the gas target.

The possibility that these observed differences in gas vs. solid target x-ray yields may be due to bremsstrahlung can be discounted for the low beam energy data. An approximate energy cutoff for secondary electron bremsstrahlung would be the maximum kinetic energy that can be transferred to the target's bound electrons [4]:

$$E_{max} \approx \frac{4mE}{MA} + 2mv_1v_2$$

where MA, E, and v_1 are the projectile mass, kinetic energy, and velocity, respectively, and m, v_2 are the electron mass and velocity of target atom K-shell electron. These energies are listed in Table I for the collision systems used in this experiment. Cutoff energies for the 10 and 20 MeV Si on Al collisions are much lower than the combined-atom energy (E_u) of 6.9 keV, thus rendering negligible bremsstrahlung contributions to the NCR yields. Yet, the NCR yields are an order of magnitude greater than the gas target yields. Although the bremsstrahlung cutoff energies for 30 and 40 MeV Si on Al collisions are higher, there does not appear to be any significant increase in the measured NCR yield at these higher beam energies. The small x-ray yield near the combined-atom limit (E_u) for the gas target collisions and the high bremsstrahlung energy cutoff does not preclude the possibility that these x rays were due to secondary electron bremsstrahlung.

The fact that the yield of x rays near the combined-atom limit (E_u) for Si on SiH_4 was small can be emphasized by comparing the

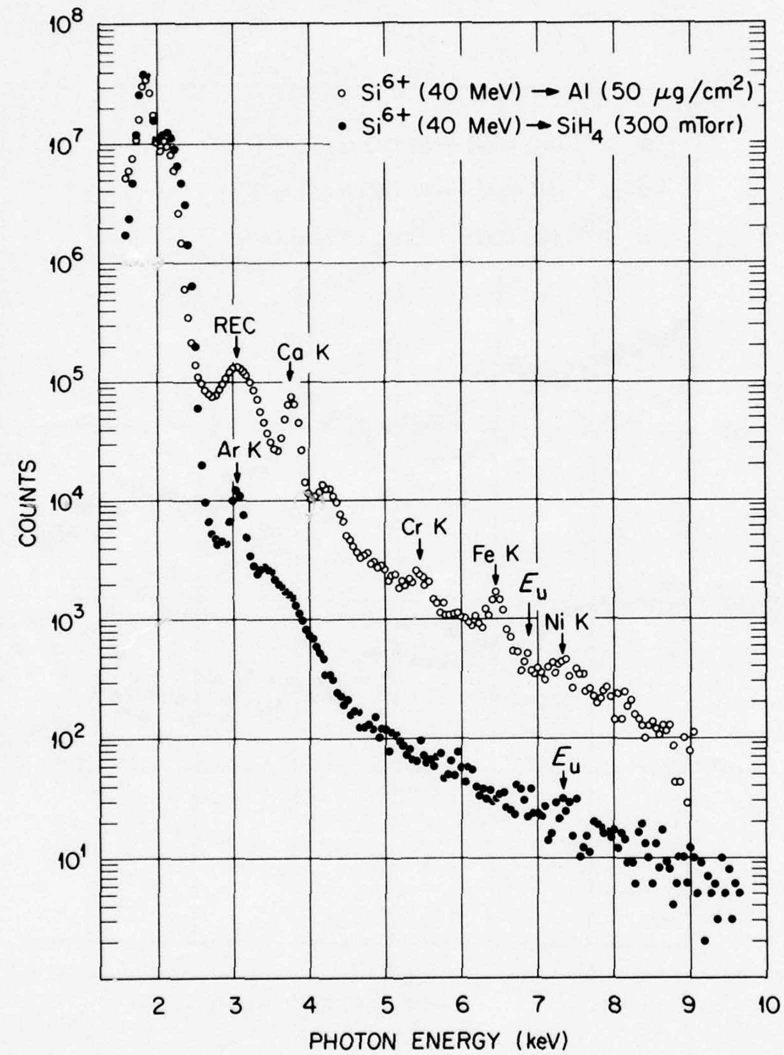

Figure 3. The x-ray spectra for 40 MeV Si^{6+} on Al and SiH_4 have been corrected for window absorption and normalized to the Si K x-ray peak. The x-ray yields near the combined-atom limits (E_u) are larger in the solid target than in the gas target.

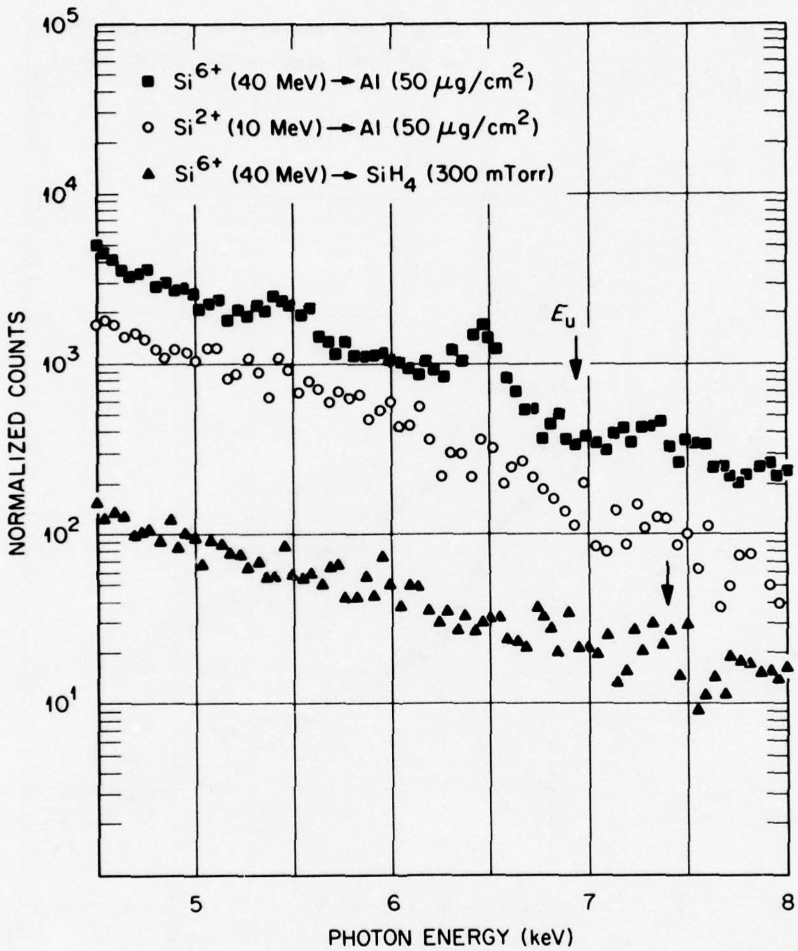

Figure 4. NCR x-ray spectra for 10 and 40 MeV Si^{x+} on Al and 40 MeV Si^{6+} on SiH_4. The NCR spectra obtained for 20, 30 MeV Si^{x+} on Al (not shown) lie between the 10 and 40 MeV solid target data. All the spectra above were normalized to the Si K x-ray lines.

TABLE I

Collision	Beam Energy (MeV)	E_{max} Maximum Kinetic Energy Transferred to Bound Electron (keV)
Si-Al	10	2.9
	20	4.6
	30	6.1
	40	7.5
Si-Si	40	7.8

ratio of integrated NCR intensities to the characteristic K x-ray line intensities (NCR/CR) for different symmetric collisions where the ratio of beam velocity to K-shell electron velocity (V/V_k) is the same. Laubert et al. [5] measured the ratio of NCR/CR for C-C and Al-Al collisions (solid targets) to be $\sim 2 \times 10^{-4}$ and $\sim 7 \times 10^{-4}$, respectively, where $\frac{V}{V_k} \simeq 0.5$. In the present experiment the NCR/CR ratio for Si-Si (gaseous target) is found to be $\sim 2 \times 10^{-5}$ for $\frac{V}{V_k} \simeq 0.5$. These results show that the NCR/CR ratios for symmetric collisions involving thin solid targets are of the same order of magnitude for different Z, whereas the present data shows that the Si-Si NCR/CR ratio, obtained with a gas target, is an order of magnitude smaller.

Because of the wide range of velocities of the projectile Si ions used on Al foils, there were correspondingly large changes in the charge state distributions of the projectile. Any changes in fluorescence yields due to these differing charge state distributions do not appear to have influenced the NCR yield with respect to the Si characteristic lines.

It appears, therefore, that the large yield of NCR in the solid targets is not due to secondary-electron bremsstrahlung or to any projectile fluorescence yield effect. The yield of NCR is not similar for gas and solid targets for the present collision systems, where the solid target collisions give NCR yields at least an order of magnitude greater than the gas target collisions.

Atomic densities in gas targets (for pressures less than 1 Torr) are several orders of magnitude smaller than atomic denities in thin, solid foils. Consequently, the inverse lifetime of a K-shell vacancy produced in a projectile traversing a gas target is much less than the frequency of collisions, whereas this inverse

lifetime for low Z projectiles is comparable to the collision frequency in solid targets.

If a single-collision model is important for NCR production, the yield of x rays near the combined-atom limit (E_u) for ion-atom collisions in gases should be comparable to the NCR yields in solid target collisions. This not being true for the collision systems studied implies that the proposed two-collision mechanism for NCR production in solid targets dominates over any single-collision processes.

REFERENCES

*Research supported in part by NSF, ONR, NASA, and by Union Carbide Corporation under contract with ERDA.

[1]. F. Bell, H.-D. Betz, H. Panke, E. Spindler, W. Stehling and M. Kleber, Phys. Rev. Lett. 35, 841 (1975).
[2]. F. W. Saris, W. F. van der Weg, H. Tawara, and R. Laubert, Phys. Rev. Lett. 28, 717 (1972).
[3]. B. L. Henke, Norelco Reporter, Vol. XIV, N 3-4 (1967), p. 127.
[4]. F. Folkmann, C. Gaarde, T. Huus, and K. Kemp, Nucl. Instr. Meth. 116, 487 (1974).
[5]. R. Laubert, H. H. Haselton, J. R. Mowat, R. S. Peterson, and I. A. Sellin, Phys. Rev. A 11, 1468 (1975).

Reprinted from: BEAM-FOIL SPECTROSCOPY, VOL. 2 (1976)
Edited by Ivan A. Sellin and David J. Pegg
Book available from: Plenum Publishing Corporation
227 West 17th Street, New York, New York 10011

ANGULAR DISTRIBUTION STUDIES OF NON-CHARACTERISTIC X-RADIATION

R. S. Thoe, I. A. Sellin, K. A. Liao, R. S. Peterson,
D. J. Pegg, J. Forester, and P. M. Griffin

The University of Tennessee, Knoxville, Tenn. 37916
and
Oak Ridge National Laboratory, Oak Ridge, Tenn. 37830

We have recently measured the polarization of the non-characteristic x-radiation emitted from collisions between energetic (10-90 MeV) Al ions in thin foils. The motivation to persue this line of research originated from the calculations of Müller and Greiner[1] which predict that in addition to the normal spontaneous emission of molecular orbital x-rays, there also exists a mechanism which gives rise to induced emission of these radiations. This mechanism is a direct result of the coriolis forces which exist in the rest frame of the quasi-molecule, whose axis of quantization is rotating with angular velocity ω_{rot}. The cross sections derived by Müller and Greiner from the two center Dirac equations are

$$\frac{d\sigma_s}{d\omega d\Omega_K d\Omega_i} = \frac{\omega^3}{2\pi\hbar c^3} |d_{Fi}|^2 \sin^2\theta_K \left(\frac{d\sigma}{d\Omega_i}\right)_{Ruth} \tag{1}$$

$$\frac{d\sigma_i}{d\omega d\Omega_K d\Omega_i} = \frac{\omega}{2\pi\hbar C^3} |\vec{\omega}_{rot} \times \vec{d}_{Fi}|^2 \sin^2\theta_K \left(\frac{d\sigma}{d\Omega_i}\right)_{Ruth} \tag{2}$$

d_{Fi} is the ordinary dipole transition matrix element and $d\sigma_s$ is the differential cross section for detecting a photon of frequency ω at angle θ_K per solid angle $d\Omega_K$ for ions scattered into solid angle $d\Omega_i$. $\left(\frac{d\sigma}{d\Omega_i}\right)_{Ruth}$ is the differential Rutherford cross section.

These two equations are equal in magnitude when $\omega^2_{rot} = \omega^2$. For photon frequencies near the united atom limit ω_{rot} is a maximum at the distance of closest approach and is $\sim \frac{T}{2m\, R_{\mu a}^{\,2}}$, in the straight line approximation for an impact parameter $b \approx 0.5 R_{\mu a}$; $R_{\mu a}$ is the radius of the united atom K shell, T is the incident kinetic energy and m is the mass of the ion - $m \sim 2Z$. Using the Bohr formula for Lyman alpha radiation gives:

$$\omega^2 = (1/4)\, \frac{(2Z)^2\, e^4}{\hbar^2\, R_{\mu a}^{\,2}}\, (3/4)^2 \tag{3}$$

$\omega^2 = \omega^2_{rot}$ implies:

$$\frac{T_o}{2m\, R_{\mu a}^{\,2}} = (1/4)\, \frac{(2Z^2)\, e^4}{\hbar^2\, R_{\mu a}^{\,2}}\, (3/4)^2 \tag{4}$$

$$T_o = \frac{Z^3}{144}\ \text{MeV}.$$

Therefore, at energies above T_o, the induced cross section should be larger than the spontaneous cross section. This expression compares very favorably with the value obtained by Betz, Bell *et al.*[2] - $T_o{}' = \frac{Z^3}{121}$ MeV, which was obtained from cross section measurements on the molecular-orbital radiation emitted from S-Al and S-Ne collisions.

The difference in the transition matrix elements in equations (1) and (2) also leads to differing polarizations between the induced and spontaneous radiation. The amount of polarization is also a strong function of subshell population, collision velocity, impact parameter, and photon frequency. In order to characterize this polarization it is necessary to consider the transformation between the laboratory rest frame and the rest frame of the quasi-molecule. In Fig. 1 the beam is moving in the -z direction, the internuclear axis is $\underline{Z}$, the rest frame of the quasi-molecule is z', x, y', and the angle between z and z' is ξ. Therefore, $0 \leq \xi \leq \pi$, and the direction ω_{rot} is coincident with the x axis. The radiation pattern of the rotating quasi-molecule for united atom radiation can be calculated most simply since for this radiation the photon frequency is $\sim$ independent of the internuclear distance.

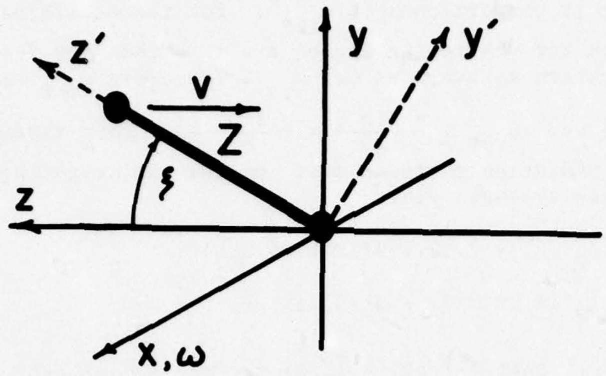

Fig. 1

Now this rotation can be represented by:

$(\hat{x}_i) = R\ (\hat{x}')$

$$R = \begin{pmatrix} 1 & 0 & 0 \\ 0 & \cos\xi & +\sin\xi \\ 0 & -\sin\xi & \cos\xi \end{pmatrix} \tag{5}$$

The two radiation patterns that have been considered are $I_1(\theta') = \sin^2\theta'$ and $I_2(\theta') = \cos^2\theta'$, where the primes indicate that these are the patterns as observed in the rotating quasi-molecular rest frame. In the lab frame these appear as

$$I_1(\theta) = x'^2 + y'^2 = x^2 + y^2\cos^2\xi + z^2\sin^2\xi \tag{6}$$

$$I_2(\theta) = z^{\ 2} = y^2\sin^2\xi + z^2\cos^2\xi . \tag{7}$$

Since this axis is rotating; (i.e., ξ goes from 0 to π), it is necessary to average these radiation patterns over all angles ξ and over all azimuthal angles θ. These averages yield:

$$\bar{I}_1(\theta) = 1/2 + 1/4\sin^2\theta \tag{8}$$

$$\bar{I}_2(\theta) = 1/4 + 1/4\cos^2\theta . \tag{9}$$

The radiation from the induced transition is somewhat different since it is proportional to ω_{rot}^2. For the collisions under consideration the scattering angles are less than one degree for impact parameters as small as 0.1 $R_{\mu a}$. Therefore ω_{rot} can be approximated by: $\omega_{rot} \simeq \frac{v \sin \xi}{Z} = \frac{v \sin^2 \xi}{b}$. Then the average of the induced radiation patterns must include the weighting factor $\sin^4 \xi$. These averages yield:

$$\bar{I}_1'(\theta) = 2/32 + 9/32 \sin^2 \theta \tag{10}$$

$$\bar{I}_2'(\theta) = 7/32 + 3/32 \cos^2 \theta, \tag{11}$$

with the result that : $\bar{I}_1'(\theta) + \bar{I}_2'(\theta) = 12/32 + 6/32 \sin^2 \theta$. Defining β as the polarization fraction (i.e., $I(\theta) = \alpha + \beta \sin^2 \theta$, $\alpha + \beta = 1$), we see that $\beta = 1/3$ even if no differential subshell alignment exists. With complete alignment β can be as large as 9/11.

If we use the maximum polarization for induced transitions and assume that the induced transition rate is proportional to the incident energy T and is equal to the spontaneous transition rate at $Z^3/121$ MeV = 18 MeV, we can describe rather accurately the behavior of the polarization β as a function of incident ion energy. The radiation pattern $I(\theta)$ is just the renormalized sum of the induced and spontaneous radiation patterns. Therefore assuming approximate isotropy of the spontaneous radiation yields

$$I(\theta) = \frac{1 + (2/11 + 9/11 \sin^2 \theta)\, T_o/18}{1 + T_o/18}$$

$$\beta(T) = \frac{9/11\, T_o}{18 + T_o} \tag{12}$$

Figure 2 is a plot of equation 12 along with the measured polarization fraction $\beta(T)$ for photons in the 5-6 keV energy interval (united atom limit) emitted from Al-Al collisions. The fit with the experimental data is remarkably good considering that equation 12 is derived from the theoretical results of **Ref.** 1 and the cross section data of Ref. 2 and contain no adjustable parameters.

Although the data of Fig. 2 fit equation 12 extremely well, there are still many unresolved problems. The effect of the beam energy on incident charge state and, hence, alignment has been completely ignored. Another major concern has to do with the rapid rotation of the quasi-molecular axis. The energies and impact

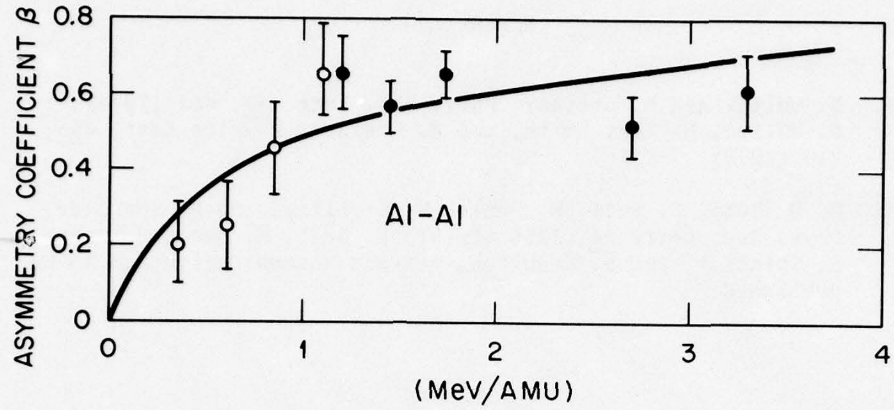

Fig. 2. Plots of the polarization β for the photon energy bins between 5 and 6 keV (inclusive) as a function of incident beam energy. Error bars represent 1 sigma. The solid line corresponds to the expression $\beta = (9/11)T/(T + 18\ \mathrm{MeV})$, where the coefficient (9/11) is derived in the text, the T dependence is derived from ω^2_{rot}, and the cross over between induced and spontaneous radiation at $\sim$ 18 MeV corresponds to the results of Ref. 2.

parameter where the rotational mechanism is important are those that give $\omega^2_{rot} \gtrsim \omega^2$. This means that the angular velocity of the internuclear axis is larger than the angular velocity of even the K-shell electrons, therefore it is difficult to understand how the electrons could be in eigenstates that are approximated by molecular orbitals. A final difficulty lies in that fact that while the molecular orbital radiation is highly polarized, which implies considerable alignment, the characteristic radiation is thought to be more nearly isotropic which implies a very small alignment.

ACKNOWLEDGMENTS

We thank Professor Myron McKay for his helpful participation in the data acquisition and the ORIC operating staff for their valuable contributions.

REFERENCES

1. B. Müller and W. Greiner, Phys. Rev. Lett. 33, 464 (1974); B. Müller, R. Kent Smith, and W. Greiner, Physics Lett. 49B, 219 (1974).

2. H. D. Betz, F. Bell, H. Panke, W. Stehling, and E. Spendler, Phys. Rev. Lett. 34, 1256 (1975); F. Bell, H. Betz, H. Panke, E. Spindler, and W. Stehling, private communication and to be published.

Reprinted from: BEAM-FOIL SPECTROSCOPY, VOL. 1 (1976)
Edited by Ivan A. Sellin and David J. Pegg
Book available from: Plenum Publishing Corporation
227 West 17th Street, New York, New York 10011

AUTOIONIZING STATES IN HIGHLY IONIZED OXYGEN, FLUORINE, AND SILICON*

J.P. Forester, R.S. Peterson, P.M. Griffin,
D.J. Pegg, H.H. Haselton, K.H. Liao, I.A. Sellin,
J.R. Mowat, and R.S. Thoe

University of Tennessee, Knoxville, Tennessee 37916

Oak Ridge National Laboratory, Oak Ridge, Tennessee 37830

INTRODUCTION

Excitation processes in atoms or ions usually involve the promotion of one of the least tightly bound outer shell electrons to a higher orbital leading to a state lying below the ionization threshold. It is possible however to form highly excited discrete states that are embedded in the continuum if one or more inner core electrons are raised to outer shells. In the present paper we report on such states in high Z 3-electron ions associated with core excited configurations of the type $1s2sn\ell$ and $1s2pn\ell$. Such states may autoionize rapidly via the Coulomb interaction unless forbidden to do so by selection rules on this process. These metastable autoionizing states either decay by radiation or autoionize at a slower rate via the weaker magnetic interactions. The lowest lying quartet state in 3-electron ions $(1s2s2p)^4P^o_{5/2}$, is metastable against both autoionization and radiation. Our previously measured lifetimes [1] for this state (in nanoseconds) are: S (1.1), Si (2.1), Ar (0.66), Cl (0.91), F (15), and O (25). Radiative decay processes involving core-excited states have also been previously observed. For example, one type of decay is an E1 transition between two metastable quartet states and another is a similar transition from a core excited state to a singly excited state. The probability of this latter transition increases as Z^4 and thus competes favorably with allowed autoionization for the depopulation of such states in higher Z ions.

EXPERIMENTAL METHOD

In the present experiment the electron decay-in-flight spectra of lithium-like O, F, and Si have been studied, using high energy beams from the Oak Ridge National Laboratory tandem accelerator. A thin carbon foil placed upstream of the viewing region of the analyzer served to both strip and excite the beam ions. The incident energy of the beam was chosen to maximize as far as possible the desired charge state downstream of the foil target. The ejected electrons were collected and energy analyzed using a second order, double focusing electrostatic cylindrical mirror analyzer, a schematic diagram of which is shown in Figure 1. This analyzer has a viewing region of 0.15 mm of the excited beam. The mean polar acceptance angle of the instrument is 42.3 degrees with a spread of ± 0.09 degrees. Electrons passing through the analyzer are detected by a low noise channeltron electron multiplier situated behind the exit slit. Spectra were obtained by sweeping the voltage on the analyzer using a linear ramp offset by a preset D.C. level. The

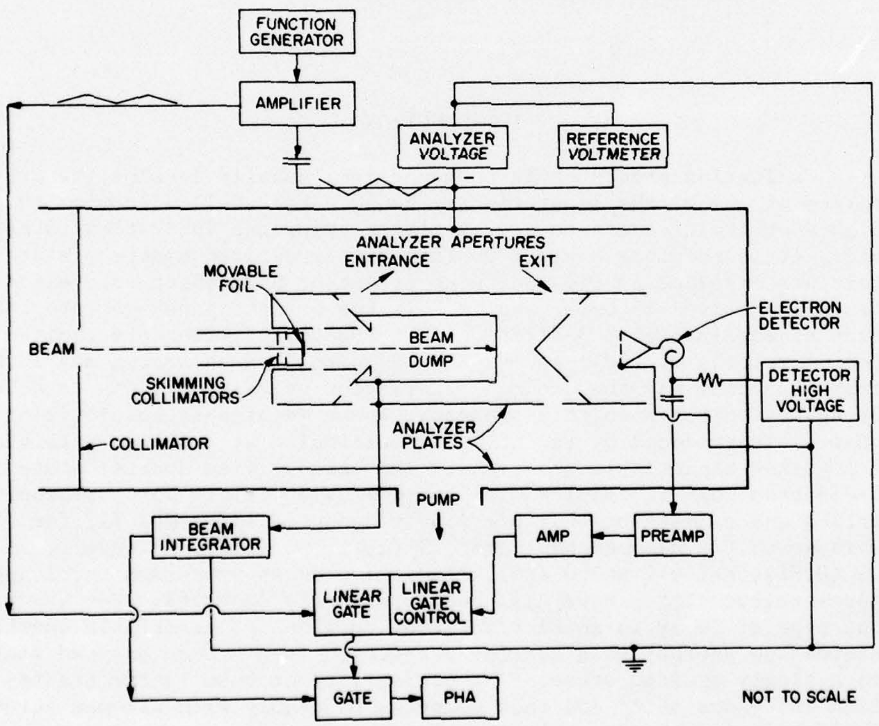

Figure 1. Schematic of the apparatus showing the electron analyzer.

spectra were then accumulated in a multichannel analyzer. The position of the foil with respect to the spectrometer viewing region could be varied in order to differentiate between short and long lived states thus aiding in the identification of the peaks.

The primary purpose of this experiment was to improve on the spectral resolution obtained in previous measurements [1] on F and O as well as to study analogous states in Si. The instrumental resolution was improved by the use of a new and larger analyzer (described previously) and by the use of thinner carbon foil targets (nominal thicknesses $2 \mu g/cm^2$) to reduce energy straggling and multiple scattering effects. The spectrometer was calibrated using Auger electrons emitted from inert gases excited by electron impact. In these spectra the measured resolution was better than 0.3%. The well established Auger energies of Werme, Bergmark, and Siegbahn[2] were used to obtain the analyzer constant.

RESULTS

Figure 2 shows the spectra of autoionization electrons emitted in flight by a 6.75 MeV highly stripped O beam following passage through a carbon foil of thickness $2 \mu g/cm^2$. The electron energy scale was established using Holøien and Geltman's [3] value of 416.2 eV for the energy of the $^4P^o(1)$ state. The notation used in this work will be that presented by Holøien and Geltman [3]. The lower of the upper two spectra corresponds to a time delay of about 0.2 nsec. with respect to the upper. The $^4P^o(1)$ — $^4P^e(1)$ splitting of 12.9 ± 0.2 eV measured in the present experiment can be compared with the previously measured value of 12±1 by Pegg et al. [1] and theoretical values of 13.1 [3], 13.0 [4], 12.2 [5], and 14.0 [6] eV. A radiative transition is also possible between these two states for which the measured splitting of 12.9 eV corresponds to a photon wavelength of 961 Å, which to our knowledge has not yet been observed. The partially blended feature on the low energy side of the $^4P^e(1)$ peak appears to be associated with the autoionization decay of the $^5P^e(1)$ state of 4-electron O. Two possible final states exist for the 3-electron ion $[(1s^2 2p)\,^2P^o,\ (1s^2 2s)\,^2S^e]$ leading to the emission of two discrete energy electrons separated by 12 eV. The higher energy of these two transitions appear to be present in our spectrum in the blended feature at 438.7 eV. Another component of this blend is associated with the decay of the $^6S^o(1)$ state in 5-electron O to the $(1s^2 2p^2)\,^3P^e$ final state of the residual 4-electron ion. Similar lines have recently been observed in the foil excited electron spectra of Be and B by Bruch et al. [7]. The structure at 434.4 eV in our spectra may be associated with the decay of the metastable $^2P^e(1)$ state in 3-electron O. The lower spectrum appearing in Figure 2 shows features of higher energy which are the result of autoionizing transitions involving $n \geq 3$. Some of the lines have been identified in Table I. The positions of the

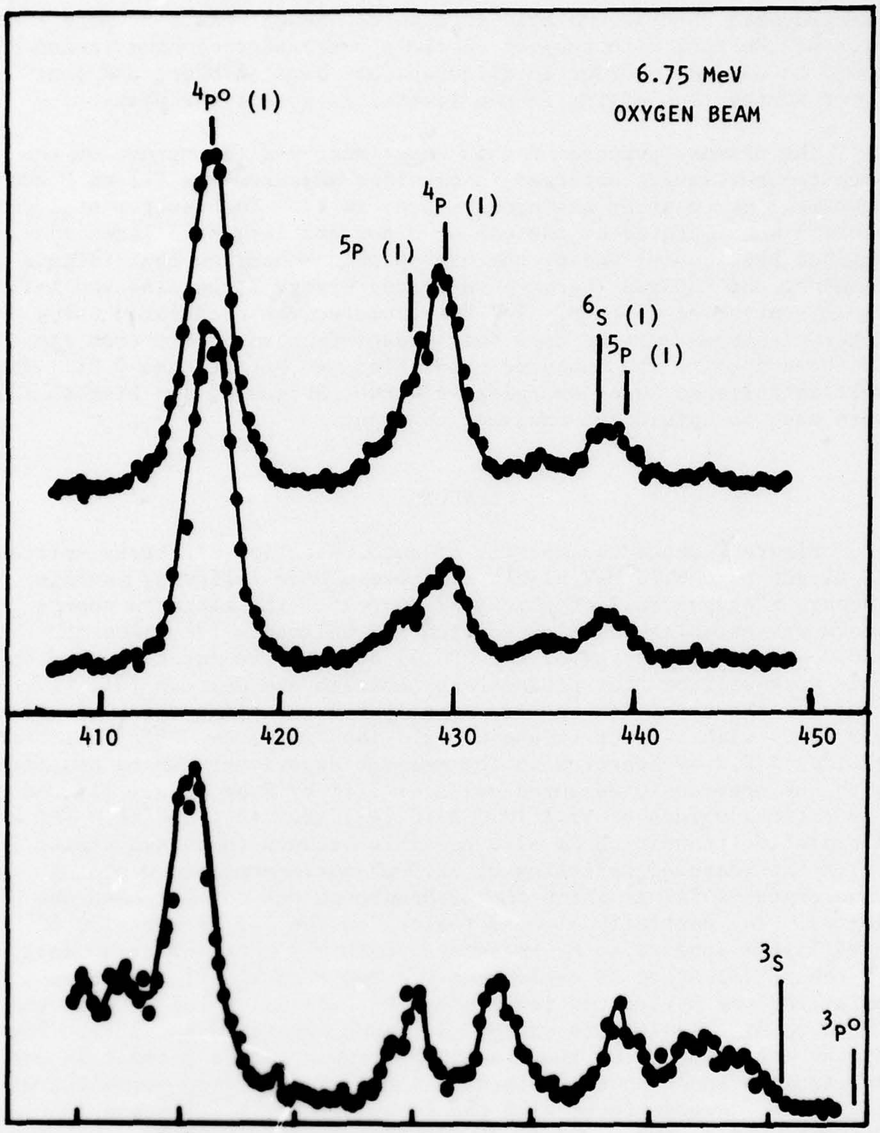

Figure 2. Spectra of electrons from highly stripped O undergoing decay in flight, plotted in the rest frame of the emitting ion. The energy scale is established by assigning a value of 416.2 to the $^4P^o(1)$ peak [3]. The continuous curve drawn through the data is drawn to aid the eye.

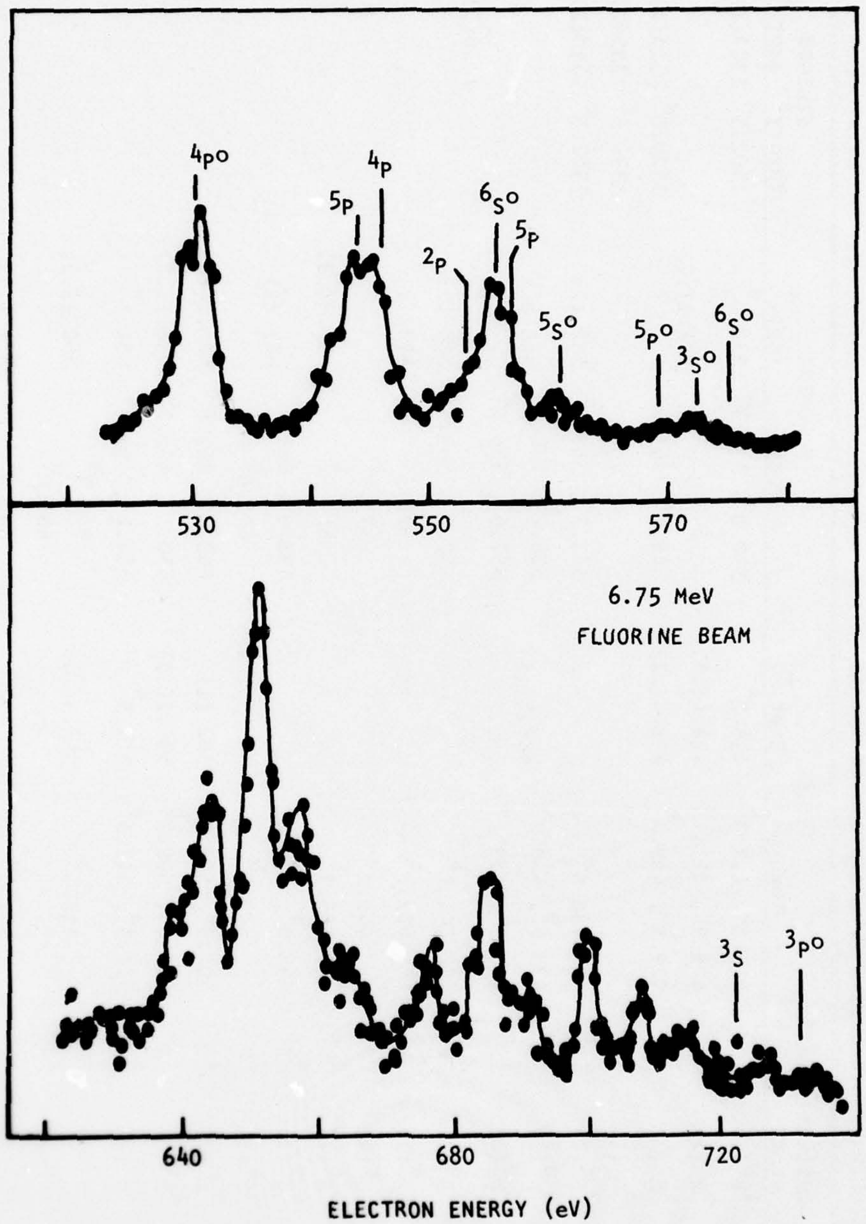

Figure 3. Spectra of electrons from highly stripped F undergoing decay in flight, plotted in the rest frame of the emitting ion. The energy scale is established by assigning a value of 530.0 eV to the $^4P^o(1)$ peak [3]. The continuous curve is drawn to aid the eye.

TABLE I. Electron energies (eV, ionic rest frame)

No. of elect.	Initial state	Final state	OXYGEN Theory[d]	OXYGEN Expt.[+]	FLUORINE Theory[d]	FLUORINE Expt.[+]	SILICON Theory[d]	SILICON Expt.[+]
3	$^4P^o(1)$	$^1S^e$	416.2[a], 417.3[b]	416.2*	530.0[a], 531.3[b]	530.0*	1302.9[a]	1303(2)
4	$^5P^e(1)$	$^2P^o$	428.3[b], 427.1[c]	426.4(.5)	543.6[b]	544.1(.7)		
3	$^4P^e(1)$	$^1S^e$	429.3[a], 429.5[b]	429.4(.2)	545.1[a], 545.3[b]		1326.0[a]	1325(1)
3	$^2D\ (1)$	$^1S^e$					1338.6[c]	1335(2)
3	$^2P^e(1)$	$^1S^e$	436.6[b]		553.7[b], 553.6[c]	552 (2)	1342.5[c]	1343(2)
5	$^6S^o(1)$	$^3P^e$	438.8[b], 438.2[c]	438.7(.5)	556.7[b], 556.4[c]	555.5		
4	$^5P^e(1)$	$^2S^e$	440.3[b], 439.1[c]		557.6[b], 556.4[c]			
4	$^5S^o(1)$	$^2P^o$	444.9[b]		562.9[b], 563.5[c]	560 (1)		1356(3)
4	$^3S^o(1)$	$^2P^o$	453.7[b]		573.5[b]	573 (1)		
5	$^6S^o(1)$	$^3P^o$	455.1[b]		575.9[b]			
4	$^3S^o(1)$	$^2S^e$	465.7[b]		587.5[b]	586.8(.8)		
3	$^4S^e(1)$	$^1S^e$	498.0[a], 500.2[b]		638.6[a], 641.4[b]	641 (1)		
4	$^5S^e(1)$	$^2P^o$	500.5[b]		641.8[b]			
3	$^4P^o(2)$	$^1S^e$	502.3[a], 503.9[b]	502 (1)	643.6[a], 645.8[b]	645.2(.4)		
3	$^4P^o(3)$	$^1S^e$	508.0[a], 508.2[b]	506.2(.5)	650.1[a], 650.3[b]	648.1(.8)		
3	$^4P^e(2)$	$^1S^e$	511.3[a], 511.5[b]	311.3*	654.1[a], 654.2[b]	654.1*		
4	$^5P^e(4)$	$^2P^o$	517.1[b]	517.3(.4)	661.0[b]	660 (1.5)		
4	$^5P^o(2)$	$^2S^e$			661.4[b]			
4	$^5P^e(3)$	$^2S^e$	521.5[b]		665.8[b]	664 (.7)		

TABLE I. Electron energies (eV, ionic rest frame)

No. of elect.	Initial state	Final state	OXYGEN Theory[d]	OXYGEN Expt.[+]	FLUORINE Theory[d]	FLUORINE Expt.[+]	SILICON Theory[d]	SILICON Expt.[+]
3	$^4S^e(3)$	$^1S^e$	527.6[a], 529.9[b]	529.7(.5)	677.9[a], 680.7[b]	679.6(.5)		
3	$^4P^e(3)$	$^1S^e$	539.6[a], 537.1[b]	537.5(.3)	691.7[a], 688.6[b]	788.4(.8)		
						701 (1)		
						704 (1)		

*These energies were set equal to those of E. Holøein and S. Geltman [3].

[a]E. Holøien and S. Geltman, Phys. Rev. 153, 81 (1967).

[b]B. R. Junker and J. N. Bardsley, Phys. Rev. A8, 1345 (1973).

[c]U. I. Safronova and V. N. Kharitonova, Opt. Spect. 27, 300 (1967).

[d]Non-relativistic values corrected using relativistic correction of R. Snyder, J. Phys. B 4, 1150 (1971).

[+]The parentheses following the experimental values contain the estimated error in eV.

$^3S^e$ and $^3P^o$ series limits are also indicated in the figure.

The autoionization electron spectra of F is shown in Figure 3. The absolute energy scale was established by assigning the value of 530.0 eV [3] to the decay of the $^4P^o(1)$ state in 3-electron F. Lines in the spectrum associated with the decay of core-excited states in 3-electron F are in many cases partially blended with contributions from similar transitions in 4-and 5-electron F. The latter transitions often leave the residual ion in excited states. The blending of such lines makes it difficult to accurately measure the separation of the 3-electron features. Some of the possible states are indicated in Figure 3. The features of the F spectra are similar to those of the O spectra. The energies of the peaks measured in this experiment as well as some theoretically calculated energies are listed in Table I.

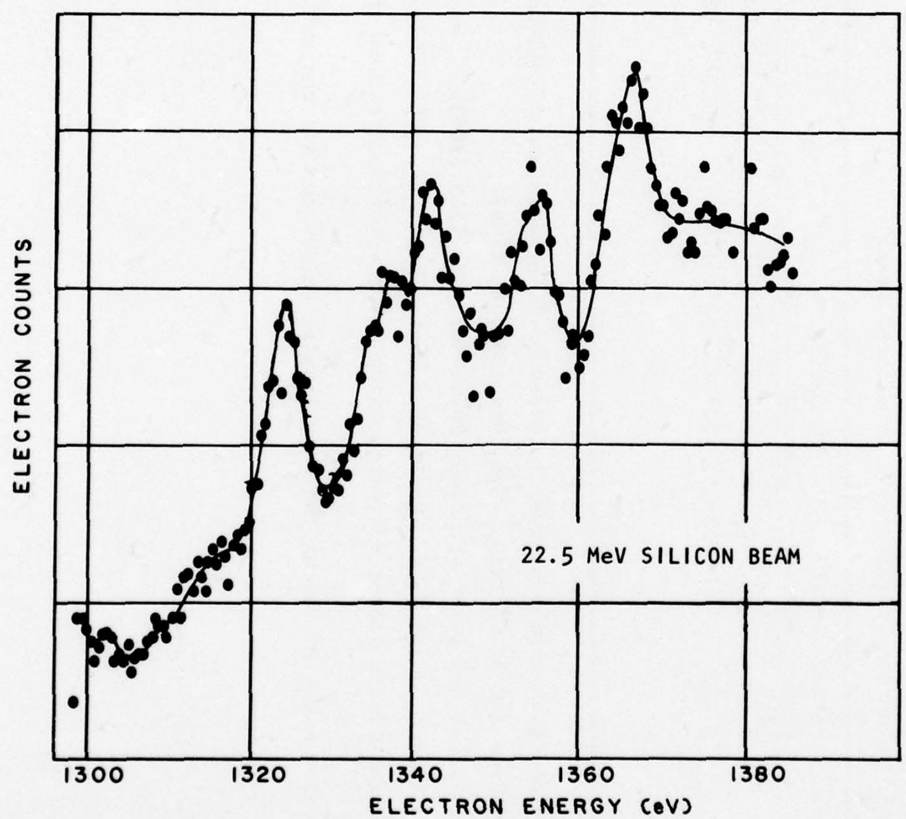

Figure 4. Spectrum of electrons from highly stripped Si, plotted in rest frame of emitting ion.

Figure 4 shows a prompt spectrum of electrons emitted from a 22.5 MeV foil-excited and highly stripped Si beam. In a similar delayed spectrum the small feature at 1303 eV became very prominent and can be associated with the $^4P^o(1)$ metastable state in 3-electron Si. The measured energy agrees very well with three independent calculations [3,4,6]. The spectral feature at 1324 eV is probably a blend of the $^5P^e(1)$ and $^4P^e(1)$ states of 4-and 3-electron Si respectively. The feature around 1340 eV is a blend of lines associated with the decay of several possible autoionizing states: $^2D^e(1)$, $^2P^e(1)$ of 3-electron Si, $^5P^e(1)$ of 4-electron Si and the $^6S^o(1)$ of 5-electron Si. Other features remain unidentified at this time.

REFERENCES

*Research supported in part by NSF, ONR, and by Union Carbide Corporation under contract with ERDA.

[1]. D. J. Pegg, I. A. Sellin, R. S. Peterson, J. R. Mowat, W. W. Smith, M. D. Brown, and J. R. MacDonald, Phys. Rev. A 8, 1350 (1973).
[2]. L. O. Werme, T. Bergmark, and K. Siegbahn, Phys. Scripta 8, 149 (1973).
[3]. E. Holøien and S. Geltman, Phys. Rev. 153, 81 (1967).
[4]. A. Gabriel, Non. Not. R. Astr. Soc., 160, 99 (1972).
[5]. B. R. Junker and J. N. Bardsley, Phys. Rev. A8, 1345 (1973).
[6]. H. Summers, Astrophys. J., 179.14 (1973).
[7]. R. Burch, J. Andra, G. Paul, Proceedings of this conference; R. Bruch, G. Paul, J. Andra, J. Phys. B. 8, L253 (1975).

(15)

Saal

[...]lle nicht ausfüllen!

DEUTSCHE PHYSIKALISCHE GESELLSCHAFT E.V.

VORTRAGSANMELDUNG FÜR DIE TAGUNG

vom .... bis März 19 77 in Mainz

Fachausschuß / Arbeitsgemeinschaft: Atomphysik

Lebensdauern und Oszillatorenstärken von n=2 Zuständen in Be-ähnlichem S.+

J.P.Forester, D.J.Pegg, S.B.Elston, P.M.Griffin, K.O.Groeneveld,* R.S.Peterson, R.S.Thoe, C.R.Vane, I.A.Sellin (Univ. Tennessee und Oak Ridge Nat.Lab.)

Aus jüngster Zeit liegen relativistische Rechnungen der Oscillatorenstärke von erlaubten Δ n=0 Übergängen in der L-Schale von isoelectronäschen Atomen der Be-Reihe vor. Wir berichten hier über Beam-Foil Messungen in allen möglichen solchen Übergängen von Be-ähnaichem S^{12+}. Für die Flugzeitmessungen stand ein Schwefelstrahl (ca. 45 MeV) des ORNL Tandems und ein "Grazing incidence" EUV Spectrometer zur Verfügung. Die theoretischen ung experimentellen Werte der Be-Reihe von Δ n=0 Übergängen werden diskutiert.

* Permanente Anschrift: Inst. f. Kernphysik der Universität, D6 Frankfurt/M
+ Gefördert durch: NSF, ONR und Union Carbide unter ERDA-Vertrag

(16)

Saal

Bitte nicht ausfüllen!

DEUTSCHE PHYSIKALISCHE GESELLSCHAFT E.V.

VORTRAGSANMELDUNG FÜR DIE TAGUNG

vom .... bis März 1977 in Mainz

Fachausschuß / Arbeitsgemeinschaft: Atomphysik

Der $2s\,^2S$-$2p\,^2P^o$ Doublettübergang in Li-ähnlichem Schwefel+

C.R.Vane, D.J.Pegg, S.B.Elston, J.F.Forester, P.M.Griffin, K.O.Groeneveld*, R.S.Thoe, I.A.Sellin, (Univ.Tennessee und Oak Ridge Nat'l. Laboratory,Tn USA)

Das $2s\,^2S$-$2p\,^2P^o$ Doublett in verschiedenen Li-ähnlichen Ionen wurde in neueren Skylabexperimenten als besonders starker Hochtemperaturübergang beobachtet und dient in Plasmauntersuchungen zur Temperaturdiagnose. Die dazu verwendeten Daten und frühere Labormessungen stimmen nicht überein. Die hier vorgelegten Daten der Doublettaufspaltung von Li-ähnlichem Schwefel nach Foliebanregung bestätigen die o.g. Skylabmessungen. Ausserdem wurden Lebensdauern von den $2p\,^2P^o_{1/2,3/2}$ Niveaux in Schwefel mit einer Beam-Foil Flugzeitmethode bestimmt. Die daraus berechneten Oszillatorenstärken werden mit werden mit neueren, relativistischen f-Wertberechnungen verglichen.

* Permanente Anschrift: Institut f. Kernphysik der Univ. D6 Frankfurt/M
+ Gefördert durch NSF, ONR und Union Carbide unter ERDA-Vertrag

Abstract for an Invited Paper
for the Lincoln-DEAP Meeting of the
American Physical Society
6-8 December 1976

High Ionization-Excitation States of Ne^{q+} Ions and their Mass-Dependent Symmetric Collision Interactions.*

I. A. SELLIN, The University of Tennessee and Oak Ridge National Laboratory, Knoxville (30 min.)

Through the use of two quite different techniques it has proved possible to study the production of excited Ne^{q+} ions (q = 1-9) and symmetric Ne^{q+}-Ne collisions (q = 1-5) in the quasi-molecular (keV energy) regime. Extraction of Ne^{q+} directly from a high power Penning discharge source at ORNL has permitted study of K ionizing collisions in Ne^{q+}-Ne collisions at beam energies $\lesssim$ 100 keV. The growth of K x-ray yields has been used to explore the exit channel effect explicitly treated within the framework of a rotational coupling model by Briggs and Macek.[1] Large, mass-dependent isotope effects have been discovered by Peterson, Laubert *et al.*[2] in the threshold region in which the K-hole production cross section rises steeply with beam energy. A striking failure of the equal velocity rule for the two isotopes ^{20}Ne, ^{22}Ne is observed. *A second method*[3] *for study of high excitation states* involves impact of highly ionized, foil transmitted heavy ions (e.g. S^{12+}) on lighter gas targets (e.g. Ne). Avoidance of a crucially limiting effect in beam-foil experiments - Doppler broadening - is an attractive goal, since not only greater accuracy in conventional beam-foil experiments but also precision resonance experiments on slow ions in high ionization-excitation states would then be possible. The likely limitations of recoil broadening and excitation cross sections have been explored recently in our laboratory in production of Ne II-V levels. Instrument limited line widths $\lesssim$ 6 meV have been observed, and attractively large production cross-sections have been demonstrated.

*Research partially supported by ONR, NSF, NASA; and by ERDA under contract with Union Carbide Corporation.

[1] J. S. Briggs and J. Macek, J. Phys. B5, 579 (1972); see also K. Taulbjerg, J. S. Briggs, and J. Vaaben, to be published in J. Phys. B.

[2] R. S. Peterson, S. B. Elston, I. A. Sellin, R. Laubert, F. K. Chen, and C. A. Peterson, to be published.

[3] J. R. Mowat, I. A. Sellin, D. J. Pegg, R. S. Peterson, J. R. Macdonald, and M. D. Brown, Phys. Rev. Lett. 31, 684 (1973); I. A. Sellin in Advances in Atomic and Molecular Physics 12, edited by D. R. Bates and B. Bederson (Academic Press, New York, 1976), p. 215.

17

Abstract Submitted

for the Lincoln, Nebraska Meeting of the

American Physical Society

December 6-8, 1976

Physics and Astronomy
Classification Scheme
Number__________

Bulletin Subject Heading
in which Paper should be placed
Atomic Collisions

Measurement of the H^++H Charge Exchange Cross Section, 0.8-2.5 MeV. L. D. GARDNER†, P. M. KOCH, J. E. BAYFIELD†, Yale Univ.; H. HAYDEN, Univ. of Connecticut; R. THOE, J. FORESTER, D. J. PEGG, I. A. SELLIN, Univ. of Tennessee.*--The total electron capture cross section for protons in atomic hydrogen was measured by passing a highly collimated high energy proton beam from the ORNL EN Tandem Accelerator through a thermally dissociated hydrogen gas target.[1] The target thickness was determined by a calibration procedure involving an auxilary low energy ion source and the observation of single electron capture by 20 keV protons and He^+ ions in argon. A dissociation fraction of 0.89 was measured using the low energy ion source by observing double electron capture by 20 keV protons from the residual molecular hydrogen. The measured cross section $\sigma_{10}(H)$ has a magnitude of $4.5 \pm 1.3 \times 10^{-22}$ cm^2 at 1 MeV and decreases with energy as $E^{-\beta}$, $\beta = 4.4 \pm 0.2$. This is in disagreement with the results of the First Born, Second Born, and first order Fadeev-Watson approximations.

†Present address: Dept. of Physics and Astronomy, Univ. of Pittsburgh.

*Supported by the Division of Physical Research of US ERDA.

[1]J.E. Bayfield, Rev. Sci. Ins. 40, 869 (1969).

Submitted by

____

L. D. Gardner

Department of Physics and Astronomy

University of Pittsburgh, Pittsburgh, Pa. 1526(

(19)

Abstract Submitted

for the Lincoln Meeting of The
(DEAP)
American Physical Society

December 6-8, 1976
Date

Physical Review
Analytic Subject Index
Number 35

Bulletin Subject Heading in
which Paper should be placed
Atomic Structure and Lifetimes

A Beam-Foil Study of the $2s^2S-2p^2P^0$ Doublet in Li-like Sulfur.* C.R. VANE, D.J. PEGG, S.B. ELSTON, J.P. FORESTER, P.M. GRIFFIN, K.-O. GROENEVELD+, R. S. PETERSON, R.S. THOE, and I.A. SELLIN, U. Tenn. and ORNL.- Recently there have been reports of observations of the $2s^2S-2p^2P^0$ doublet in highly stripped Li-like ions made aboard Skylab during solar flare events. This doublet was among the strongest of the high temperature lines observed and was used as a diagnostic of the plasma temperature. It appears that there is a disagreement between the doublet splittings obtained there and from an earlier laboratory measurement. We have investigated this doublet splitting in Li-like sulfur using foil-excitation and the results confirm the aforementioned Skylab data. In addition, we have measured the radiative lifetimes of the $2p^2P^0_{1/2,3/2}$ levels employing the usual beam-foil time-of-flight method and have derived corresponding oscillator strengths which will be compared with recent relativistic f-value calculations.

*Research supported in part by NSF, ONR, and Union Carbide Corporation under contract with ERDA.

+Permanent Address: Inst. für Kernphysik, Universität Frankfurt/M, W. Germany.

Submitted by

P M Griffin
Signature of APS Member

P. M. Griffin
Same name typewritten

Oak Ridge National Laboratory
Address

Oak Ridge, Tennessee 37830

UCN-9168
(3 5-69)

(20)

Abstract Submitted

for the Lincoln Meeting of The
(DEAP)
American Physical Society

December 6-8, 1976
Date

Physical Review
Analytic Subject Index
Number 35

Bulletin Subject Heading in
which Paper should be placed
Atomic Structure and Lifetimes

Radiative Lifetimes and Oscillator Strength for the n=2 States of Be-like Sulfur.* J.P. FORESTER, D.J. PEGG, S.B. ELSTON, P.M. GRIFFIN, K.-O. GROENEVELD+, R.S. PETERSON, R.S. THOE, C.R. VANE, I.A. SELLIN, U. Tenn. and ORNL.-- There has been considerable theoretical activity recently in calculating relativistic oscillator strengths for allowed $\Delta n=0$ transitions within the L shell of ions in the Be-sequence. We report here on a beam-foil investigation made in our laboratory on all possible such transitions in the Be-like ion, S^{12+}. The time-of-flight lifetime measurements were made using an $\sim$ 45 MeV sulfur ion beam from the ORNL tandem accelerator and a grazing incidence spectrometer to collect and disperse the resulting foil-excited EUV radiation. Comparisons between theory and experimental beam-foil results will be made along the Be-sequence for the $\Delta n=0$ transitions studied here.

*Research supported in part by NSF, ONR, and Union Carbide Corp. under contract with ERDA.

+Permanent Address: Inst. für Kernphysik, Universität Frankfurt/M, W. Germany.

Submitted by

Dand J Pegg

Signature of APS Member

D. J. Pegg

Same name typewritten

University of Tennessee

Address

Knoxville, Tennessee 37916

UCN-9168
(3 5-69)

(21)

Abstract Submitted

for the Lincoln Meeting of The (DEAP) American Physical Society

December 6-8, 1976
Date

Physical Review Analytic Subject Index Number 13.2

Bulletin Subject Heading in which Paper should be placed Atomic Collisions

Mass Dependence of Ne K X-Ray Yields from Ne^{+}-Ne Collisions at keV Energies.* R.S. PETERSON, S.B. ELSTON, I.A. SELLIN, Univ. of Tennessee and Oak Ridge National Laboratory, R. LAUBERT, F.K. CHEN, and C.A. PETERSON, New York University.-- Ne K x-ray yields from $^{A}Ne^{+}$-^{B}Ne collisions for A,B = 20,22 have been measured for beam energies between 60 keV and 220 keV. While x-ray yields were found to scale with equal relative velocities for the highest beam energies used, significant deviations from this scaling were measured at the lower beam energies. The possibility of equal center-of-mass energy scaling was tested; the measurements indicated deviations from this scaling for all beam energies for symmetric mass collisions. Comparisons of this mass dependence for symmetric collisions have been found to agree well with new theoretical calculations.

*Research supported in part by NSF, ONR, and Union Carbide Corporation under contract with the Energy Research and Development Administration.

Submitted by

Stuart B. Elston
Signature of APS Member

S. B. Elston
Same name typewritten

University of Tennessee
Address

Knoxville, Tennessee 37916